Optical Characterization of Solar Collectors from Outdoor Measurements

Incidence Angle Dependence of Asymmetric Collectors

Anna Helgesson

Division of Energy and Building Design
Department of Construction and Architecture
Lund University
Lund Institute of Technology, 2004
Report EBD-T--04/1

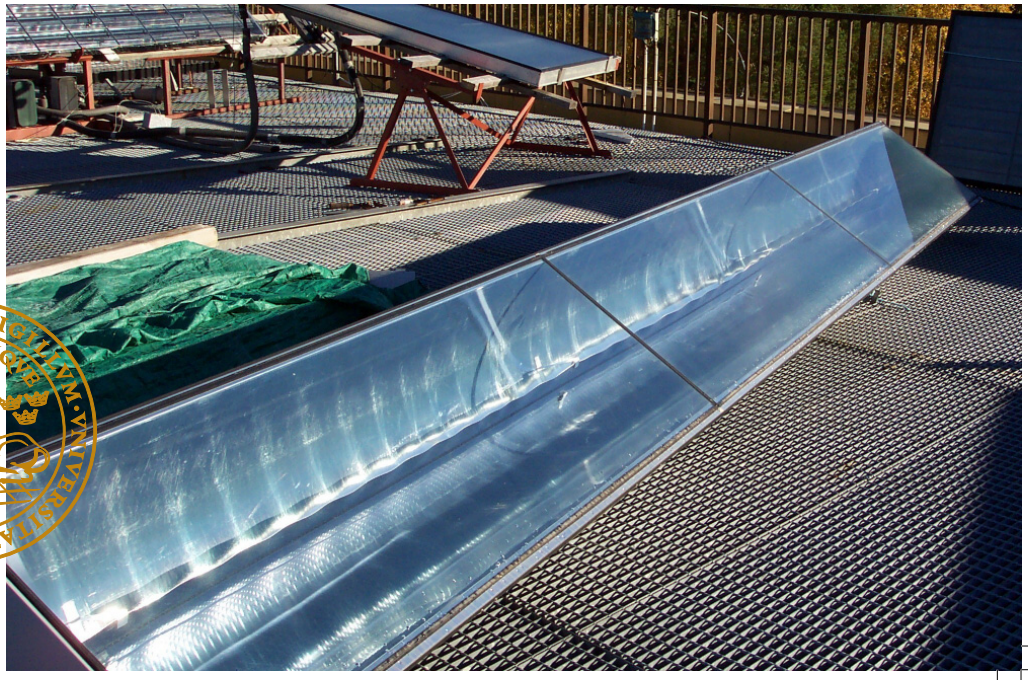

Lund University

Lund University, with eight faculties and a number of research centres and specialized institutes, is the largest establishment for research and higher education in Scandinavia. The main part of the University is situated in the small city of Lund which has about 101 000 inhabitants. A number of departments for research and education are, however, located in Malmö. Lund University was founded in 1666 and has today a total staff of 6 006 employees and 41 000 students attending 90 degree programmes and 1 000 subject courses offered by 88 departments.

Department of Construction and Architecture

The Department of Construction & Architecture is part of Lund Institute of Technology, the technical faculty of Lund University. The main mission of the Department of Construction & Architecture is to pursue research and education on topics related to the built environment. Some of the topics of interest are: restoration and maintenance of buildings, construction management, design processes, construction, energy efficiency, climatization and design of ventilation and heating systems, demolition, disposal and re-use of building materials.

These topics are treated from both a Swedish and an international perspective and collaboration between actors from mutidisciplinary fields of competence forms a particularly important aspect of research and education at the Department. The Department is divided into 5 subdepartments or divisions: Architectural Conservation & Restoration, Computer Aided Architectural Design, Construction Management, Energy & Building Design, and Housing Development & Management.

Division of Energy and Building Design

Reducing environmental effects of construction and facility management is a central aim of society. Minimising the energy use is an important aspect of this aim. The recently established division of Energy and Building Design belongs to the department of Construction and Architecture at the Lund Institute of Technology in Sweden. The division has a focus on research in the fields of energy use, passive and active solar design, daylight utilisation and shading of buildings. Effects and requirements of occupants on thermal and visual comfort are an essential part of this work. Energy and Building Design also develops guidelines and methods for the planning process.

Optical Characterization of Solar Collectors from Outdoor Measurements

Incidence Angle Debendence of Asymmetric Collectors

Anna Helgesson

Licentiate Thesis

Key words

Incidence angle dependence, Optical efficiency, Asymmetric solar collectors

The English language corrected by L. J. Gruber BSc(Eng) MICE MIStructE
Layout: Hans Follin, LTH, Lund

Printed by KFS AB, Lund 2004

Report No EBD-T--04/1
Optical Characterization of Solar Collectors from Outdoor Measurements. Incidence Angle Dependence of Asymmetric Collectord.
Department of Construction and Architecture, Lund University, Division of Energy and Building Design, Lund

ISSN 1651-8136
ISBN 91-85147-07-9

Lund University, Lund Institute of Technology
Department of Construction and Architecture
Division of Energy and Building Design
P.O. Box 118
SE-221 00 LUND
Sweden

Telephone: +46 46 - 222 73 52
Telefax: +46 46 - 222 47 19
E-mail: ebd@ebd.lth.se
Home page: www.ebd.lth.se

Abstract

Due to high installation costs and relatively low output, the active use of solar energy is limited. The output from a collector can be improved e.g. by using a selective absorber, AR-treated cover glass or transparent insulation. The output/cost ratio can also be improved by the use of reflectors. The performance of a collector depends highly on the incidence angle dependent optical efficiency. In this report, detailed methods for measuring the optical efficiency is developed.

In order to evaluate the performance of a collector, measurements are needed. For the evaluations in this work, a dynamic test method has been used. The collector output is modelled as:

$$\dot{q}_u = \eta_{0b} K_{\tau\alpha}(\Theta) I_b + \eta_{0d} I_d - k\Delta T - (mC)_e (dT_f/d\tau)$$

where η_0 is the optical efficiency, I the irradiance, k the heat loss factor, ΔT the temperature difference between collector and ambient air, and $(mC)_e$ the effective collector thermal capacitance. $K_{\tau\alpha}(\Theta)$ is a modifier accounting for the dependence of varying incidence angles during the day. It is often modelled as:

$$K_{\tau\alpha}(\Theta) = 1 - b_0(1/\cos(\Theta) - 1)$$

where b_0 is the "incidence angle modifier coefficient". In order to evaluate the energy output from different collector types, measurements were made on a number of collector prototypes. In the analysis, the collector parameters were identified by MLR on the measured data. In order to verify the determined parameters, the modelled output was compared with the measured output. The annual energy output was then estimated by using the collector parameters in the simulation program MINSUN.

In one study in the work, the incidence angle dependence of the absorptance was investigated by outdoor testing. The tested absorbers had coatings of nickel-pigmented aluminum oxide (Ni-Al_2O_3), and sputtered nickel/nickel oxide (Ni-NiO_x). The results showed that the Ni-Al_2O_3 absorber has a slightly better performance than the Ni-NiO_x absorber at high incidence angles. In another study, detailed comparative

tests were made on different glazings in order to study the influence of AR treatment on the collector output. The tests indicated that the AR treatment can increase the annual output by 9% (at T_{op} = 50°C). Usually a structured glass is installed with the structures facing the absorber. The evaluation indicates, however, that facing the structure outwards can increase the annual performance by 4%. A detailed study showed that the b_0 factor generally depends on the incidence angle.

MaReCo collectors are studied in the work. This is a reflector collector, specially designed for northern latitudes. The MaReCo principally consists of an asymmetric reflector trough with a single, double-sided selective, absorber that runs along the trough. The purpose of the MaReCo is to replace the collector box, insulation, and some of the absorber material by a reflector. The standard MaReCo has an acceptance angle interval of 20° - 65°, outside which the reflector is not active and the absorber only works with radiation direct from the sun. The MaReCo concept is flexible and can be used for stand-alone as well as building integrated applications. Several MaReCo prototypes have been tested in the work. The estimated yearly energy output at 50°C from a stand-alone MaReCo with Teflon and from a Roof-MaReCo, both at a tilt of 30°, were 282 and 336 kWh/m² respectively. The Spring/Fall-MaReCo is a special version that has a low optical efficiency during the summer. In this way, a larger collector area can be installed for increasing the solar fraction of the system without increasing the risk of overheating. The test results estimate a yearly energy output of 222 kWh/m² from this collector.

For an asymmetric collector (e.g. the MaReCo), the incidence angle dependence will be different in different directions. The angular analysis then has to be made in two perpendicular planes (longitudinal and transverse) of the collector. In the transverse plane, not only the properties of glass and absorber affect the output, but also the reflectivity and shape of the reflector. In order to handle this, a biaxial incidence angle modifier should be used. One example is the common "product model": $K_{\tau\alpha}(\Theta) = K_L(\Theta_L,0)K_T(0,\Theta_T)$. Shortcomings of this model are that it is not correct for plane collectors and that it is not defined for concentrators where normal incidence is outside the acceptance interval. In this work, a new expression for a biaxial incidence angle modifier is suggested: $K_{\tau\alpha} = f_L(\Theta)g_{TL}(\Theta_T)$. The factor $f_L(\Theta)$ gives information about the influence of the glazing and $g_{TL}(\Theta_T)$ accounts for the influence of the reflector. This expression differs in principle from the product model, since Θ_L is not used. In order to study the suggested model, measurements were made on MaReCo collectors. The "no-loss efficiency" was determined by eliminating the effect of heat losses from the measured output. The factor $f_L(\Theta)$ was decided from measurements in the L direc-

tion made around the equinox (when Θ_T is constant). The factor $F_T(\Theta_T)$ was determined from measurements in the T direction for constant Θ_L. In order to keep Θ_L constant, the collector was rotated to a north/south direction. The results were then used to calculate the reflector factor, $g_{TL}(\Theta_T)$, as the ratio $F_T(\Theta_T)/f_L(\Theta_T)$. The parameters were then used to model the energy output. The analyses indicate that the new suggested biaxial expression can be used to model the collector output for asymmetric collectors where the standard model does not work. One drawback of the method is, however, that it requires measurements to be made around either spring or autumn equinox. The new suggested model has also been tested for modelling the angular performance of PV modules with concentrators.

Contents

Nomenclature

Abbreviations and definitions

Symbol	Explanation	Unit
A	Area (of surface i, $_a$=aperture, $_c$=collector, $_r$=absorber)	m²
A_i	Anisotropy index	–
B_0	Analysis factor defined as (1/cos(Θ) - 1)	–
b_0	Incidence angle modifier coefficient ($_L$ in longitudinal and $_T$ in transverse plane)	–
C	Concentration ratio	–
c	Speed of light (= $3.0 \cdot 10^8$ m/s)	m/s
c_p	Specific heat of the fluid	J/kg,K
D	Correction factor for extrapolation of η_{0b}	–
d	Thickness of material	m
E_B	Radiation emitted by a blackbody (λ: wavelength distribution)	W/m²
E_{50}	Estimated yearly energy output (valid for T_{op} = 50°C)	kWh/m²,yr
$E_{July,yr}$	Collector energy production during July or year	kWh/m²
F	Fin efficiency factor	–
F'	Collector efficiency factor	–
$F(\Theta)$	Acceptance function for a concentrator	–
$F_T(\Theta_T)$	Total dependence function in T-direction	–
$F'U_{w/sky}$	Wind speed or Sky temperature dependence of heat loss coefficient	Ws/m³,K W/m²,K
F_{12}	View factor between surfaces 1 and 2	–
$F_{glas}(\Theta)$	Incidence angle dependence due to the cover	–
$f_{T,L}(\Theta)$	Function for modelling the incidence angle dependence in the T- or L-direction	–
G_{sc}	Solar constant (=1 367 W/m²)	

$g_{TL}(\Theta_T)$, $G_{refl}(\Theta_T)$, $R_T(\Theta_T)$	Incidence angle dependence due to reflector	–
h	Heat transfer coefficient (for convection ($_{conv}$) or radiation ($_{rad}$) between plate ($_p$), cover ($_c$), and ambient ($_a$). $_w$=h for wind convection.)	W/m²,K
H_{coll}	Insolation onto the collector plane	kWh/m²
H_{eff}	Effective solar height	°
I	Radiation ($_{tot}$=total, $_b$=beam, $_d$=diffuse; $_t$=on tilted surface, $_n$=normal direction, $_{\lambda i}$=incident, monochromatic, $_{bi}$=beam in incidence angle interval i. $_{T,L}$=projected in the transverse or longitudinal plane and $_{//}$=parallel to the glazing.) i, r = incident and reflected	W/m²
$\mathbf{I}$	Beam radiation vector	
I_B	Blackbody intensity	W/m²,°
I_{SC}	Short-circuit current (from module in *conc*entrator or from *plan*ar module)	A
K	Extinction coefficient	m^{-1}
$K_{\tau\alpha}$	Incidence angle modifier for beam ($_b$) $(1-b_0(1/\cos(\Theta)-1))$ and diffuse ($_d$) radiation	–
$K_{\tau\alpha L,T}(\Theta)$	Incidence angle dependence in L- and T-direction	
$k = F'U$	Heat loss coefficient Temperature dependence is modelled as: $k = k_1 + k_2\Delta T$; $U = U_0 + U_1\Delta T$	W/m²,K
L	Thermal conductivity of material	W/m,K
$L_{July/yr}$	Heat load during July or year	kWh
l	Path length	m
$(mC)_e$	Effective collector thermal capacitance	J/m²,K
n	Average number of reflections	—
n	Day number	—
$\mathbf{n}$	Normal vector to collector surface	
n_i	Index of refraction (*sub*strate, *film*)	—
$P_{model/measure}$	Modelled and measured collector output	W/m²
p	Focal length of parabola	m
$\dot{Q}_u$ $\dot{q}_u$	Collector outputCollector output per collector area ($_m$=measured)	WW/m²
$\dot{Q}$	Heat transfer ($_l$=conduction, $_c$=convection, $_r$=radiation)	W

$\dot{q}_{loss,top}$	Heat losses from the top of the collector	W/m²
R	Solar reflectance ($_{hemi}$=hemispherical, $_{s}$=specular)	—
R	Electric resistance	W
R_b	Geometric factor	—
R_i	Heat transfer resistance	$(W/m^2,K)^{-1}$
R^2	Coefficient of determination	
r	Reflection of radiation	–
S	Absorbed solar radiation	W/m²
T	Temperature (of fluid at collector *in-* or *out*let, $_{amb}$=ambient air temp near the collector, $_{abs}$=absorber, $_{c}$=cover, $_{f}$=fluid, $_{p}$=plate, $_{w}$=wall)	°C or K
T_{op}	Operating temperature (= $(T_{in}+T_{out})/2$)	°C
ΔT	Temperature difference between collector and the surroundings ($T_{f,mean} - T_{amb}$)	°C
ΔT_{sky}	Temp difference ($T_{amb} - T_{sky}$)	°C
$\frac{dT_f}{d\tau}$	Mean time derivative for fluid temperature	K/s
U	Heat loss coefficient ($_{L}$=overall, $_{t}$=top, $_{b}$=bottom, $_{e}$=edge)	W/m²,K
U_P	Piping heat loss coefficient (per m² of collector)	W/m²,K
V	Voltage	V
$\dot{V}$	Fluid flow	m³/s
w	Wind speed near the collector	m/s
α	Solar absorptance (λ = monochromatic)	–
α_p	Profile angle	°
α_s	Solar altitude angle	°
β	Collector tilt	°
δ	Declination	°
ε	Thermal emittance (λ = monochromatic)	–
ε_i	Emittance of surface i ($_{c}$=cover, $_{p}$=plate)	–
ϕ	Latitude (north positive)	°
γ	Azimuth angle ($_{c}$=collector surface, $_{s}$=solar) (east negative)	°
η	Collector efficiency	–

η_0 = $F'(\tau\alpha)_e$	Optical (or "zero loss") efficiency for beam ($_b$), and diffuse ($_d$) radiation at normal incidence. (When calculated from measured output, η_0 is called "no-loss efficiency".)	–
λ	Wavelength	m
ν	Frequency	s^{-1}
Θ	Angle of incidence of beam radiation onto the collector plane (=angle between incident radiation and surface normal)	°
$\Theta_{T,L}$	Incidence angle for beam radiation projected in the Transverse or Longitudinal planes respectively	°
Θ_a	Acceptance half-angle	°
Θ_z	Solar zenith angle	°
$\Theta_{1,2}$	Angles of incidence $_{(1)}$ and refraction $_{(2)}$	°
ρ	Density of fluid (water/glycol)	kg/m^3
ρ	Reflectance ($_d$=for diffuse radiation, $_s$=specular, $_\lambda$=monochromatic $_g$=ground reflectance)	–
σ	Stefan-Boltzmann constant (5.6697×10^{-8} $W/m^2,K^4$)	
τ	Solar transmittance ($_\lambda$ = monochromatic)	–
τ_{CPC}	Transmittance of a CPC accounting for the influence of the reflectance of the concentrator.	–
τ_{IR}	IR-transparency	–
$(\tau\alpha)$	Transmittance-absorptance product ($_{av}$=average, $_n$=normal direction)	–
υ	Hour angle	°

AR = Antireflection
CIGS = Copper indium gallium diselenide
CPC = Compound Parabolic Concentrator.
EPS = Expanded PolyStyrene
FP = Flat-plate collector
IR = Infra red
MaReCo = Maximum Reflector Collector
MLR = Multiple Linear Regression
PV = Photovoltaic
RD&D = Research, Development and Demonstration
SF = Solar Fraction (= collector output/heat load)

Further explanations

Air Mass (m) is the ratio of the mass of atmosphere through which beam radiation passes to the mass it would pass if the sun were at zenith (m = 1/ cos(Θ_z) for Θ_z < 70°).

Irradiance (G) [W/m²] is the rate at which radiant energy is incident on a surface per unit area of surface.

Irradiation [J/m²] is the incident energy per unit area on a surface, found by integration of irradiance over a specified time (usually hour, I, or day, H). (The term insolation is specifically used for solar energy irradiation.)

Beam (or direct) radiation is the solar radiation received from the sun without having been scattered by the atmosphere.

Diffuse radiation is the solar radiation received from the sun after its direction has been changed by scattering by the atmosphere.

Total solar radiation is the sum of beam and diffuse radiation on a surface. (The total radiation on a horizontal surface is often referred to as global radiation.)

Emissive power [W/m²] is the rate at which radiant energy leaves a surface per unit area, by emission only.

Solar time is the time based on the apparent angular motion of the sun across the sky, with solar noon the time the sun crosses the meridian of the observer. (= standard time + 4(Lst – Lloc) + E, where E is the equation of time and Lst is the standard meridian for the local time zone (=-15° for Sweden).

Transverse plane (“T-plane”) is the plane perpendicular to collector.
Longitudinal plane (“L-plane”) is the plane parallel to collector axis.
S, E, W, N = South, East, West, North

Acknowledgements

This work is part of a large Swedish RD&D[1]-programme concerning solar heating (Helgesson et al, 2000b and 2004, and Larsson, 2003). The aim of the programme is to improve the output/cost relation for solar collectors and thereby make the use of solar energy more competitive. The programme is mainly financed by the Swedish Energy Agency (Energimyndigheten) and different energy utilities. The presented work has been made at Vattenfall Utveckling AB in Älvkarleby with some collaboration with Uppsala University and Lund Institute of Technology.

I would like to thank everybody who has helped me and been involved in my work. This includes a large number of persons who have helped me in different ways. First of all, I would like to mention my supervisor prof. Björn Karlsson, who has also been my largest "solar energy guru" during the work. Thanks for helping me with this work Björn! Special thanks are also given to Lennart Spante (for being a supportive boss), Peter Krohn (who has helped me with measurement techniques and computer problems), Bengt Perers (for introducing me to the world of solar energy theory), and Susanne Eriksson (for many laughters). Also a number of other colleagues – not mentioned here – have been of great help. Furthermore I wish to thank all my co-authors (without them, my work would only have been "half"), teachers and friends during different (solar) energy courses, and all those persons helping me "in the last minute" with this work. Finally, I wish to give a big hug to my parents (for always being there and supporting me).

1. Research, Development and Demonstration.

1 Introduction

The energy from the sun can be used for both heating purposes (of water and buildings) and for electricity generation. In order to utilize the heat, thermal solar collectors are used, and in order to generate electricity, solar cells (or PV-modules) are used. In this work, the focus has been on solar collectors. Some of the results and described reflector arrangements can, however, also be used for solar electricity applications.

Solar energy is an environmentally friendly energy source that does not cause unwanted emissions of CO_2, other pollution or noise disturbance. The fuel, i.e. the sun's rays, is also abundant and free of charge. The contribution from solar energy to the total energy mix is nevertheless very small. In Sweden about 220 000 m² of solar collectors have been installed (2001) (Larsson, 2003). Assuming each solar collector gives a yearly output of 400 kWh/m² (an optimistic figure), the Swedish collectors produce about 85 GWh per year. This is only a very small part of the approximate[2] 90 TWh required for heating water and buildings in Sweden during a year. The total installation in the EU amounts (2002)[3] to almost 11 million m², with a target of 100 million m² in year 2010[4]. One difference between Swedish and European systems is that combisystems (for both space heating and warm water preparation) dominate (approx 90%) in Sweden, whereas hot water systems dominate in the rest of Europe.

Why is the energy from the sun not utilized to a greater extent? One of the major reasons is the high cost associated with the solar energy technology. The problem here is that the production volume of solar collectors is not large enough to motivate investments in automatic manufacturing techniques. This results in expensive collectors, few customers and a continued low production. Another reason, maybe the most obvi-

2. Statistics from the Swedish Energy Agency (www.stem.se).

3. European Solar Thermal Industry Federation: *Sun in Action II – A solar thermal strategy for Europe*, Vol 1, Market overview, perspectives and strategy for growth, 2003.

4. Communication from the European Commission: *Energy for the future: Renewable sources of energy*, White paper for a community strategy and action plan, COM(97)599 final, 1997.

ous, is that the sun does not always shine when heat is needed. This is illustrated in figure 1.1, showing a "normal case" for Swedish conditions. The hot water load is almost constant during the year, whereas the need for space heating is larger during the winter than during the summer. The low availability of solar energy during the winter season necessitates the use of some other energy source during that period, and this will affect the total cost of the energy system. Some of the solar energy can be stored (e.g. in a water tank) from sunny days to times when the heat is needed. Usually, the storage is designed for a couple of days. A seasonal storage needs to be very large and is not of any interest for most applications. The storage makes the system both more complex and more expensive. Also non-technical and non-economic reasons may influence the use of solar energy. Examples of this are aesthetics (ugly collectors?!), and architecture (difficulties to implement collectors in the existing building stock, and architects are not aware of the possibilities of using solar energy).

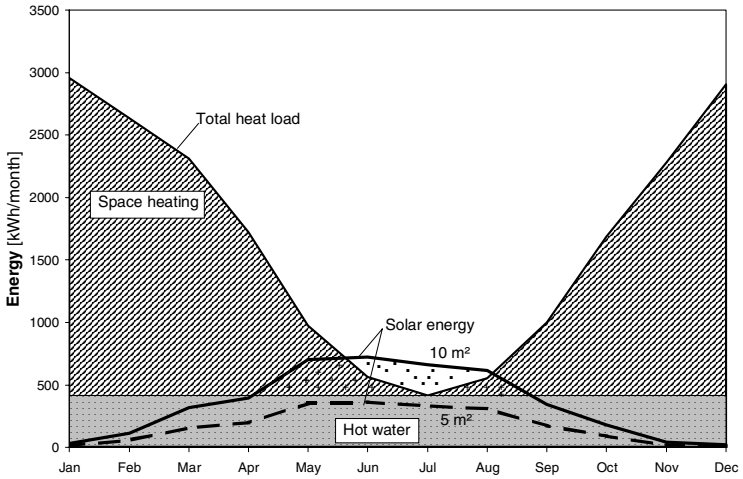

Figure 1.1 *Approximate annual heating demand for hot water (5 000 kWh) and space heating (15 000 kWh) for a single family house in Sweden, and output from two solar collector systems with different collector areas (5 and 10 m² respectively). The crossed area is the extra solar energy contribution from the larger system that can be used for space heating, and the dotted area is the unusable overproduction during the summer.*

One of the major obstacles to the utilization of solar energy for heating purposes is the high cost/output ratio. This ratio can be decreased by either reducing the costs of the solar collector or increasing the energy performance. The costs can be reduced e.g. by using:

- cheap (standard) materials
- rational manufacturing methods
- reflectors that replaces more expensive absorbers.

The collector energy output depends on the incident solar radiation and on the collector properties (optical and thermal). The optical properties (absorptance, transmittance, and reflectance) depend on the choice of material and on the incidence angle of the radiation onto the collector. Since the sun "moves" across the sky during the day, the incidence angle varies and the optical properties of the collector therefore change during the day. This makes theoretical evaluation of the energy output from a solar collector a difficult task. The performance evaluation will be even more complex if the collector has an asymmetric geometry. In that case, the performance also depends on the direction of the collector.

The output from a collector can be increased in a number of ways, e.g. by using:

- a selective absorber coating
- antireflection treated cover glass
- a well insulated collector box
- transparent insulation between absorber and collector glazing
- reflectors.

Some of these methods are studied in e.g. (Hellström, et al, 2000). An increase in solar absorptance (α)[5] from 0.95 to 0.97 combined with a decrease in thermal emittance (ε) from 0.10 to 0.05 increases the energy output by about 7%, at an operating temperature (T_{op}) of 50°C. The use of a Teflon film between absorber and glazing can increase the energy output by 6% (at T_{op} = 50°C). Commercially available antireflection (AR) treatment increases the normal solar transmittance (τ) of the glass by 4%, increasing the annual energy output by 6.5% at 50°C. By using an external booster reflector of anodized aluminum, the annual output can be increased by 26% at 50°C.

5. The symbols used in the text are collected and explained in the nomenclature list.

In order to evaluate the performance of a collector, measurements are needed. These measurements should be performed in a standardized way in order to facilitate comparisons of the results from different evaluations. For the evaluations in this work, a dynamic test method (Perers, 1995) has been used (chapter 5 and 6).

During the period 1996 - 2003, there were two large Swedish national Research, Development, and Demonstration programmes (RD&D programmes) concerning solar heating (Helgesson et al, 2000b and 2004). These programmes were mainly financed by STEM[6] and different Swedish energy companies. The aim of the RD&D work was to reduce the cost of solar energy and thereby make the technology more competitive in the energy market. A lot of different subprojects have been carried out in a collaboration between researchers, scientists and the manufacturing industry. Examples of project areas are development of antireflection treatment of glass, improvement of the selective surface of absorbers, and design of different reflector collectors. Also manufacturing methods and system design have been studied within the RD&D programme.

At Vattenfall Utveckling AB (VUAB), work has been performed regarding cost reductions and output improvements. One result from this work is a specially designed reflector collector called MaReCo (Maximum Reflector Collector). The name indicates the purpose of the design, to reduce the collector costs by replacing some of the expensive absorbers with cheaper reflector material. The MaReCo has a reflector geometry that is specially adapted for the insolation conditions in Sweden. The collector principally consists of a reflector trough with a single absorber fin running along the trough. Due to the asymmetric yearly distribution of the solar radiation in Sweden, the reflector trough should be asymmetric. This influences the optical properties of the collector. In order to include this effect in the collector evaluation method, the incidence angle dependence of asymmetric reflector collectors has been studied in different projects (Papers VII - IX).

In my work, I have studied a number of solar collectors and collector components. The focus has been on the energy output from different kinds of collectors, specially the asymmetric MaReCo. The different collectors were evaluated by performing outdoor measurements, followed by simulation of the yearly energy output, on some collector prototypes

6. The Swedish Energy Agency.

placed at VUAB's laboratory in Älvkarleby (Sweden). In my work, I have also studied the incidence angle dependence of the optical efficiency. A new biaxial expression for modelling the incidence angle dependence has been suggested and tested on some different collectors. In the following text, the MaReCo is described, the asymmetric insolation in Sweden is discussed, and some equations for modelling the collector performance are given. Furthermore, the results from the collector evaluations are presented together with a description of the new suggested method for characterising the incidence angle dependence of an asymmetric collector. The results from my work are also reported in the papers listed in appendix D.

2 Insolation

The solar energy irradiation, i.e. insolation, on a surface varies both over the day and during the year, and is also different for different locations depending on latitude and local climate. The total yearly insolation on a horizontal surface located in Sweden is in the range of 800 kWh/m² (northern part of Sweden) to 1 000 kWh/m² (southern part). For a horizontal surface, more insolation is available during the summer than during the winter. If the surface is tilted, the available insolation can be increased. Tilting the surface also affects the distribution of the seasonal output (figure 2.1a). Figure 2.1b shows that there is an optimum tilt which maximizes the available radiation onto a collector.

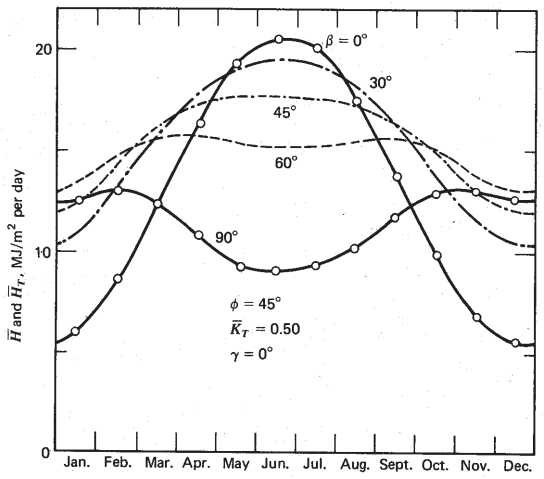

a)

b)

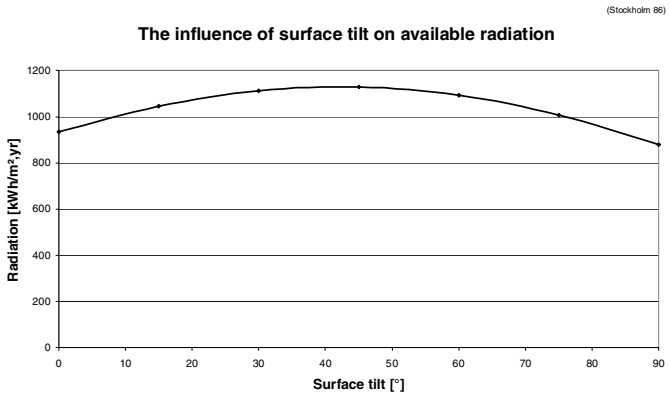

Figure 2.1 *a) The influence of surface tilt on the estimated average daily radiation on a south-facing surface over the year for a latitude of 45° (Duffie and Beckman, 1991).*
b) The influence of surface tilt on the available irradiation in Stockholm (ϕ H" 60°N). An optimum can be found at a tilt of approximately 45°.

In order to maximize the incident radiation, the collector should face the equator (i.e. south in the northern hemisphere). If the surface is turned away from south, the amount of available insolation will be reduced. According to figure 2.2 a deviation of ± 15° is, however, not critical. A shift in azimuth angle of 15° shifts the daily maximum of available energy by about one hour. This can be used to affect the performance of a system with regular diurnal variations in the energy demand. Figure 3.14 (in chapter 3) illustrates the output from a tested special collector when facing either east (-90°) or west (+90°).

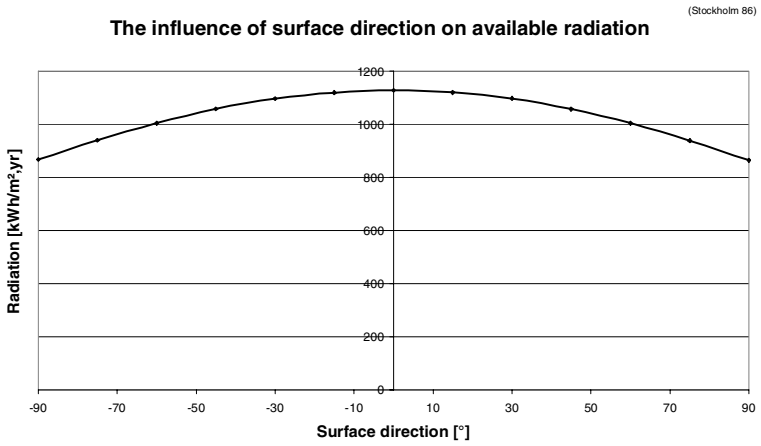

Figure 2.2 *The influence of surface direction on the available irradiation. The surface has a tilt of 45°.*

Figure 2.3 shows the yearly distribution of the beam radiation (projected in a vertical north-south plane) onto a collector surface as a function of the effective solar height (H_{eff}). The effective solar height is the angle between the south horizontal axis and the projection of the solar vector on the plane drawn by the south and the vertical axes. The diagram shows a peak of irradiation for effective solar heights between 50° and 55°. This peak corresponds mainly to summer radiation around noon. The tail at higher angles comes from mornings and evenings during the summer, and the radiation at low angles mainly corresponds to the winter period (compare with figure 6.5) (Karlsson and Wilson, 2000a). At lower latitudes, two peaks are found; one around the summer solstice and one around the winter solstice (figure 2.4). The loss of the winter peak at high latitudes is due to the low solar altitude during the winter months, causing high absorption of the direct radiation in the atmosphere (Rönnelid and Karlsson, 1997a).

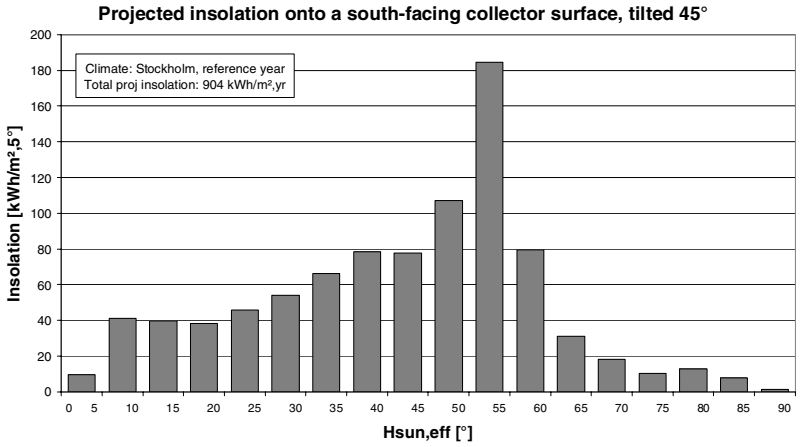

Figure 2.3 *Annual distribution of beam irradiation projected on a vertical north-south plane as a function of the effective solar height.*

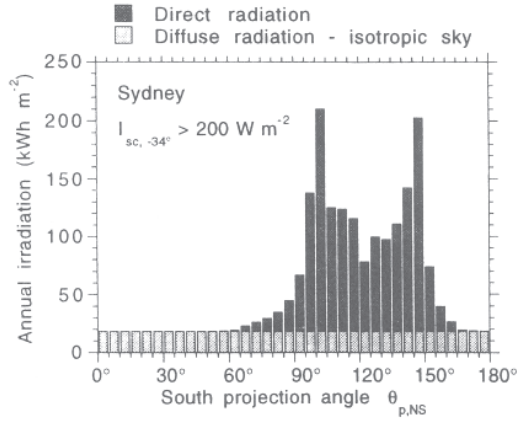

Figure 2.4 *Annual distribution of direct and diffuse irradiation in a north-south vertical plane for Sydney (ϕ = 33.9°S).* ***(Rönnelid and Karlsson, 1997a)***

Figure 2.3 is a good illustration of why a solar collector in Sweden should be designed so that it can utilize all radiation up to an effective solar height of about 65°. The asymmetric irradiation distribution in Sweden, with low direct radiation during the winter, is very suitable for the utilization of east-west oriented concentrators with little (or no) sun tracking

(Helgesson et al, 2004, and Rönnelid et al, 1996b). When designing a CPC collector for northern latitudes, advantage can be taken of the fact that a large part of the energy is concentrated to a narrow angle interval (50 - 55°). The collector can then be designed with a narrow acceptance half-angle (Θ_a) covering the summer solstice peak, leading to a high concentration ratio (C). For lower latitudes, where two irradiation peaks occur, a larger acceptance angle is required if both peaks are to be accepted by an east/west concentrator without having to retilt the construction during the year. The extremely asymmetric annual irradiation for a northern latitude implies that a concentrator optimized for this location should have an asymmetric geometry. A collector designed for Stockholm should have an acceptance angle interval of 20 - 65° in order to maximize the collector output.

According to a rough rule of thumb, the surface tilt (β) should equal the latitude (ϕ) for maximum annual energy availability (Duffie and Beckman, 1991). During the winter (summer), when the solar altitude is low (high), a larger (smaller) collector tilt is advantageous. In order to maximize the winter (summer) availability the collector should therefore be tilted 10 - 15° more (less) than the latitude. Since the irradiation distribution is highly asymmetric at high latitudes, this "rule of polar mount" is not valid. The optimum tilt is instead primarily determined by the position of the summer peak, and is for mid-Sweden ($\phi \approx 60°$) about 45° (figure 2.1) (Rönnelid et al, 1996b).

The annual heat output from a conventional flat-plate collector is about 350 - 400 kWh/m² (at T_{op}, = 50°C) [7]. If the collector is directed away from south or given a tilt that is not optimal, the output will be reduced. Figure 2.5 shows how the relative output from a flat-plate collector depends on tilt and direction. The relative output is the output at a certain condition compared with the output from a south-facing reference collector with a tilt of 45° ("optimum"). The figure indicates that it is better to have a lower than a higher tilt and that a deviation from south of approximately 25° is acceptable for a collector with a tilt of 45°. The influence on the output of tilt and direction is also discussed in (Adsten and Perers, 1999). One conclusion in that reference is that different collectors have different dependence on tilt and azimuth angle. In general, a more advanced solar collector (with lower heat losses) has a weaker dependence. The dependence on tilt and azimuth angle means that it is

7. Energies will be stated at an operating temperature of 50°C throughout the text, unless otherwise noted.

important to distinguish between the output provided by the manufacturer (valid for a certain, optimal, tilt and azimuth angle) and the output for the actual case.

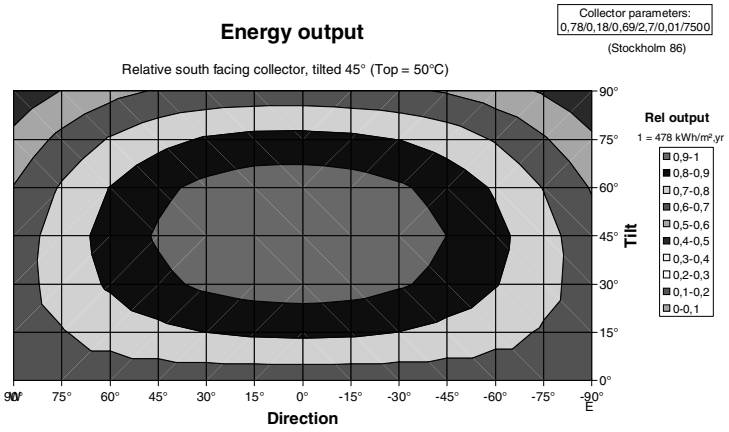

Figure 2.5 *Illustration of how the energy output from a flat-plate collector, with a selective absorber and a Teflon film between absorber and glass, is affected if the collector is faced away from south or given another tilt than 45°. The collector is placed in Stockholm (N 59.3°, E 18.1°) and has an operating temperature of 50°C. The simulations were made with the program MINSUN, using climatic data for Stockholm 1986. The cerise (i.e. the middle) area corresponds to an output of at least 90% of the output in the optimum case.*

Also variations in climate for different years and different locations influence the actual output from a system. Some examples of this can be seen in figures 2.6, 2.7 and 2.8. This means that standardized climatic data should be used when performing simulations of the energy output in order to compare different collectors tested in different years in different parts of the country. This is also mentioned in (Adsten et al, 2002a). In this work, hourly average climatic data for Stockholm 1986 has been used for most of the energy simulations. The "Stockholm reference" year is compiled from SMHI[8] measurements during the period 1984 – 1992.

8. Swedish Meteorological and Hydrological Institute.

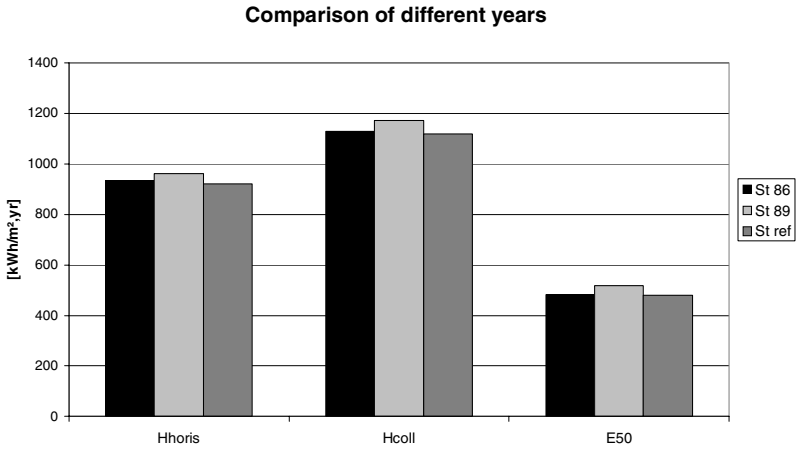

Figure 2.6 *Illustration of how the irradiation (horizontal and on collector plane tilted 45°), and the estimated collector output (E50) depend on variations in the climate during different years.*

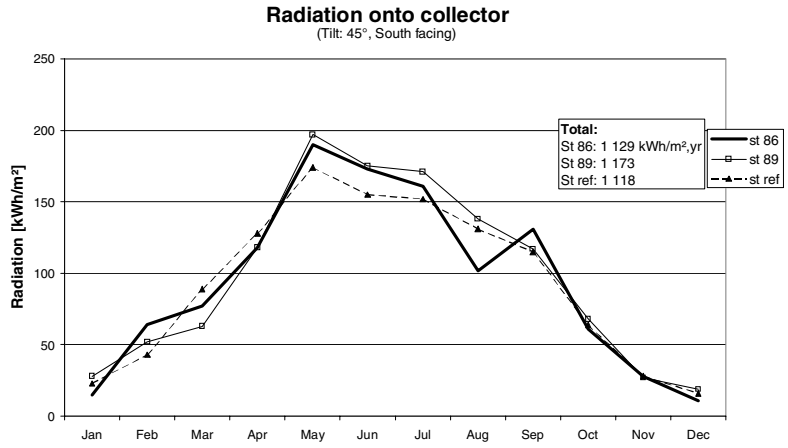

Figure 2.7 *Comparison of monthly total radiation onto a collector surface (tilted 45°) during different years.*

Figure 2.8 shows the variation between different years of the monthly total radiation onto a surface tilted 45° placed in Älvkarleby, where the evaluations in this work have been made. Figure 2.9 shows a comparison between the climate (total insolation onto a horizontal surface, and tem-

perature) in Stockholm (a "normal year" during the period 1961 – 1990)[9] and the climate in Älvkarleby (an average year during the period 1997 – 03). As can be seen from this diagram, there is no major difference in insolation and temperature for these two locations (Stockholm: N 59.3°, E 18.1°; Älvkarleby: N 60.6°, E 17.4°).

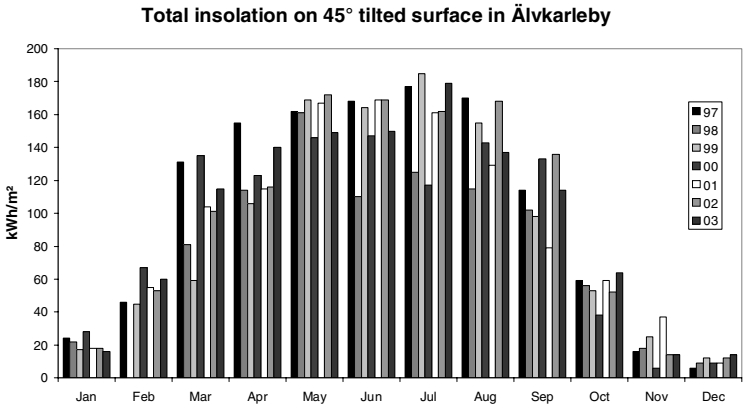

Figure 2.8 *Total measured insolation onto a surface tilted 45° placed in Älvkarleby during different years.*

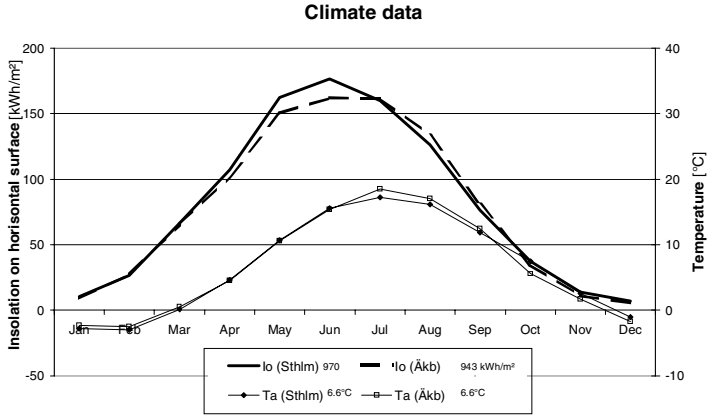

Figure 2.9 *Comparison of insolation and temperature in Stockholm and Älvkarleby. Data compiled from several years of measurements.*

9. Data from SMHI.

3 The Maximum Reflector Collector (MaReCo)

3.1 The use of booster reflectors

In large collector fields, e.g. for district heating purposes, the collectors are placed in rows behind each other. At high latitudes, the distance between adjacent collector rows must be large (usually about 2 - 2.5 times the collector height) in order to minimize shading effects. This means that a large part of the incident solar radiation falls on the ground between the collectors. One way to improve the energy output from a collector field is therefore to use booster reflectors placed between the collector rows (figure 3.1). In this way, the solar radiation that would otherwise be lost to the ground is redirected onto the collector. The use of external flat booster reflectors can increase the annual performance by 30% (100 – 120 kWh/m²) (Perers and Karlsson, 1993b). A parabolic shaped reflector can increase the energy output even more than a flat reflector with the same reflector width/collector height ratio. The increased annual performance can be used either to increase the yield from a given ground area or to reduce the system area for a given load. For Swedish conditions, it is usually cost effective to install external reflectors (Nostell et al, 1997).

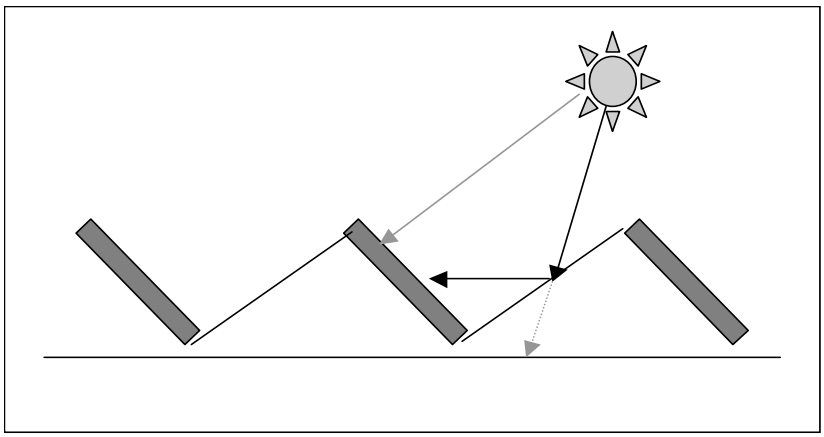

Figure 3.1 *Illustration of the use of external reflectors to redirect the solar radiation and thereby increase the energy output from a collector field.*

For Swedish latitudes, the collector should be tilted 45° and the reflector approximately 25° for optimal performance. A large amount of solar radiation then falls onto the reflector at an angle of approximately 60°, and optical characterisation should therefore be made at this angle (Nostell et al, 1997). Both beam and diffuse reflected radiation contribute to the incident radiation onto the collector. The amount of direct radiation during the collector operation is approximately 75% of the total irradiation onto the collector (Rönnelid and Karlsson, 1999). The diffuse radiation is often assumed to be isotropic (i.e. independent of angle). If the collector and the reflector are assumed to be infinitely long (collector length at least approximately 10 times the collector width), end effects can usually be neglected.

3.2 Parabolic reflectors

In order to achieve temperatures in excess of approximately 80°C from a solar collector, the solar radiation has to be concentrated. By using internal reflectors, the hot absorber area can be reduced and this reduces the heat losses. CPCs (Compound Parabolic Concentrators) are here the optimal choice, since they approach the thermodynamic limit of concentration (C). For two dimensions, the concentration factor is given by (Rabl, 1976):

$$C = C_{\max} = \frac{1}{\sin(\Theta_a)} \tag{3.1}$$

where C is defined as the ratio of the aperture area and the total[10] absorber surface area ($C = A_d/A_r$), and Θ_a is the "acceptance half-angle" formed by the axis of the right or left parabola and the collector mid-plane (figure 3.2). All rays incident on the aperture within the acceptance angle, and none of the rays outside, pass to the absorber. The parabola is described by the equation:

$$y = \frac{x^2}{4p} \tag{3.2}$$

where p is the focal length of the parabola.

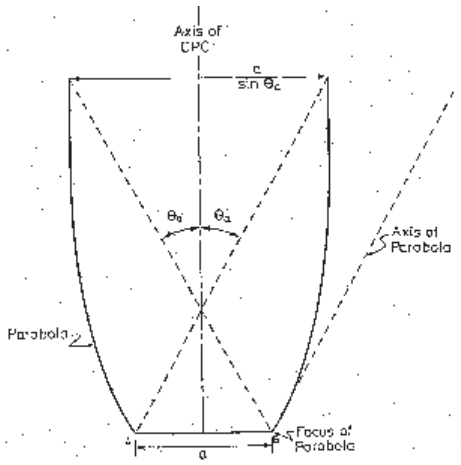

Figure 3.2 *A compound parabolic concentrator. a is the absorber width and Θ_a is the acceptance half-angle. (Norton et al, 1991)*

The design and performance of different CPC configurations are described in numerous references (e.g. Norton et al, 1991, Rabl et al, 1980, Rabl et al, 1979, and Tripanagnostopoulos et al, 2000). Different kinds of concentrators are also discussed in (Nostell et al, 1998b, and Mills and Giutronich, 1978). The basic design of a two-dimensional CPC arose almost at the same time in three different countries. Since the CPC requires a smaller amount of (expensive) absorbing material, it can be a

10. For a bifacial absorber both sides of the absorber should be counted.

cost effective alternative compared with a flat-plate collector. It does, however, require a durable reflecting material with acceptable reflectance. Due to reflections in the reflector, a CPC usually has a lower optical efficiency than a flat-plate collector. Thanks to the relatively small (warm) absorber area, a CPC can achieve a good performance at high operating temperatures. Combining a CPC reflector with an evacuated receiver tube, a very good high temperature performance can be gained.

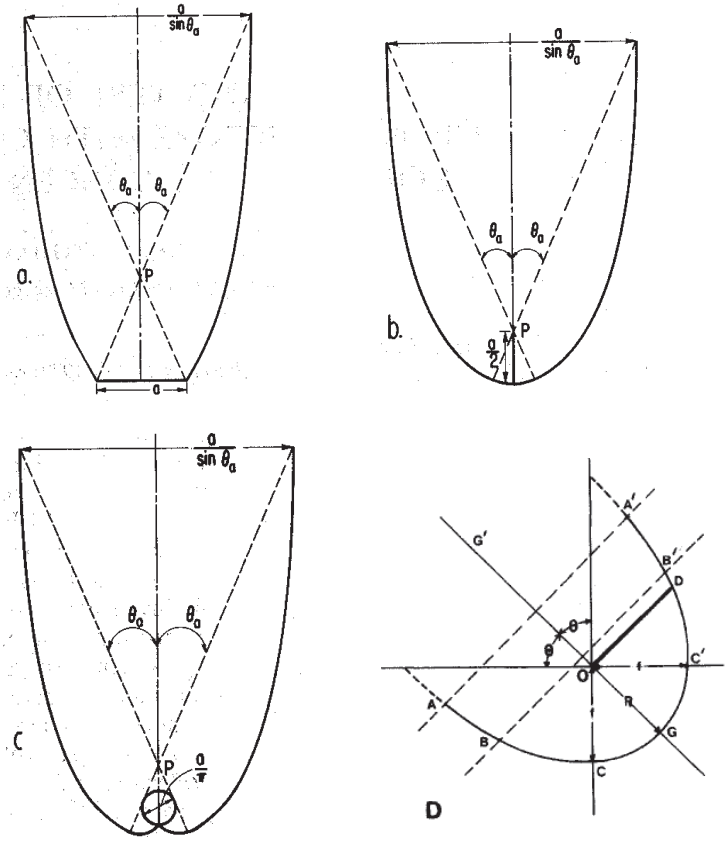

Figure 3.3 *Different configurations of CPC collectors: a) flat one-sided receiver, b) fin receiver, c) tubular receiver. (Rabl, 1980) d) An alternative position of the absorber in order to form a hot air space trap (Tripanagnostopoulos, 2000).*

CPC reflectors can be designed for different absorber shapes, and some examples are given in figure 3.3. These different configurations have slightly different properties. Configuration a has higher conduction losses through the back side than the ”backless” configurations b or c. Further-

more, configuration b only requires half as much of the relatively expensive absorber material than configuration a, and configuration b is also less deep. The receiver in a CPC collector absorbs radiation both directly from the sun and after reflections in the reflector. This means that the reflectance of the mirror is important for the collector performance. The surface does not need to be perfectly specular, but the total reflectance should be as high as possible. The flat absorber can be placed with different tilts, and if it is placed parallel to the cover (config d), a hot air trap space will form between the absorber and the reflector, reducing the convection thermal heat losses. A parallel placing to the cover tilt also increases the optical efficiency of the front side, since the fraction of directly absorbed light then increases.

The absorption of solar radiation increases the temperature of the absorber surface, resulting in increased heat losses. In order to reduce the thermal losses by convection and radiation from the front absorber surface to the cover, a selective coating (with low emittance compared with a black surface) is recommended. The heat losses can also be reduced by introducing a transparent material between the absorber and the cover. Heat losses also occur by conduction through the reflector and the thermal insulating material. In order to avoid thermal losses from the absorber to the mirror, there should be an air gap between those two. This gap, however, introduces optical losses since solar rays can then pass through it without being absorbed.

Also the reflector is heated by absorbed radiation, resulting in heat losses to the cover by convection and radiation. This effect also increases the average temperature of the absorber environment, reducing the heat losses from the absorber.

The optical performance of a concentrating collector depends on the optical properties of the cover, absorber and reflector, the fraction of the incoming solar radiation that is reflected, and the average number of multiple reflections (Tripanagnostopoulos, 2000). Also any gap between absorber and reflector, concentrator contour, errors in tracking, and displacement of the absorber from the focus affect the optical performance. At high temperatures, there is a risk that the absorber deforms and moves away from its design position. This means that some concentrated radiation will be missed. In order to minimize the optical losses and to reduce the sensitivity to misalignment and thermal deformation, it is recommended to oversize the absorbers (by about 20%) relative to the reflector profile (Rabl, 1980). (One drawback of this is that the concentration ratio is then reduced.)

The distribution of the image at the receiver depends on the incidence angle. For a CPC shaped reflector all specular radiation onto the reflector will hit the absorber as long as the incidence angle is within the ac-

ceptance angle interval of the collector. Beyond that, all specular radiation will be lost (Perers and Karlsson, 1993b). This can be expressed by the use of the acceptance function, $F(\Theta)$, defined as the fraction of the rays incident on the aperture at an angle Θ that reaches the absorber (Carvalho et al, 1985). The acceptance function is affected by the smoothness of the reflector surface (Rönnelid and Karlsson, 1998). Figure 3.4 gives an example of the acceptance function. For trough like concentrators, it is only the transversely projected incidence angle (Θ_T) that is of importance (chapter 6). The acceptance function for an ideal (untruncated) 2D concentrator can be expressed as:

$$\begin{cases} F(\Theta_T) = 1 & |\Theta_T| \le \Theta_a \\ F(\Theta_T) = 0 & |\Theta_T| > \Theta_a \end{cases} \tag{3.3}$$

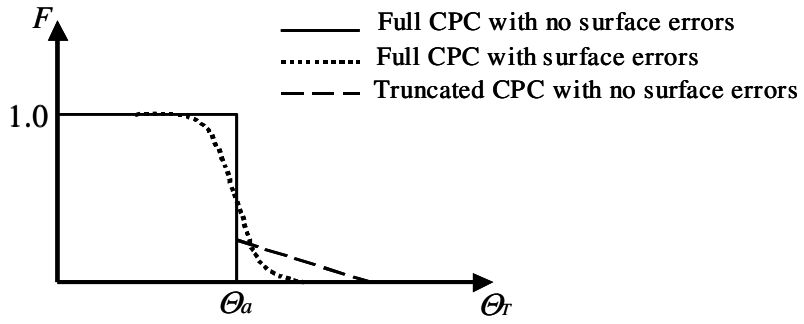

Figure 3.4 *Acceptance function F(Θ) of radiation incident on the absorber surface.*

Since the top part of a CPC reflector is nearly normal to the aperture, it only gives a minor contribution to the concentration. In order to save reflector material (reduce collector cost) and to reduce the collector depth, the CPC is usually truncated, i.e. cut off before it reaches it full length. The truncation affects the long-term collectible energy in different ways, and the trade-off between optical and thermal losses implies that there is an optimal degree of truncation (Carvalho et al, 1985):

⊕ The truncation allows some rays beyond the nominal acceptance half-angle to reach the absorber, increasing the acceptance of beam insolation. This can be seen in figure 3.4. The acceptance of isotropic diffuse insolation can be calculated as 1/C.

⊕ When the reflector is truncated, the average number of reflections is decreased, resulting in reduced optical losses.

⊖ The heat losses per aperture area increase with truncation.

3.3 Description of the MaReCo design

Since the absorber is one of the most expensive components of a collector, it is desirable to minimize the absorber area. By using internal reflectors, some of the expensive absorber material can be replaced by cheaper reflector material. In this way, the material cost can be reduced. The reduced warm absorber area also results in reduced heat losses. This increases the useful energy output from the collector and reduces the need of insulating material, further reducing the cost of the collector. This concept has been used in the so-called MaReCo (Maximum Reflector Collector). This is a truncated, stationary, asymmetric reflector collector specially designed for northern latitudes. The collector has been developed by Vattenfall Utveckling AB and Finsun Energy AB. The main purpose of the MaReCo is to maximize the annual performance for a given reflector area (Karlsson and Wilson, 2000a). The collector principally consists of an asymmetric reflector trough with a single absorber fin that runs along the trough (figure 3.5).

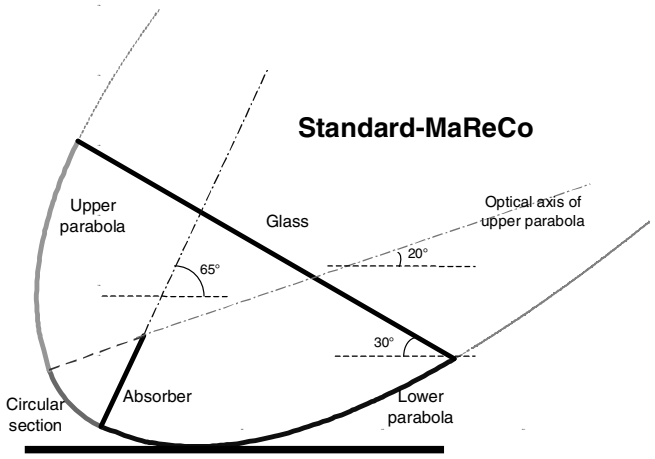

Figure 3.5 *Schematic sketch of a MaReCo consisting of a parabolic reflector trough and a double-sided selective absorber. The trough extends in the east-west direction and the collector does not have to be retilted during the year.*

In order to achieve a minimum absorber area, the reflector should be designed to reflect the solar radiation onto both sides of the absorber. This means that the absorber should have a selective coating on both the front and the rear sides, i.e. it should be bifacial.

The MaReCo is designed according to the principle of maximizing the annual irradiation per absorber area within a determined acceptance angle interval, with the restriction of a given reflector width (Karlsson and Wilson, 2000a). A rough estimation of the useful output from a CPC collector can be gained from irradiation distribution diagrams (Rönnelid and Karlsson, 1997a). Since the annual irradiation at northern latitudes is extremely asymmetric (figure 2.3), the reflector in an east-west extended collector should be asymmetric in order to maximize the yield. Considering the irradiation distribution and the profile of the load, the concentrator should operate between March 15 and October 15 (corresponding to effective solar heights in the interval 20 - 65°). The upper limit means that the collector does not operate in early mornings and late afternoons during the summer months. The collector is tilted in such a way that the profile angle of beam radiation will be within the acceptance angle interval of the collector during times when output is wanted (compare figure 6.5). A large part of the available solar radiation is then collected without the need for tracking, which otherwise would increase the investment and maintenance costs. The asymmetric geometry results in an uneven distribution of radiation onto the absorber. A large part of the radiation is found on the focal point (at the tip of the absorber). It is therefore important to use an absorber that has a high fin efficiency (F).

Figure 3.6 shows the profile of a MaReCo reflector. The reflector consists of three parts, two parabolas (A and C) and one semi-circular part (B). Parabola C is the front side (or “lower”) reflector part and it has an optical axis that is tilted 65° from the horizon, corresponding to the upper acceptance angle of the collector. Parabola A is the back side (or “upper”) reflector and it has an optical axis tilted 20°, corresponding to the lower acceptance angle. The focal point of the two parabolas coincides at point 5 in the figure (which is the top of the absorber that extends between points 1 and 5). The circular part B, with centre at point 5, transfers the light falling between point 2 and point 5 onto the back side of the absorber. In this way, the circular part replaces an absorber fin between points 5 and 2 with the back side of the double-sided selective absorber between points 5 and 1. The lower tip of the absorber can be placed anywhere between points 1 and 2. A MaReCo with this design will accept all radiation that has an effective solar height between 20° and 65°, i.e. all radiation within this angle interval will be reflected onto the absorber (figure 3.7). When the sun is outside the acceptance angle in-

terval, the reflector is no longer active and the absorber only works with beam radiation direct from the sun and with diffuse radiation from sky and reflector. This means that the optical efficiency is lower for effective solar heights outside the acceptance angle interval. The acceptance half-angle (Θ_a) of the construction is in this case 22.5°. According to equation 3.1 this corresponds to a maximum concentration factor (C) of 2.6 for the construction.

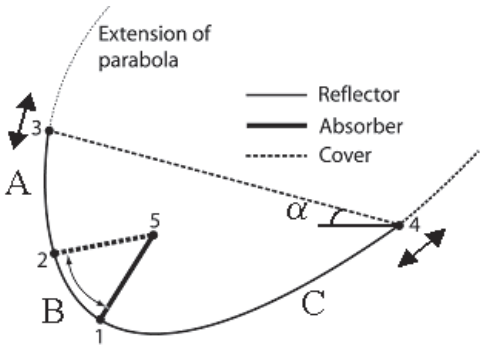

Figure 3.6 *Cross section of the reflector profile of a standard MaReCo optimized for location in Stockholm (Paper IV). Parts A and C are parabolas and part B is a circular sector. Point 5 is the focal point of the parabolas and the centre point of the circular part. The absorber extends between points 5 and 1 and the cover glass is placed between points 3 and 4. α is the tilt of the aperture.*

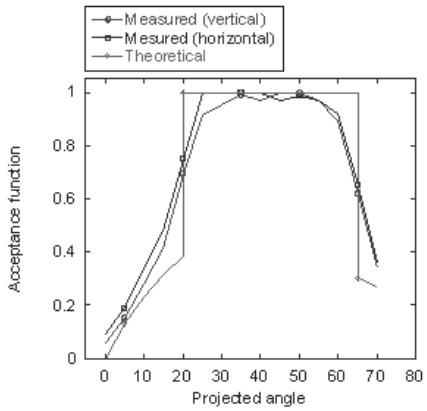

Figure 3.7 *Acceptance functions for a stand-alone MaReCo. The measured functions are calculated from solar simulator measurements with the absorber placed vertically and horizontally. (Paper V)*

In order to avoid too long reflectors, the reflector is truncated before it reaches its full length. The truncation of the reflector profile (using a certain width of the reflector material) is determined so that the annual irradiation onto the absorber is maximised (Rönnelid, 2003). For a MaReCo placed in Stockholm, the optimal glass tilt is around 30°.

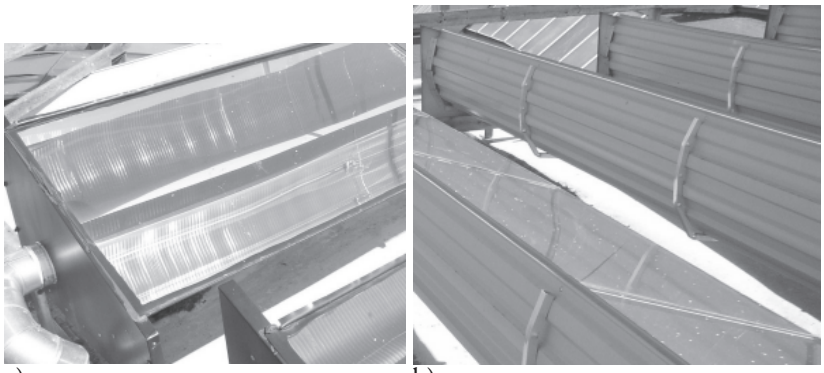

a) b)

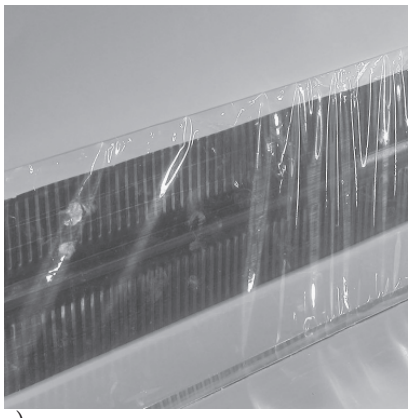

c)

Figure 3.8 *Photo of a stand-alone MaReCo. a) from the front side, b) from the back side, c) close-up of the "Teflon-tent" around the absorber.*

Figure 3.8 shows a "standard" stand-alone MaReCo. The reflector trough is constructed of a corrugated steel sheet. Square tubes are formed to a profile in order to give the reflector the desired shape (Karlsson et al, 2000b). The antireflection treated cover glass is attached to the trough by silicon and forms, together with the glass, a strong and rigid structure. The reflector is made of anodized aluminum and has a width of 1 m. The

double-sided selective absorber is fixed in a holder, which allows some movements. By using a "Teflon-tent" around the absorber the heat losses can be suppressed (the U-value can be reduced by approximately 1 unit). The Teflon film hangs over a spring that extends along the entire trough. The standard MaReCo has an absorber with a width of 143 mm and the glazing has a width of 620 mm. According to (Adsten et al, 2001), the absorber should be tilted 20° instead of 65° usually used in the MaReCo. The same reference also shows that the annually collected energy increases by 6 - 8% if the thickness of the absorber fin is increased from 0.5 mm to 1 mm. In (Adsten et al, 2002b), the influence of different designs on the heat losses from a MaReCo is described. This reference shows e.g. that the use of Teflon and horizontal mounting of the absorber can reduce the U-value significantly, and that the use of high emitting absorbers (black) results in high U-values. The methods of decreasing the convective heat losses by using a plastic film around the absorber or changing the position of the absorber to horizontal are also discussed in (Hollands et al, 1991). This reference also discusses the benefits to be obtained by increasing the reflectance of the reflector.

3.4 Different types of MaReCos

According to eq 3.1, a small acceptance angle interval will result in a large concentration factor. The design of a stationary concentrator collector is therefore a problem of optimization regarding concentration factor and the period when the reflector is active. It is therefore important to design the reflector according to the application and location of the collector. The MaReCo design concept is flexible and can be used for different conditions: stand-alone on the ground or flat roofs (figure 3.8 and 3.9) or integrated in walls or roofs with different tilts and directions (figures 3.10, 3.12, 3.13, and 3.15).

Several prototypes of MaReCos for stand-alone, roof, and wall installations have been built and tested at VUAB's laboratory. The evaluations were made in accordance with the dynamic testing method described in chapter 7. The results from some of these tests are described in Paper IV and briefly summarized in table 3.1 and the text below. The tested MaReCos have low U-values thanks to the small absorber area compared with the total glazed area. Also the effective thermal capacitance is low in most cases. This is partly explained by the low material content of the collectors, resulting in a low collector weight.

Table 3.1 Summary of some collector parameters for different evaluated MaReCo designs. E_{50} is the annually delivered energy output at T_{op} = 50°C (**Paper IV). (Data for the Spring/Fall-MaReCo is from Paper VI.) For the energy simulation, climatic data for Stockholm reference year (1983 – 92) was used, except for the Spring/Fall-MaReCo where data for Stockholm 1986 was used.**

Collector	η_{0b} [–]	b_0 [–]	η_{0d} [–]	k_1 [W/m²,K]	$(mC)_e$ [J/m²,K]	E_{50} [kWh/m²,yr]
Stand-alone MaReCo	0.59	0.37	0.37	2.4	2 980	253
Roof-MaReCo	0.69	0.29	0.56	2.4	1 950	336
Wall	0.61	0.22	0.27	2.0	1 130	142
East	0.58	0.13	0.25	2.0	6 250	135
West	0.60	0.16	0.35	2.0	4 890	174
Spring/Fall-MaReCo	table 3.2	0.26	0.44	*	2 701	222

*$k = 2.4 + 0.01\,\Delta T$

A ***stand-alone MaReCo*** (figure 3.9) with an aperture tilt of 30° was tested both with and without a Teflon film around the absorber. Due to lower heat losses, the MaReCo equipped with Teflon has a higher annual energy output (282 kWh/m² compared with 253 kWh/m²). At higher operating temperatures the improvement by using a Teflon film is even higher. It is, however, important that the Teflon does not touch the absorber surface.

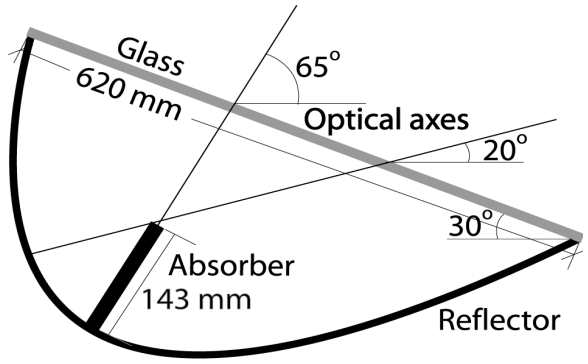

Figure 3.9 Schematic sketch of a standard MaReCo with an acceptance angle interval of 20 - 65° and an aperture tilt of 30°.

Also another stand-alone MaReCo version has been tested (Helgesson, 1999). This MaReCo is made of blocks of Expanded PolyStyrene (EPS), which constitutes both insulation and support for the reflector. The energy output, when laminated Al foil was used as reflector, was 288 kWh/m². One advantage of the EPS-MaReCo is that the collector is easy to handle, which reduces the installation costs. One disadvantage though is that the EPS material is sensitive to temperatures over 90°C, which is a temperature that can arise if stagnation occurs. In order to avoid these high temperatures, a MaReCo with ventilation channels in the EPS was designed. Temperature measurements and long-term stagnation on this collector showed that there seems to be no risk of overheating the EPS material.

Figures 3.10, 3.12, and 3.15 illustrate three different MaReCo geometries. Figure 3.10 shows a ***standard Roof-MaReCo*** designed for a south-facing roof with a tilt of 30°. In order to fit into the roof, the Roof-MaReCo has a smaller collector depth than the stand-alone version. The glass is placed between points 2 and 4 in figure 3.6, and the absorber is placed just below the cover glass. The optical axis is normal to the glass and all radiation from the horizon up to the glass normal is accepted by the reflector. Figure 3.11a shows the ideal acceptance function of the collector together with the annually projected radiation. This figure clearly shows that the reflector accepts most of the irradiation. Figure 3.11b shows the acceptance function together with the measured optical efficiency in the transverse plane. The Roof-MaReCo has a rather high optical efficiency for beam radiation (0.69) and a rather high annual energy output (336 kWh/m²). This is, however, somewhat lower than the output from a conventional flat-plate collector without Teflon (approx 370 kWh/m²). One advantage of the Roof-MaReCo is that it can be mounted on roofs with a tilt of 30° or lower. For Swedish conditions, the optimum tilt of a flat-plate collector is 45°, but most roofs have a lower tilt than that.

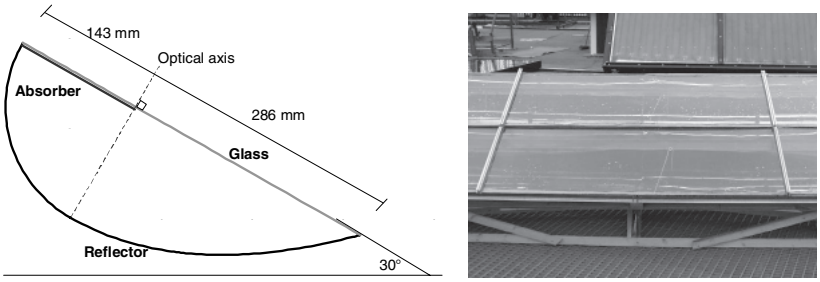

Figure 3.10 Schematic sketch and a photo of a Roof-MaReCo designed for a roof tilt of 30°.

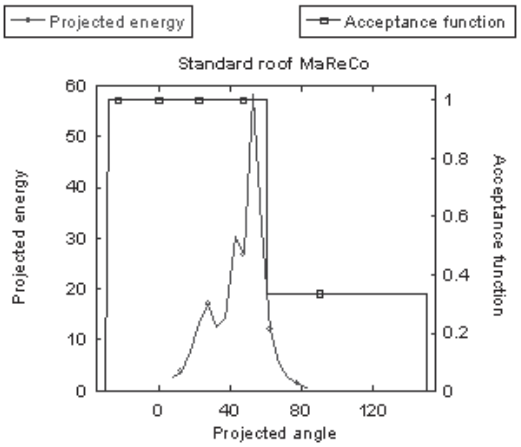

a)

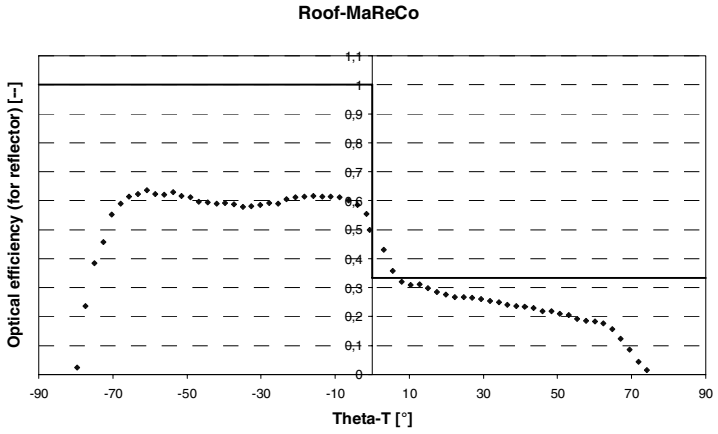

b)

Figure 3.11 *a) Projected energy incident on the aperture and theoretical acceptance function for the standard Roof-MaReCo. b) Ideal acceptance function and the optical efficiency for the reflector in the transverse direction (i.e. the $R_T(\Theta_T)$-function). Note that the two diagrams do not have the same angle on the x-axis.*

Figure 3.12 shows the geometry of a ***Wall-MaReCo***. Since this type of collector is integrated in the building construction, a minimum thickness is wanted. The annual energy output is rather low (142 kWh/m²), partly due to the unfavourable vertical alignment. A vertical flat-plate

collector has, for comparison, an output of about 190 kWh/m²,yr. An analysis shows that the optical axis should be lowered to around 10°. This will, however, reduce the concentration ratio.

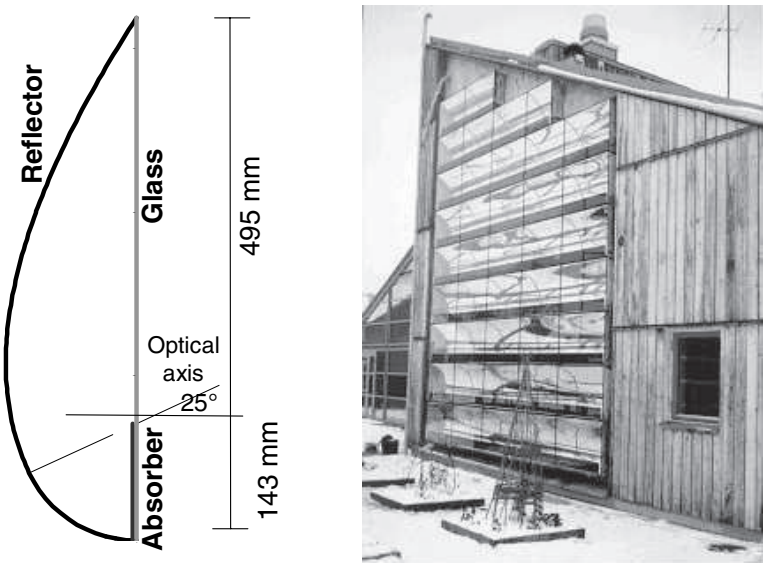

a) b)

Figure 3.12 *a) Schematic sketch of a Wall-MaReCo designed for a south-facing wall.*
b) A photo of a Wall-MaReCo installed in Aneby, Sweden.

Since all existing buildings do not have suitable roofs facing south, an alternative MaReCo has been designed to be used for "non-south installations". Figure 3.13 shows a photo of such an ***East/West-MaReCo***. The energy output from the East/West-MaReCo is lower than from the standard south-facing construction. This means that it is important that the East/West-MaReCo is very cheap. Although the solar radiation is symmetric around noon, the west facing part gives a higher output than the east facing part (W: 174 kWh/m²,yr and E: 135 kWh/m²,yr respectively). One reason for this is that the ambient temperature is often higher in the afternoon, resulting in lower heat losses. Figure 3.14 shows a daily diagram of the output from the tested East/West-MaReCo. Here it is seen that the east part of the collector starts to operate earlier during the day than the west part.

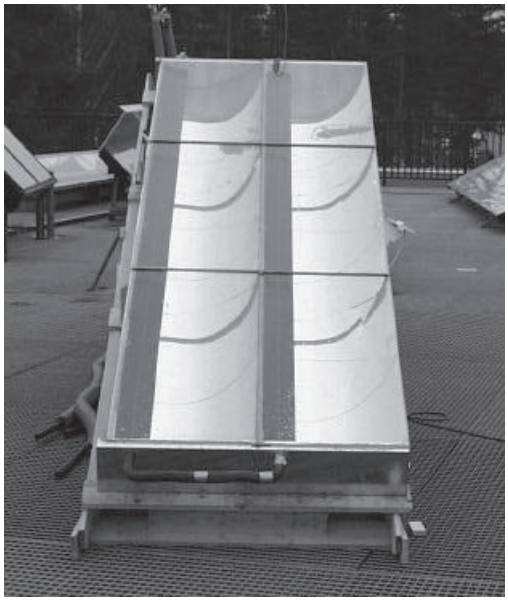

Figure 3.13 *A photo of the west side of an East/West-MaReCo with a collector tilt of 25°. (North is to the left in the figure.)*

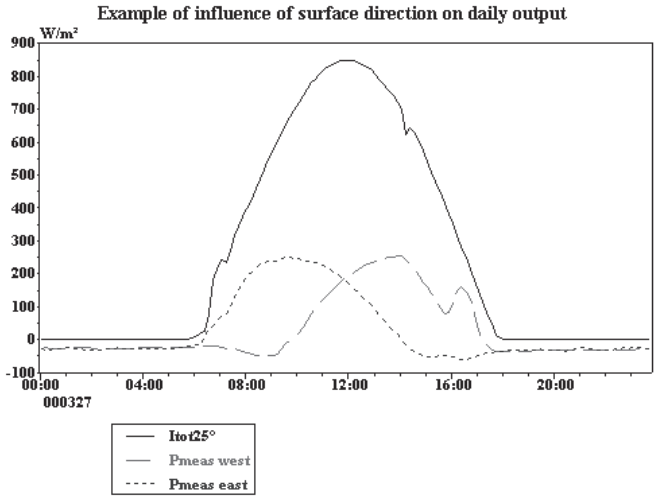

Figure 3.14 *A daily diagram showing the output from the east and the west parts of the tested East/West-MaReCo. The total insolation on a south-facing plane (tilted 25°) is also shown. The west collector is shaded around 16:00.*

The MaReCo can also be designed in order to achieve a high annual solar fraction of the system. According to figure 1.1, a larger collector area is needed to cover more of the heat demand during spring and fall. A larger area may, however, cause overheating problems during the summer. The ***Spring/Fall-MaReCo*** is specially designed to adapt the collector output to the load, i.e. with a lower efficiency during the summer. In this way, a larger collector area can be installed in order to utilize more solar energy during the heating season (spring and fall), without increasing the risk of overheating during the summer (Paper V & VI). (The concept of using asymmetric collectors for seasonal load adaptation is also discussed in (Mills et al, 1994, and Kerskes et al, 2003).) Figure 3.15a shows a schematic sketch of the Spring/Fall-MaReCo. This MaReCo is very similar to the Roof-MaReCo, but it has another tilt of the optical axis. In this case, radiation from angles over 45° relative to the horizon is reflected out of the collector. This affects the period when the reflector is active and solar radiation is accepted. This is seen in figure 3.16a that shows the ideal acceptance function for the collector together with the annually projected radiation (compare also figure 6.5). Figure 3.15b shows a photo of a Spring/Fall-MaReCo prototype that was long-term tested by VUAB. The evaluation showed that the optical efficiency, just as wanted, is higher during spring/fall than during summer (figure 3.16b).

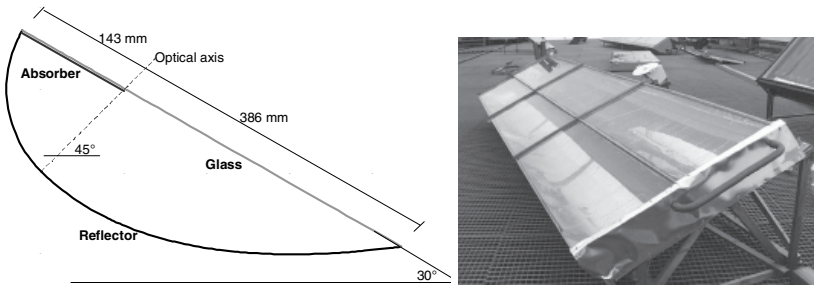

a) b)

Figure 3.15 *a) Schematic sketch and b) a photo of an evaluated prototype of a Spring/Fall-MaReCo. The Spring/Fall-MaReCo is designed for a roof tilt of 30° and the optical axis is tilted 45° from the horizon.*

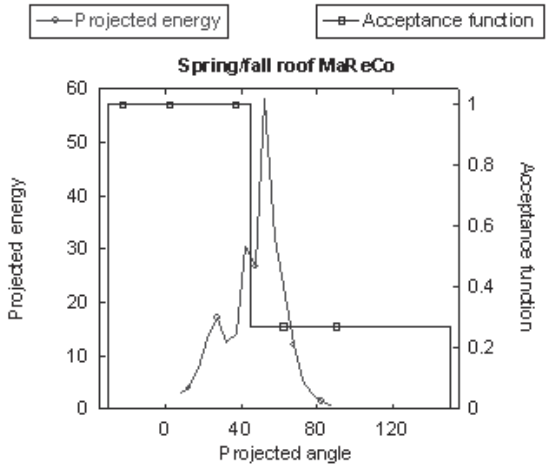

a)

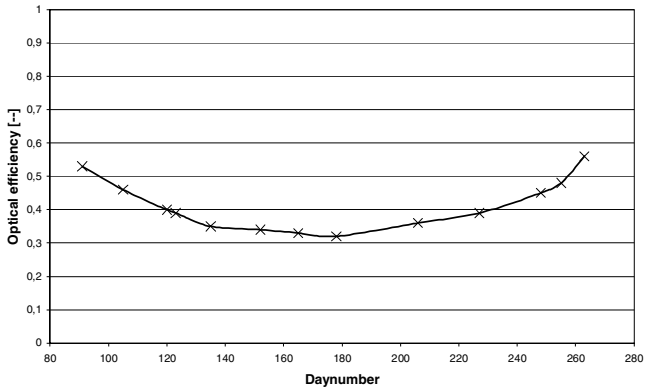

b)

Figure 3.16 *a) Projected energy incident on the aperture and theoretical acceptance function for the Spring/Fall-MaReCo. b) Variation of the optical efficiency during the evaluation period April - September for the Spring/Fall-MaReCo.*

In order to estimate the annual output, a MINSUN simulation was made using monthly mean values of the optical efficiency from figure 3.16b together with estimated values for the winter period (table 3.2). The winter values were obtained from extrapolation of the efficiency curve in figure 3.16b. The simulation result is given in figure 3.17, where the output from a reference MaReCo, with the same yearly mean optical efficiency, is also given. The figure clearly shows that the Spring/Fall-MaReCo has a lower output during the summer than the reference col-

lector. Also the total yearly energy output from the Spring/Fall-MaReCo is lower than that from the reference (222 compared with 332 kWh/m²). It is nevertheless possible to achieve a higher solar fraction (SF, defined as "solar collector output/total heat need") of the system by using a larger Spring/Fall-MaReCo instead of using a "better" collector dimensioned not to give excess heat during the summer. This will, however, require that the cost of the Spring/Fall-MaReCo is low enough to allow the use of a larger area. Thanks to the low material content of a MaReCo, the collector cost can be kept low, whereby this requirement may be fulfilled. In the tested case, the reference collector will give an overproduction at an area of 5.8 m² (SF = 0.38). A Spring/Fall-MaReCo needs an area of 8.6 m² for the same SF, but overheating occurs first at an area of 11.3 m² (SF = 0.50) (Paper V).

Table 3.2: Mean monthly optical efficiencies ($\overline{\eta}_{0b}$) for beam radiation used for energy simulation. Other collector parameters are given in table 3.1.

month	Jan	Feb	Mar	Apr	May	Jun	Jul	Aug	Sep	Oct	Nov	Dec	year
$\overline{\eta}_{0b}$	0.882	0.882	0.882	0.536	0.352	0.268	0.274	0.378	0.636	0.882	0.882	0.882	0.645

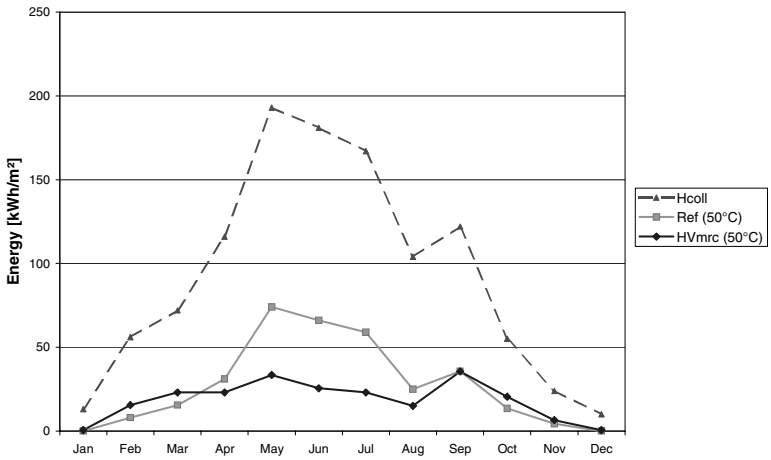

Figure 3.17 *Results from the MINSUN simulation of collector outputs (at T_{op} = 50°C) from the Spring/Fall-MaReCo (HVmrc) and from a reference collector (Ref). Hcoll is the total insolation on the collector plane (Hcolltot = 1 113 kWh/m²,yr). Climatic data used: Stockholm 1986.*

The concentrator concept can also be used in **PV** applications in order to reduce the need for expensive solar cell area. In this way, the cost of solar electricity can be reduced. One problem in concentrating the sunlight on a solar cell is that the cell temperature then rises, resulting in a reduced electrical output. The performance can be improved if the cells are cooled with circulating water. The heated cooling water can then also be used for heating purposes. This concept is used in a so-called hybrid collector, giving both heat and electricity. One example of such a hybrid collector is the ***Hybrid-MaReCo*** (figure 3.18), developed by VUAB (Helgesson et al, 2002b, and Karlsson et al, 2003). During 2004, 30 m² of this collector has been installed in a new residential area in Stockholm. The used hybrid absorber is made of an aluminum profile with solar cells laminated onto the front side and cupper tubes for the circulating water placed on the back side. In order to increase the solar absorption, the absorber surface is anodized. The first Hybrid-MaReCo reflector was made as a sandwich structure. This, however, caused problems due to thermal expansion, and a new construction with a reflector made of a single steel sheet laminated with an aluminized plastic foil has therefore been developed. Energy simulations indicate a possible yearly energy output of 50 $kWh_{electricity}$ and around 150 kWh_{heat} per m² glass at 50°C.

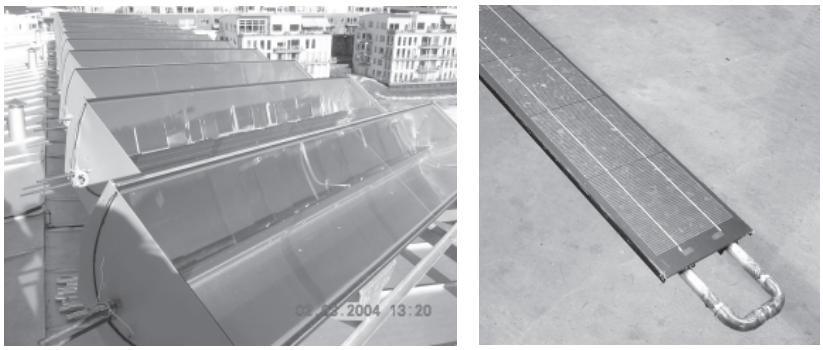

Figure 3.18 *Photo from the installation of the Hybrid-MaReCo (left) and of the developed hybrid absorber with solar cells on the front side (right).*

3.5 Example of larger MaReCo-installations

The MaReCo has also been used in some demonstration plants in Sweden:

- 100 m² MaReCo connected to the district heating net in Falun

- 150 m² MaReCo in two installations in Älvkarleby
- 500 m² MaReCo connected to the district heating net in Torsåker
- 400 m² MaReCo in combination with flat-plate collectors and bio energy in Fränsta.

Results from different systems indicate that the annual output (per glazed area) from a MaReCo system is in the order of 80% of that from a system with conventional flat-plate collectors (Karlsson and Wilson, 2000a). One reason for the lower performance is optical losses in the reflector. Although the output is lower, the specific cost of the MaReCo (in SEK/kWh) can be lower than that of a flat-plate collector thanks to the lower material content. This means that the MaReCo has the potential to become a cost effective alternative in large systems where the collectors are placed on the ground or on flat roofs.

The MaReCos in Torsåker (figure 3.19) were built on site in 1999. These collectors are connected to a district heating net, also including a pellet burner. The MaReCos are constructed of corrugated sheet steel and have reflectors of anodized aluminum. A Teflon film is mounted around the absorber in order to reduce the convection losses. Each collector has a length of 40 m. According to measurements of collector output and solar irradiation, the annual energy output from this collector system is estimated to approximately 300 kWh/m² (at T_{op} = 45°C) (Helgesson, 2001).

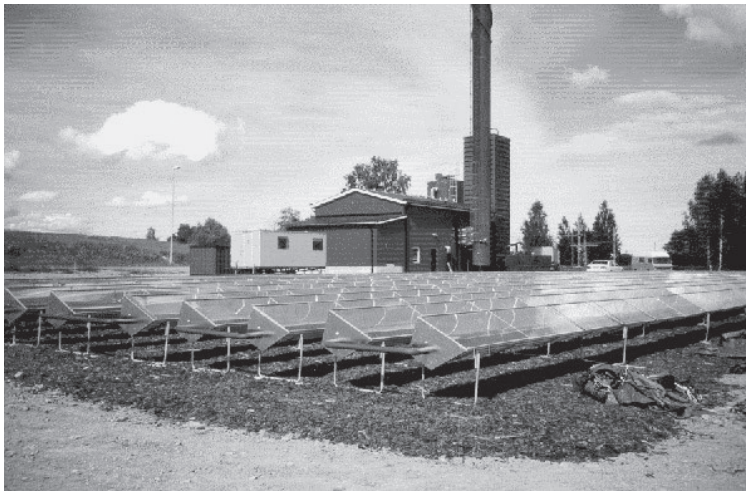

Figure 3.19 *Photo of the field with 500 m² stand-alone MaReCos in front of the bio fuel burner in Torsåker, Sweden.*

4 Collector performance

Figure 4.1 shows a cross section of a conventional flat-plate collector. The most important component is the absorber that collects the incoming solar heat and transfers it to a circulating medium. In order to reduce the heat losses, the absorber is placed in a well insulated collector box. The box is covered with transparent glazing that reduces convection and radiation losses and protects the interior of the collector. Usual materials are copper and aluminum in the absorber, and glass or plastics as cover. The use of Teflon film suppresses the convection losses and is a good design option for collectors working at high temperature (>70°C).

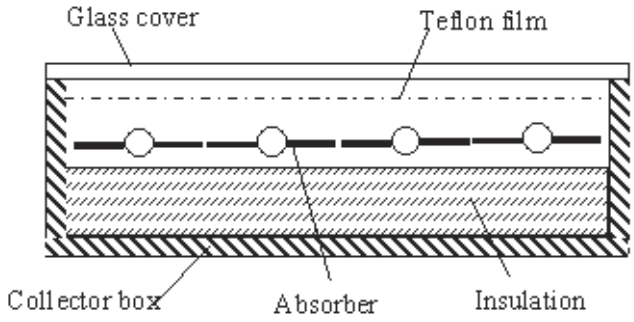

Figure 4.1 Cross section of a conventional flat-plate solar collector.

The performance of a solar collector, in steady state, is described by an energy balance (Duffie and Beckman, 1991):

$$\dot{Q}_u = A_c\left[S - U_L\left(T_p - T_{amb}\right)\right] \quad [\mathrm{W}] \tag{4.1}$$

In this equation, $\dot{Q}_u$ is the useful energy output, A_c the collector area, U_L the heat loss coefficient, T_p the mean absorber plate temperature, T_{amb} the ambient temperature, and S the solar radiation absorbed by the collector per unit area. S is equal to the difference between the incident solar radiation and the optical losses and can in principle be calculated as:

$$S = (\tau\alpha)_{av} I_t \tag{4.2}$$

where I_t is the incident solar radiation onto the collector surface, and $(\tau\alpha)_{av}$ is the average transmittance-absorptance product.

The equations above show that the energy output depends both on incident solar radiation and on collector properties (optical and thermal). The optical properties (absorptance, transmittance, and reflectance) as well as the amount of radiation that reaches the collector at a certain time of the day depend on the position of the sun, i.e. on the incidence angle of the radiation. This fact makes the theoretical evaluation of the energy output from a solar collector a difficult task. The performance evaluation will be even more complex if the collector has an asymmetric geometry, since the performance, in that case, also depends on the direction of the collector.

4.1 Optical properties

4.1.1 Absorptance, Emittance, Transmittance, and Reflectance

Radiation falling onto a surface can either be transmitted, absorbed or reflected. Important properties for solar energy calculations are the solar *absorptance* (α), the long-wave, or thermal, *emittance* (ε) and the solar *transmittance* (τ). The absorptance is a figure that expresses how much of the incident radiation is absorbed by the surface. The emittance is the ratio of the energy emitted from a surface to the energy the surface would emit if it was a blackbody at the same temperature. For conditions of thermal equilibrium Kirchoff's law states that:

$$\varepsilon_\lambda = \alpha_\lambda \tag{4.3}$$

The data that are generally available are measurements of monochromatic[11] *reflectance* (ρ_λ). The spectral reflectance is measured with a spectrophotometer. For an opaque surface, energy from all directions (either monochromatic or total) is either absorbed or reflected so that:

$$\rho_\lambda + \alpha_\lambda = \rho_\lambda + \varepsilon_\lambda = 1 \tag{4.4}$$

11. I.e. at a certain wavelength (λ).

This means that it is only necessary to know the reflectance in order to find the absorptance and emittance properties of an opaque surface. For solar energy applications, the spectral distribution of terrestrial solar radiation is a suitable choice for the calculation of α. The total absorptance for a surface is calculated as:

$$\alpha = \frac{\int_0^\infty \alpha_\lambda I_{\lambda i} d\lambda}{\int_0^\infty I_{\lambda i} d\lambda} \tag{4.5}$$

where $I_{\lambda i}$ is the incident energy spectrum and $\alpha_\lambda = I_{\lambda absorbed}/I_{\lambda i} = 1\text{-}\rho_\lambda$. For solar absorptance, the integration should include the wavelength interval 0.3 - 2.5 μm.

The emittance of a surface depends on the nature of the surface and its temperature. In this case the blackbody spectrum is used in the calculations. The total emittance is calculated as:

$$\varepsilon = \frac{\int_0^\infty \varepsilon_\lambda E_{\lambda B} d\lambda}{\int_0^\infty E_{\lambda B} d\lambda} = \frac{\int_0^\infty \varepsilon_\lambda E_{\lambda B} d\lambda}{\sigma T^4} \tag{4.6}$$

where $E_{\lambda B}$ is the energy emitted from a blackbody at a certain temperature (T) at wavelength λ, and $\sigma = 5.6697 \cdot 10^{-8}$ W/m²,K^4 is the Stefan-Boltzmann constant.

For a (partly) transparent surface, also the transmittance is of interest. The transmittance, reflectance and absorptance of the glazing depend on the incoming radiation and on the thickness, refractive index, and the extinction coefficient of the material. For smooth surfaces, the Fresnel expressions can be used to calculate the reflection (r) of unpolarized radiation passing from medium 1 to medium 2:

$$r_\perp = \frac{\sin^2(\Theta_2 - \Theta_1)}{\sin^2(\Theta_2 + \Theta_1)} \tag{4.7a}$$

$$r_{//} = \frac{\tan^2(\Theta_2 - \Theta_1)}{\tan^2(\Theta_2 + \Theta_1)} \tag{4.7b}$$

$$r = \frac{I_r}{I_i} = \frac{r_\perp + r_{//}}{2} \tag{4.7c}$$

where Θ_1 and Θ_2 are the angles of incidence and refraction (figure 4.2). These angles are related to the refractive indexes (n)[12] by Snell's law:

$$\frac{n_1}{n_2} = \frac{\sin(\Theta_2)}{\sin(\Theta_1)} \tag{4.8}$$

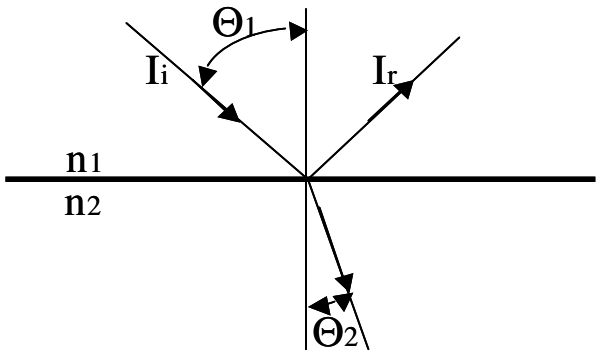

Figure 4.2 *Angles of incidence and refraction (Θ_1 and Θ_2) in media with refractive indexes n_1 and n_2. I_i is incident radiation and I_r is reflected radiation.*

In solar applications, the radiation is transmitted through a slab, meaning that it passes two interfaces per cover. Only considering reflection losses, the transmittance of initially unpolarized radiation can be calculated as:

$$\tau_r = \frac{\tau_{//} + \tau_{\perp}}{2} = \frac{1}{2}\left(\frac{1-r_{//}}{1+r_{//}} + \frac{1-r_{\perp}}{1+r_{\perp}}\right) \tag{4.9}$$

The absorption of radiation in a partly transparent medium depends on the distance (l) the radiation has travelled and the extinction coefficient (K)[13] of the material. If only the absorption losses are considered, the transmittance is calculated as:

$$\tau_a = e^{-(Kl/\cos\Theta_2)} \tag{4.10}$$

12. $n_{air} \approx 1$ and $n_{glass} \approx 1.526$.
13. K_{glass} is between 4 and 32 m^{-1}.

The transmittance of a single collector cover can then, in a simplified way, be calculated as:

$$\tau = \tau_a \tau_r$$

The transmittance is usually a function of the wavelength of the incident radiation and the total transmittance is calculated as:

$$\tau(\Theta) = \frac{\int_0^\infty \tau_\lambda(\Theta) I_{\lambda i}(\Theta) d\lambda}{\int_0^\infty I_{\lambda i}(\Theta) d\lambda} \tag{4.11}$$

where $I_{\lambda i}(\Theta)$ is the incident monochromatic solar intensity arriving at the cover system from the incidence angle Θ.

In order to consider the transmittance for diffuse radiation, an equivalent angle of incidence is defined. For isotropic diffuse radiation, this angle is approximately 60° for a wide range of conditions encountered in solar collector applications (Duffie and Beckman, 1991).

For a concentrating collector, using a reflecting material, another optical property, the reflectance, is also important. If the incident radiation is contained within a small solid angle, two limiting distributions of the reflected radiation exist: specular and diffuse (figure 4.3). Specular reflection is mirrorlike (i.e. the reflected polar angle equals the incident polar angle), whereas the diffuse reflection is distributed uniformly in all directions. The general case is a mixture of these two limiting cases. The monochromatic specular reflectance ($\rho_{\lambda s}$) is defined as the ratio of specularly reflected monochromatic intensity ($I_{\lambda s}$) to the incident monochromatic intensity ($I_{\lambda i}$). Specular reflectance is, in general, wavelength dependent and, for a particular spectral distribution of incident energy, it is calculated as:

$$\rho_s = \frac{\int_0^\infty \rho_{\lambda s} I_{\lambda i} d\lambda}{\int_0^\infty I_{\lambda i} d\lambda} \tag{4.12}$$

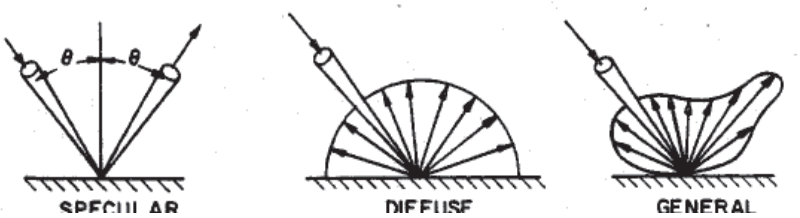

Figure 4.3 *Specular, diffuse, and general reflected radiation from a surface. (Duffie and Beckman, 1991)*

Absorption losses in the reflector affect the overall optical properties of a concentrating collector. This effect can be taken into account by using the factor τ_{CPC}, which is the fraction of radiation transmitted through the aperture that reaches the absorber (Carvalho et al, 1985):

$$\tau_{CPC} = \rho^n \tag{4.13}$$

where ρ is the reflectivity of the reflector and n is the average number of reflections. n depends on the incidence angle.

4.1.2 Transmittance-absorptance product

Some of the radiation passing the cover system is absorbed directly by the absorber and some is reflected back to the cover system. A part of the reflected radiation is then reflected back to the absorber, where it can be either absorbed or reflected. The fraction of the incident energy that is ultimately absorbed, after multiple reflections of diffuse radiation, is given by equation 4.14 (Duffie and Beckman, 1991)[14]. The $(\tau\alpha)$-product depends on the incidence angle. The incidence angle dependence will be further discussed in chapters 6 and 8.

$$(\tau\alpha) = \frac{\tau\alpha}{1-(1-\alpha)\rho_d} \approx 1.01\tau\alpha \tag{4.14}$$

The optical efficiency of a *CPC* having a cover with transmissivity τ, and an absorber with absorptivity α, is given by $\eta_0 = \tau\alpha\rho^n$ (Carvalho et al, 1985).

14. As an example, ρ_d = 0.12 for a glass with *KL* = 0.037 (at 60°).

4.2 Heat transfer

4.2.1 Conduction, Convection, and Radiation

Heat can be transferred through conduction, convection or radiation. The conductive heat transfer ($\dot{Q}_l$) through a material is calculated as:

$$\dot{Q}_l = \frac{L}{d} A(T_a - T_b) \tag{4.15}$$

where L is the thermal conductivity of the material, d the material thickness, A the area through which the energy is transferred, and T_a and T_b the temperatures on both sides of the body.

The convective heat transfer ($\dot{Q}_c$) from a wall to a fluid is calculated as:

$$\dot{Q}_c = h_{conv} A(T_w - T_f) \tag{4.16}$$

where h_{conv} is the heat transfer coefficient, T_w the temperature of the wall, and T_f the temperature of the fluid.

In the area of solar collector operation, the radiation heat transfer plays a more significant role than in most usual engineering practice. Radiation is electromagnetic energy that is propagated through space at the speed of light (c). It has a frequency (ν) such that:

$$c = \lambda \nu \tag{4.17}$$

where λ is the wavelength. The spectrum of electromagnetic radiation is divided into different wavelength bands (figure 4.4). Thermal radiation is emitted from all bodies by virtue of their temperature. The wavelengths of importance in solar energy applications are in the ultraviolet to near-infrared range (approximately 0.3 - 25 µm). This range includes the visible spectrum (0.38 - 0.78 µm) and the solar radiation (approx 0.3 - 2.5 µm).

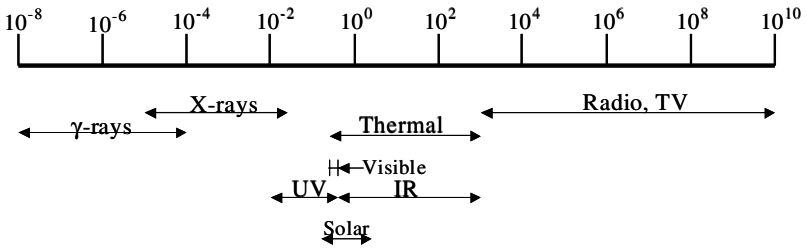

Figure 4.4 *Spectrum of electromagnetic radiation. The scale shows wavelength in μm.*

For theoretical studies, the blackbody concept is very useful. A blackbody is a perfect absorber that absorbs all incident radiation. A blackbody is also a perfect emitter of thermal radiation. The wavelength distribution of radiation emitted by a blackbody is given by Planck's law:

$$E_{\lambda B} = \frac{3.7405x10^{-16}}{\lambda^5\left[\exp\left(0.0143879/(\lambda T)\right)-1\right]} \tag{4.18}$$

By integrating Planck's law over all wavelengths, the total energy, per unit area, emitted by a blackbody is found to be:

$$E_B = \int_0^\infty E_{\lambda B} d\lambda = \sigma T^4 \tag{4.19}$$

The wavelength corresponding to the maximum intensity of blackbody radiation is found by Wien´s displacement law:

$$\lambda_{\max} T = 2897.8 \ \ \mu\text{m K} \tag{4.20}$$

The directional characteristics of a radiation field are described by using the radiation intensity (I). The intensity is defined as the energy passing through an imaginary plane per unit area per unit time and per unit solid angle whose central direction is perpendicular to the imaginary plane. The blackbody emissive power is related to the blackbody intensity by:

$$E_B = \pi I_B \tag{4.21}$$

The radiation heat transfer ($\dot{Q}_r$) between two surfaces (i = 1 and 2) with temperature T_i, area A_i, and emittance ε_i can be calculated as:

$$\dot{Q}_r = \frac{\sigma\left(T_2^4 - T_1^4\right)}{\frac{1-\varepsilon_1}{A_1\varepsilon_1} + \frac{1-\varepsilon_2}{A_2\varepsilon_2} + \frac{1}{A_1 F_{12}}} \tag{4.22}$$

where F_{12} is the view factor between the two surfaces. This expression can be simplified for two interesting cases:

- For radiation between two infinite parallel plates (e.g. absorber and cover in a flat-plate collector): $A_1 = A_2$, and $F_{12} = 1$.
- When a small convex object (1, e.g. a flat-plate collector) is surrounded by a large enclosure (2, e.g. the sky), the ratio A_1/A_2 approaches zero, and $F_{12} = 1$.

In order to simplify the expression a radiation heat transfer coefficient (h_{rad}) is defined so that the radiation heat transfer can be expressed as:

$$\dot{Q}_r = A h_{rad}\left(T_2 - T_1\right) \tag{4.23}$$

4.2.2 Heat loss coefficient

Heat is lost from a solar collector through a combination of conduction, convection and radiation. The energy loss through the top is the result of convection and radiation between parallel plates. Below, this is shown for a system with two covers. The loss (per unit area) between the absorber plate and the first cover can be calculated as (Duffie and Beckman, 1991):

$$\dot{q}_{loss,top} = h_{conv,p-c1}\left(T_p - T_{c1}\right) + \frac{\sigma\left(T_p^4 - T_{c1}^4\right)}{\frac{1}{\varepsilon_p} + \frac{1}{\varepsilon_{c1}} - 1} = \left(h_{conv,p-c1} + h_{rad,p-c1}\right)\left(T_p - T_{c1}\right) \tag{4.24}$$

where index p denotes the absorber plate and index $c1$ the first cover. $h_{conv,p\text{-}c1}$ is the convection heat transfer coefficient between two inclined parallel plates and $h_{rad,p\text{-}c1}$ is the radiation heat transfer coefficient between the plates. The heat transfer resistance (R_3) between the plate and the first cover can be written as:

$$R_3 = \frac{1}{h_{conv,p-c1} + h_{rad,p-c1}} \tag{4.25a}$$

A similar expression can be written for the resistance (R_2) between the two covers. The resistance from the top cover to the surroundings (R_1) is given as:

$$R_1 = \frac{1}{h_w + h_{rad,c2-a}} \tag{4.25b}$$

where $h_{rad,c2\text{-}a}$ is the radiation heat transfer coefficient for radiation exchange with the sky, and h_w is the wind convection heat transfer coefficient of the collector surface.

For the two-cover system, the top loss coefficient from the collector plate to the ambient air is then calculated as:

$$U_t = \frac{1}{R_1 + R_2 + R_3} \tag{4.26}$$

In the absence of a selective surface (section 4.4), radiation is the dominant mode of heat transfer. If a selective surface with low emittance is used, convection is the dominant heat transfer mode between the selective surface and the cover, but radiation is still the largest term between the two cover glasses in a two-cover system.

The energy loss through the bottom of the collector depends on the insulating material and is calculated as:

$$U_b = \frac{L}{d} \tag{4.27}$$

where L and d are thermal conductivity and thickness of the insulation respectively.

The edge losses, described by U_e, can be estimated by assuming one-dimensional sideways heat flow around the perimeter of the collector.

If it is assumed that all losses occur to the common sink (ambient) temperature T_{amb}, the collector overall loss coefficient (U_L) is the sum of the top, bottom and edge loss coefficients:

$$U_L = U_t + U_b + U_e \tag{4.28}$$

The heat losses can be measured by using a so-called ”hot box” with an electrically heated absorber (Adsten, 2002b). The absorber temperature is measured with thermocouples at several points on the surface. In thermal equilibrium, the U-value can be calculated as:

$$U = \frac{\left(V^2/R\right)}{A \cdot \left(T_{abs} - T_{amb}\right)} \tag{4.29}$$

where V is the measured voltage and R is the resistance of the electric heating foil. In order to take the temperature dependence of the heat losses into account, the following model is used:

$$U = U_0 + U_1\left(T_{abs} - T_{amb}\right) \tag{4.30}$$

4.2.3 Collector efficiency factor (*F'*)

The useful output ($\dot{q}_u$) from a collector can, in principle, be expressed as:

$$\dot{q}_u = F'\left[(\tau\alpha)I - U_L \Delta T\right] \tag{4.31}$$

where F' is the collector efficiency factor, which is the ratio of the actual useful energy gain to the useful gain that would result if the collector absorbing surface had been at the local fluid temperature (Duffie and Beckman, 1991). F' accounts for the temperature difference between absorber surface and fluid, and the value of F' depends on the ability of the absorber to transfer the energy absorbed in the fin to the fluid in the tubes. The efficiency factor is given by the ratio:

$$F' = {R_{pa}}\Big/{R_{fa}} \tag{4.32}$$

where R_{pa} is the heat transfer resistance from the absorber plate to the ambient air and R_{fa} is the heat transfer resistance from the fluid to the ambient air. F' is nearly independent of concentration ratio, and when water is used, F' is very close to unity (Rabl, 1980). The derivation of efficiency factors for uneven irradiation on a fin absorber is discussed in (Hellström, 2004).

4.3 Reflectors

In concentrating solar collectors a reflecting material is used to direct the beam component of the solar radiation onto the receiver. The increase in annual collector output by using a booster reflector is approximately equal to the additional irradiation from the reflector multiplied by the optical efficiency of the collector. The annual performance increase (in kWh/

m²) due to an external reflector is almost independent of the operating temperature (Perers and Karlsson, 1993b). This means that the relative increase due to the reflector is usually higher at a higher temperature. For good performance, the reflector material should have a high specular reflectance for radiation in the solar spectrum wavelength range. Examples of good reflector materials are *silver* and *aluminum*, with a solar hemispherical reflectance (R_{hemi}) of 96% and 92% respectively (Nostell et al, 1998a). The optical performance of a bare aluminum surface will, however, deteriorate quickly (due to oxidation, abrasion, and dirt) when it is exposed to outdoor environment. One method to prevent the decrease in reflectance is to use a thin protective surface cover. *Rolled aluminum sheets lacquered with* PVF_2 (polyvinyl di-fluoride) have good mechanical strength and long-term optical stability, but also rather low specular reflectance. This material is commercially produced as roofing material and has been used as corrugated reflectors in some large collector fields in Sweden and Denmark. Another solution is to use a second surface *silver mirror*. This has a good specular reflectance (roughly 95% (Hellström et al, 2000)), but might suffer from insufficient mechanical strength. If a back-surface coating is used, the transparency of the glass influences the optical properties. A material with good long-term properties and mechanical strength, but with inferior optical properties compared with silver or aluminum, is *stainless steel* (R_{hemi} = 66% (Nostell et al, 1998a)). The cost of this material is however too high to make it an attractive alternative. A long-term stable material with high specularity can be achieved by *vacuum evaporation of* an *aluminium* foil. Also this material has a rather high cost.

In an evaluation of a stand-alone MaReCo, two different reflector materials were tested: anodized aluminium and laminated aluminum foil (Helgesson et al, 2000a). The collector with anodized reflector showed a somewhat higher annual energy output (298 compared with 288 kWh/m²). The lower cost of the laminated foil may, nevertheless, result in a lower cost per produced kWh. The measurements also showed that the temperature of the reflector is lower and more evenly distributed if anodized aluminium is used. The reason for this is that the anodized aluminum has a higher thermal conductivity and therefore distributes heat better than the laminated foil.

In a collector plant in Falun, MaReCos with reflectors made of aluminum films laminated on cardboard have been tried. One disadvantage of these reflectors is that the cardboard absorbs moisture, resulting in reduced durability and performance of the reflector. Another reflector material that has been tested in a MaReCo is a steel plate laminated with an aluminized plastic foil. This material has a reflectance of about 80%

(Helgesson et al, 2002b). The same reference also gives the reflectances for Anodized aluminum and the reflectance enhanced aluminum reflector MIRO as 83% and 90% respectively.

The reflectances for some different reflector materials are summarized in table 4.1. As an example, the hemispherical reflectance for PVF_2 coated anodized aluminum is also given in figure 4.5.

Table 4.1: Solar hemispherical reflectance (in %) for different reflector materials. The reflectance is measured, in the wavelength range 300 – 2 500 nm, with a Beckman spectrophotometer equipped with an integrating sphere. (*Rs* = specular component.)

	Reflectance	**after 4 year aging**	**reference**
Rolled roofing aluminum	88 Rs: 66	Not long term stable, since no protective coating	Nostell, 1997
Anodized aluminum	86 Rs: 80	76 Rs: 35	Perers et al, 1992
PVF_2 lacquered anodized aluminum	83 Rs: 75	79 Rs: 64	Nostell et al, 1998a
Vacuum evaporated aluminum foil coated with PMMA	86 Rs: 85	83* Rs: 81	Nostell et al, 1998a
Stainless steel	66 Rs: 51	64 Rs: 42	Nostell et al, 1998a

* *after 6 year aging*

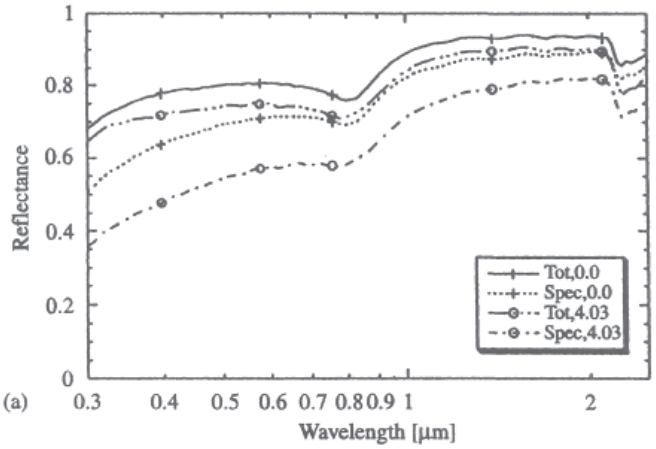

Figure 4.5 *Hemispherical and specular reflectance for a PVF_2-coated anodized aluminum sample for different aging times. (Nostell et al, 1998a)*

The standard method to measure specular and diffuse reflectance with an integrating sphere can give misleading results. In such an instrument, the specular component is defined as light reflected within a narrow cone around the specular direction (e.g. 3.5°). For large collector fields, a considerable part of the diffuse light (i.e. light scattered more than 3.5°) will, however, still hit the collector aperture (Perers et al, 1992).

A reflector surface does not have to be mirrorlike. Also diffuse materials, e g rolled aluminum, perform well. With equal total reflectance, the rolled material may even perform better than a mirror material (Perers et al, 1994). The scattered reflected light from rolled aluminum is distributed along a circular arc. The intensity increase occurs for hours when part of the specular reflected radiation is lost above the collector but some scattered light still hits the collector. Also trapezoidal corrugated aluminum sheets can be used for booster reflector applications. One advantage of a trapezoidal reflector over a flat one is that it has higher mechanical strength. The combination of strength and optical performance determines the optimum corrugation pattern for solar reflector application. For Swedish conditions, a corrugation angle of about 10° is most favourable (Rönnelid and Karlsson, 1999). For booster reflectors with large corrugation angles and low specular reflectance, multiple reflections reduce the annual reflected irradiation. As long as the total reflectance is acceptable, the tolerance for high surface roughness is fairly large. When mounting a reflector, grooves (or other surface textures) should preferably be directed parallel to the collector azimuth.

4.4 Modification of the collector properties

4.4.1 Selective absorber surface

The basic collector model eq 4.31 clearly shows that the collector performance ($\dot{q}_u$) depends on the optical ($\tau\alpha$) and thermal (U_L) properties of the collector and on the surrounding climate (radiation, I, and temperature, T_{amb}). Furthermore, the performance also depends on the operation of the collector and on the system to which the collector is connected (affects T_f).

$$\dot{q}_u = F'\left[(\tau\alpha)_{av} I_t - U_L\left(T_f - T_{amb}\right)\right] \tag{4.31}$$

In order to absorb as much solar energy as possible, the glazing should have a high transmittance and the absorber should have a high absorptance for solar radiation. In order to reduce the heat losses, the absorber surface

should also have a low emittance for thermal radiation. According to Kirchhoff´s law (eq 4.3), there is a conflict between a high absorptance and a low emittance. However, the maximum temperature of the absorber surface is usually about 200°C, corresponding to thermal radiation with wavelengths above approximately 3 μm. The solar radiation, on the other hand, has wavelengths less than 3 μm. Since the solar and the thermal radiation only slightly overlap (figure 4.6) it is possible to design an absorber surface with selective properties, i.e. high solar absorptance and low thermal emittance (figure 4.7). An ideal selective absorber would have α = 1.0 throughout the solar spectrum and ε = 0 in the thermal range.

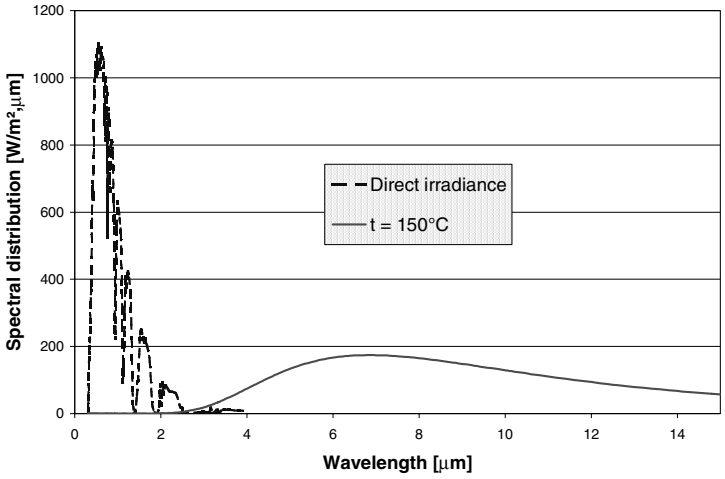

Figure 4.6 *Spectral distribution of short wave solar radiation (AM1.5, ISO 9845-1) and longer wave thermal radiation (for a blackbody with temperature 150°C).*

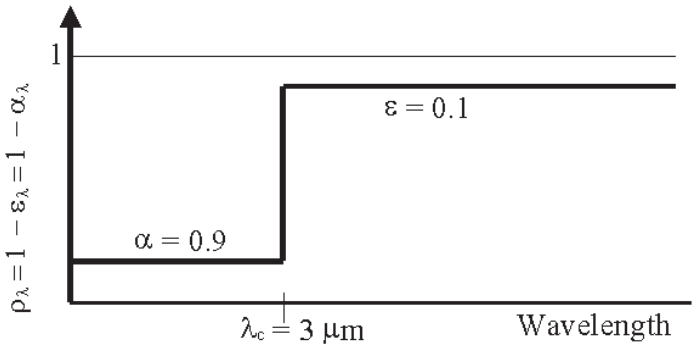

Figure 4.7: A hypothetical selective surface with a cut-off wavelength at 3 μm.

The possibility of producing practical selective absorber surfaces was first shown in the mid 1950s. The most common type of selective absorber is a tandem absorber, obtained by depositing a coating with high solar absorptance onto a substrate (usually a metal) with low thermal emittance (high IR-reflectance). The optical performance of the selective absorber depends on the properties of both the coating and the substrate, and also on the thickness of the coating. Many of the coating materials used are metal oxides. One example of a selective surface is Nickel-pigmented aluminum oxide, prepared by first anodizing an aluminum plate in dilute phosphoric acid (to produce a porous aluminum film) followed by electroplating metallic nickel particles within the pores from a nickel salt aqueous solution (Tesfamichael and Wäckelgård, 2000). The selective surface can also be produced by reactive DC-magnetron *sputtering* in vacuum in a roll-coating device. The substrate is here placed in a vacuum chamber together with a "target" of the material to be deposited. Ions of an inert gas (e.g. argon) are accelerated, by means of a potential difference, towards the target, knocking out atoms of the target material. These atoms then build up a thin film on the substrate. A strong magnetic field can be used to concentrate the plasma near the target in order to increase the deposition rate. One example of this is the Sunstrip absorber with a coating consisting of three layers with a total thickness of about 200 nm. The first layer is a nickel barrier (corrosion protection) layer deposited on the aluminum substrate. The next layer is an absorbing graded-index nickel-nickel oxide layer. The oxygen inlet during the sputtering process is designed to give a gradual decrease of nickel content and an increasing amount of nickel oxide from the substrate to the front surface, resulting in a graded index structure with a refractive index that is decreasing from

the substrate to the front surface. (The ideal case is to have a refractive index of 1, and an extinction coefficient of 0 at the front surface (Adsten et al, 2000).) The last (outermost) layer is a transparent anti-reflection layer. Typical values of α, and ε for a spectrally selective absorber are 0.93 - 0.96 and 0.05 - 0.25 respectively (Adsten, 2002c). The Sunstrip absorber[15] has a solar absorptance of 96% and a thermal emittance of 7%. Properties of selective surfaces are discussed in more detail in section 7.3.

4.4.2 Antireflection treatment

The most common cover material in solar collectors is glass. Low-iron glass has the best transmittance. Glass with a high Fe_2O_3 content (having a "greenish" appearance) absorbs in the infrared portion of the solar spectrum. The higher the Fe_2O_3 content, the higher is the infrared absorption. For that reason low-iron glass should be chosen for collector applications. Typical values of the solar transmittance (τ) are for ordinary float glass 83 - 85% and for low iron glass 90% (Adsten, 2002c).

An increase of 1% in transmittance yields an increase of approximately 2% in the annual system performance (Nostell et al, 1999a). The transmittance of the cover can be increased by depositing a thin antireflection (AR) layer onto the cover surface (figure 4.8). The index of refraction of the coating (n_{film}) should, for best result, equal the square root of the refractive index of the substrate (n_{sub}), assuming air to be the surrounding medium. Since most materials used for collector covers have $n_{sub} \approx 1.5$, the film should have $n_{film} \approx 1.22$, or, as a rule of thumb, a refractive index that is lower than 1.3. This is a very low index, and the usual way to achieve this is to fabricate a porous film on the surface of the substrate.

AR-treatment can be made by e.g. *etching* (Cathro et al, 1984, Nostell, 2001, Nostell et al, 1999a, and Nostell et al, 1998b). Dipping the glass in a silica saturated fluosilic acid solution gives a long-term stable AR-treatment, with an increase in solar transmittance of up to 5%. Measurements on a glass AR-treated by an etching technology show an increase in transmittance of 4%, resulting in an increase in the annual energy output at T_{op} = 50°C by 9%. The chemicals involved in the etching process are, however, too harmful for the technology to be interesting in a large scale. A more environmentally friendly method is to prepare the AR-film by using silica sols in a *dip-coating process*. The sol consists of monodisperse silica particles mixed with ethanol and water. Hydrochloric acid might

15. www.sunstrip.se.

be added in order to avoid coagulation. For a good result, it is important that the surface is thoroughly cleaned before dipping. The film thickness, which controls the wavelength of the reflectance minimum, is controlled by the withdrawal rate.

Apart from being more environmentally friendly, the dip-coating process is also rather fast. One problem though is that the adhesion between the substrate and the film made with this technology tends to be low. The mechanical properties can, however, be improved by baking and tempering the glass. The best AR-film prepared by the dip-coating method has shown an increase in solar transmittance by 5.4% (Nostell et al, 1999a).

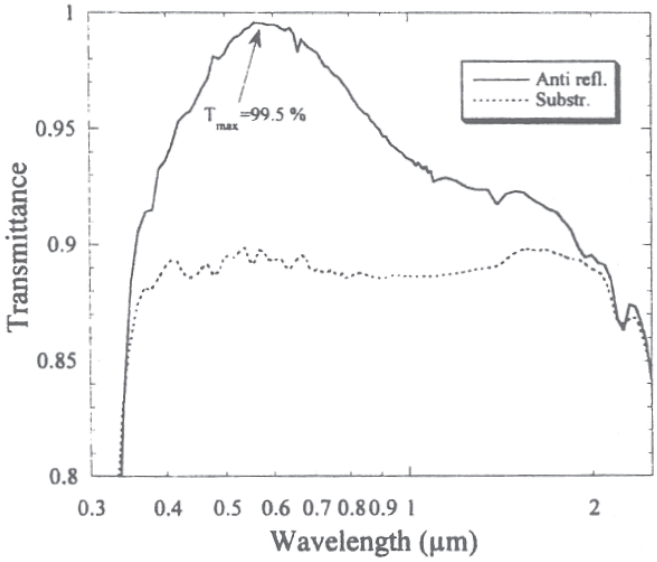

Figure 4.8 *Transmittance spectrum for a glass sample with and without AR-treatment. (Nostell et al, 1999a)*

4.4.3 Transparent insulation

The heat losses from a collector depend on the absorber emittance and on the collector insulation (section 4.2.2). For a collector with internal reflectors, the conductivity and the emittance of the reflector material also influence the heat losses. In order to block thermal conduction, an air gap between absorber and reflector is often recommended. By using a transparent insulation, placed between the absorber and the glazing, the heat losses (especially for high temperature applications) can be reduced. The transparent insulation reduces the convection losses, but also the transmittance of the glazing, meaning that the use of transparent insula-

tion is a problem of optimization. The total performance also depends on the IR-transparency (τ_{IR}) of the insulating material (Rönnelid and Karlsson, 1996a). A high τ_{IR} increases the radiative part of the losses between the absorber and the outer glazing. For non-selective absorbers the importance of secondary glazing with low τ_{IR} increases.

A common transparent insulating material is Teflon, which has a high thermal stability (up to 200°C), a low weight, and a high solar transmittance (τ = 0.96) (Rönnelid and Karlsson, 1996a). A *flat Teflon film* can increase the performance by 6% (at T_{op} = 50°C) and can be a cost effective choice for high temperature applications (Hellström, 2000). Since the MaReCo is intended for use at relatively high temperatures, it is recommended to use a Teflon film in a MaReCo (Paper IV). Figure 4.9 shows two different types of transparent insulations. Using a honeycomb Teflon insulation the performance can be increased by 12% (Hellström et al, 2000). One problem with this is the material cost, since the honeycomb structure requires a lot of material. For a flat-plate collector, the Teflon film is mounted flat between the absorber and the cover glass (figure 4.10a). If the collector has several internal reflector troughs, the Teflon film can be mounted on the top of the reflector edges (figure 4.10b). In a MaReCo, the Teflon film can be mounted as a tent around the absorber fin (figure 4.10c). When transparent insulation is used, it is important that the Teflon film is mounted so that it does not come in contact with the warm absorber surface. (If the Teflon film sticks to the absorber the selectivity of the absorber will be destroyed since Teflon has an emittance of 0.53.) It is also important to avoid tension, which otherwise can cause the film to tear, drastically reducing the collector performance.

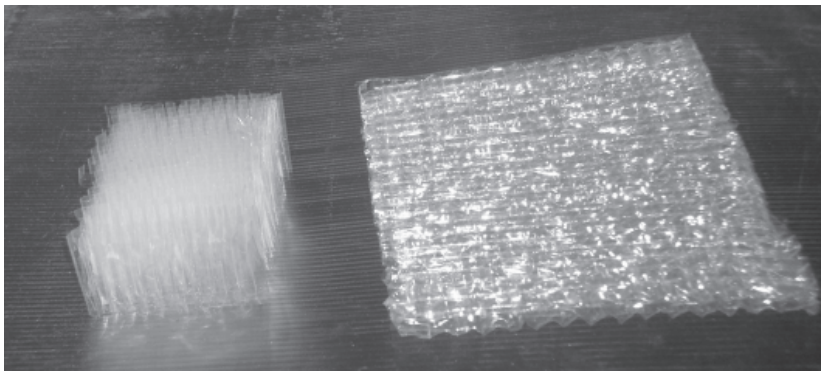

Figure 4.9 Photo of two different transparent insulations.

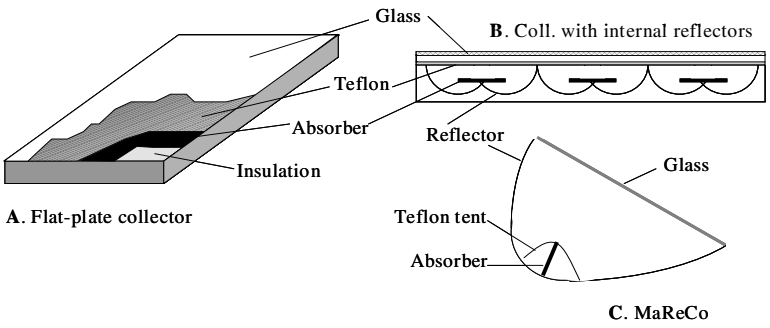

Figure 4.10 *Mounting of a Teflon film in order to reduce the heat losses in a) a flat-plate collector, b) a collector with internal reflector troughs, and c) a MaReCo.*

5 Basic solar energy theory – Measurements

5.1 Collector measurements

In order to predict the performance of a collector and to study how different designs will affect the energy output, measurements are needed. The most straightforward way is to build a prototype and measure the performance during a whole operating season. This method is, however, time consuming and expensive, and the result is only valid for conditions similar to those during the measurement period.

In the standard testing of a solar collector (ISO 9806-1[16]), the performance is measured at clear sky conditions with high radiation levels at near normal incidence angles to the collector and with a low fraction of diffuse radiation. One shortcoming of the classical stationary collector testing is that these ideal operating conditions are not so common in Sweden. This means that the testing time will be long and that the collector performance predicted may not be representative for a longer period of operation, especially since some energy is also delivered at high incidence angles and for diffuse fractions of solar radiation. It is therefore of interest to use a method that accurately predicts the annual collector performance for a variety of climates and operating conditions from a shorter period of measurements. This matter is considered in a quasi-dynamic method for outdoor testing of solar collectors (Perers, 1997, and Perers, 1993a), which is included in the European standard "EN 12975:2000"[17] (Fischer et al, 2001, and Veenstra, 1999). This standard is used by SP[18] for testing solar collectors. In (Nayak and Amer, 2000) the Perers method is compared with eight other dynamic test methods. By running the pump in the collector array continuously during the test period, a large variety

16. ISO 9806-1.2, "*Thermal performance tests for solar collectors – Part 1: Glazed liquid heating collectors*".

17. EN 12975:2000; "*Thermal solar systems and components – Solar Collectors*".

18. Swedish National Testing and Research Institute.

of operating conditions are used for the evaluation of the collector. This makes the prediction of the energy output during a longer period more realistic. The dynamic test method therefore gives a more complete characterisation of the collector performance from a shorter period of measurements (Perers, 1993a). This reference concludes that the Perers method accounts for almost all theoretical effects and that the test set-up and the sequences of tests involved more or less follow the ASHRAE standard. It is also shown that the theoretical predictions of the method agree reasonably well with experimental measurements. The problem of predicting long-term performance of solar collectors is also discussed in (Collaires-Pereira and Rabl, 1979).

The expected energy output from a collector can be determined by using the "dynamic collector parameters" in a standard simulation program (e.g. TRNSYS or MINSUN). In this work, the MINSUN program has been used for the energy simulations. The complete MINSUN simulation and optimization program models a solar energy system containing solar collectors, storage, auxiliary heaters, and consumers (Chant, 1985). The program consists of two parts; a solar collector array model and a system model. In this work, only the collector array part (UMSORT) was used for the simulations. Instead of using detailed system information, a fixed average operating temperature ($T_{op} = (T_{in} + T_{out})/2$) is applied. Since no system effects are included, the comparison between different collector designs is facilitated. As input parameters, the zero loss efficiencies for beam and diffuse radiation (η_{0b} and η_{0d}), the incidence angle modifier coefficient (b_0), the heat loss coefficients (k_1 and k_2), and the effective collector thermal capacitance ($(mC)_e$) are given together with collector tilt (β) and orientation (γ_c), and location latitude (ϕ). The collector parameters are identified by multiple linear regression (MLR) on data obtained from measurements on the collector. One advantage of the dynamic method is that datagaps can be accepted (Perers, 1993a). This makes it possible to delete erroneous data. For the identification, standard multiple linear regression routines, available in most spreadsheet programs (e g Excel), can be used. The reflectance of booster mirrors cannot, however, be determined with the MLR method, since the correlation between direct irradiance and irradiance from the reflector exhibit too strong a correlation. Since the same model is used in the simulation as for parameter identification, the determined parameters can be used directly in the simulation program. In order to run the simulation, hourly climatic data (of radiation and ambient temperature) during a year for the location in question are needed. In this work data from 1986 for Stockholm (N 59.3°, E 18.1°) were used for most of the simulations (figure 2.7). The total insolation in this case was 934 kWh/m² onto a hori-

zontal surface and 1 129 kWh/m² onto a surface tilted 45°. Running the program creates a log file with a summary of the monthly and annual values of radiation, and collector energy output and operating time at five different operating temperatures.

In an extended MLR method, the zero loss efficiency can be identified for different intervals of incidence angles (Perers, 1997). In this method, the beam radiation is divided into different classes, depending on the incidence angle onto the collector. This makes it possible to identify the incidence angle dependence angle by angle and thereby to study collectors with special incidence angle effects.

A simple relation for estimating the yearly energy output for a solar collector in Sweden is the "Karlsson formula" (Perers and Karlsson, 1990). This equation is based on estimates of the useful irradiance and average ambient temperature over a year. Eq 5.1 given below is valid only for a collector temperature of 50°C.

$$E_{50} = \tau\alpha \cdot 800 - U \cdot 47 \tag{5.1}$$

5.2 Solar radiation

5.2.1 The sun

The sun is a sphere consisting of very hot gases with a density estimated to be about 100 times that of water. Its diameter is $1.39 \cdot 10^9$ m and its average distance from the earth is $1.5 \cdot 10^{11}$ m (figure 5.1). The surface of the sun has an effective blackbody temperature[19] of 5 777 K.

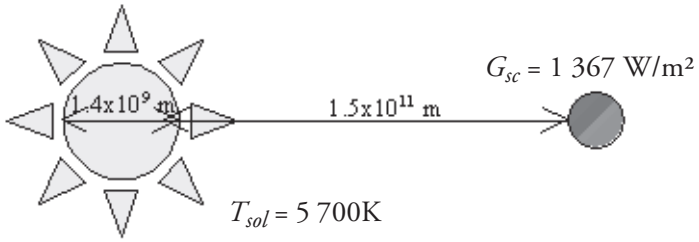

Figure 5.1 The sun-earth relationship.

19. The effective blackbody temperature is the temperature of a blackbody radiating the same amount of energy as the body in question does.

The sun is a huge fusion reactor in which hydrogen combines to form helium. The mass being lost in the reaction is converted to energy that is transported from the interior of the solar sphere to the surface from where it is radiated out into space. The intensity of solar radiation outside the earth's atmosphere is nearly fixed and is described by the solar constant, G_{sc}. The World Radiation Center (WRC) has adopted a value of 1 367 W/m² for this constant (Duffie and Beckman, 1991). The WRC standard spectral irradiance curve at mean earth-sun distance (outside the atmosphere) is given in figure 5.2. This "extraterrestrial" radiation is the radiation the earth would receive in the absence of the atmosphere. Due to the eccentricity of the earth's orbit, this radiation varies over the year. The solar radiation that is received at the surface of the earth is reduced due to atmospheric scattering (by air molecules, water and dust) and atmospheric absorption (by O_3, H_2O, and CO_2). The degree to which scattering occurs depends partly on the path length of the radiation (described by the "air mass"[20]). Figure 5.2 shows the spectral distribution of beam irradiance for different air masses. Solar radiation outside the atmosphere has most of its energy in the wavelength range of 0.3 - 3 μm. Most of the solar radiation that reaches the earth is found in the wavelength range of 0.29 - 2.5 μm.

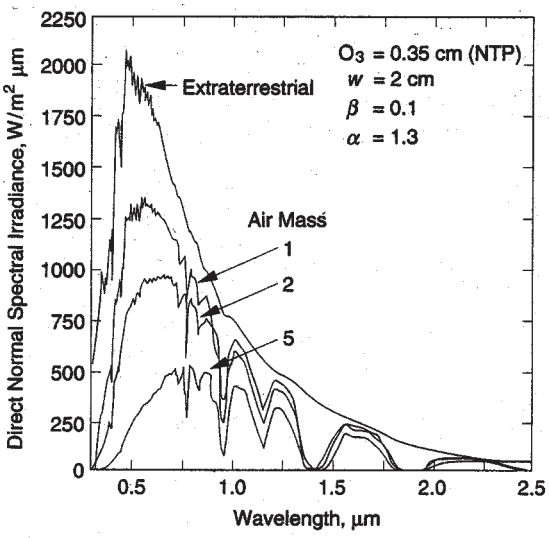

Figure 5.2 *The WRC standard spectral irradiance curve for extraterrestrial radiation at mean earth-sun distance and examples of the spectral distribution of beam irradiance for different air masses (Duffie and Beckman, 1991).*

20. $m = 1/\cos(Q_z)$ (for $0 < Q_z < 70°$).

5.2.2 Radiation measurements

Solar (short-wave) radiation is radiation originating from the sun in the wavelength range of 0.3 - 3 μm. Long-wave radiation originates from sources at temperatures near ordinary ambient temperatures. This radiation has wavelengths greater than approximately 3 μm.

For measuring solar radiation, different instruments are used. A *pyrheliometer* uses a collimated detector for measuring the (beam) solar radiation from the sun and from a small portion of the sky around the sun at normal incidence. A *pyranometer* is used for measuring the total (beam + diffuse) hemispherical solar radiation. If the detector is shaded from the beam radiation by a shading ring, the pyranometer can be used for measuring the diffuse radiation. Since the ring shades the pyranometer from part of the diffuse radiation, a correction for this shading must be made.

The pyranometer can either be placed horizontally or mounted in the same plane as the collector surface in order to measure the radiation onto the collector plane. Horizontally measured beam radiation (I_b) can be recalculated to radiation on a tilted surface (I_{bt}) by the following equation (see also figure 5.3):

$$I_{bt} = I_b \frac{\cos(\Theta)}{\cos(\Theta_z)} = I_b R_b \tag{5.2}$$

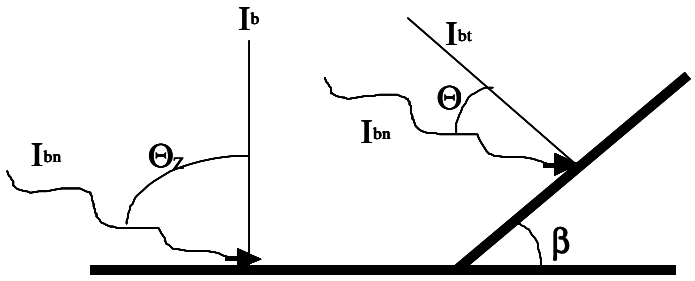

Figure 5.3: *Beam radiation on horizontal (I_b) and tilted surfaces (I_{bt}). I_{bn} is beam radiation measured on a plane normal to the direction of propagation. Θ_z is the zenith angle and Θ is the angle of incidence onto the tilted surface.*

Different models can be used for determining the total radiation onto a tilted plane from radiation measurements on the horizontal plane. The different methods treat the diffuse part in different ways. One such method is the Hay and Davies model (Duffie and Beckman, 1991), which is used in MINSUN.

$$I_t = I_b R_b + I_d \left[(1 - A_i) \left(\frac{1 + \cos(\beta)}{2} \right) + A_i R_b \right] + I \rho_g \left(\frac{1 - \cos(\beta)}{2} \right) \quad (5.3)$$

where A_i is the anisotropy index, which determines the portion of the horizontal diffuse radiation that is to be treated as forward scattered. (If A_i is zero, the diffuse radiation is considered to be completely isotropic.)

6 The dynamic collector model and incidence angle dependence

6.1 Collector performance model and incidence angle modifier

The purpose of the dynamic collector test method is to characterize the solar collector performance from a short testing period with no requirement for stable climatic conditions. The mathematical model given in eq 6.1 is used for characterizing the collector output ($\dot{q}_u$) (Perers, 1993a). This model is based on a standard collector model, augmented by correction terms for beam and diffuse incidence angle modifiers, thermal capacitance, wind speed, and sky temperature. This results in a rather complete characterisation of the collector. If an external booster reflector is used, the extra reflected radiation has to be added (Perers, 1997, and Perers and Karlsson, 1998b). The contribution of the reflector to the irradiance on the collector cannot, however, be separated from the direct contribution from the sun onto the collector, since the components are strongly correlated.

$$\dot{q}_u = F'(\tau\alpha)_e K_{\tau\alpha b}(\Theta) I_b + F'(\tau\alpha)_e K_{\tau\alpha d} I_d - F'U_0 \Delta T - F'U_1 (\Delta T)^2 - (mC)_e \frac{dT_f}{d\tau} - \\ - F'U_w \Delta T w - F'U_{sky} \Delta T_{sky} - U_p \Delta T \tag{6.1}$$

In the equation $F'(\tau\alpha)_e$ (later on denoted η_0) is the so-called "zero loss efficiency", I_b and I_d are the beam and diffuse radiation components respectively, $F'U$ (later on denoted k) is the heat loss factor, and ΔT is the temperature difference between the collector and the collector surroundings

($\Delta T = \frac{T_{in} + T_{out}}{2} - T_{amb}$). The factor $(mC)_e$ is the effective collector thermal capacitance and $\frac{dT_f}{d\tau}$ is the mean time derivative for the average fluid temperature (T_f). The wind speed (w) and sky temperature (T_{sky}) parameters may be excluded for most glazed collectors. In this work, the piping heat losses (U_p) have also been omitted, resulting in a study of only the collector.

The factor $K_{\tau\alpha b}(\Theta)$ is an incidence angle modifier (for beam radiation) that takes into account the effects of varying incidence angles (Θ) during the day. For flat-plate collectors, the modifier can be modelled with the standard b_0 equation (Duffie and Beckman, 1991, and Perers, 1993a):

$$K_{\tau\alpha}(\Theta) = \frac{(\tau\alpha)}{(\tau\alpha)_n} = 1 - b_o\left(\frac{1}{\cos(\Theta)} - 1\right) \tag{6.2}$$

where b_0 is a constant called the incidence angle modifier coefficient. (A higher b_0 factor results in a quicker decrease in the optical efficiency with the incidence angle.) One advantage of this equation for collector calculations is that it gives a cut off angle before Θ = 90°, just as the shading effect. Using equation 6.2, the zero loss efficiency for beam radiation can be expressed as:

$$\eta_{0b}(\Theta) = \eta_{0b} K_{\tau\alpha b}(\Theta) = \eta_{0b}\left[1 - b_o\left(\frac{1}{\cos(\Theta)} - 1\right)\right] \tag{6.3}$$

where η_{0b} is taken at normal incidence.

According to equation 6.3, a plot of $\eta_{0b}(\Theta)$ versus the factor (1/cos(Θ)-1) should form a single straight line with intercept η_{0b} and a negative tilt corresponding to the product $\eta_{0b}b_0$. An analysis of the incidence angle dependence of the solar collector indicates, however, that using a single b_0 factor might lead to errors in the estimated output (Paper III). Figure 6.1 shows the optical efficiency obtained from measurements on a flat-plate collector. The figure shows that two different lines can be fitted to the dots, indicating that the b_0 factor depends on the incidence angle. The problem is that the standard b_0 function decreases monotonically from 0°, while the true optical efficiency curve is often almost constant up to about 40°. For larger incidence angles, η_{0b} then decreases noticeably. Since most of the useful energy is delivered at low incidence angles, the use of a constant b_0 factor for all incidence angles usually underesti-

mates the output. One solution to this problem can be to use different b_0 factors in different incidence angle intervals, or to use another function to model the output. This will be further discussed in chapter 8.

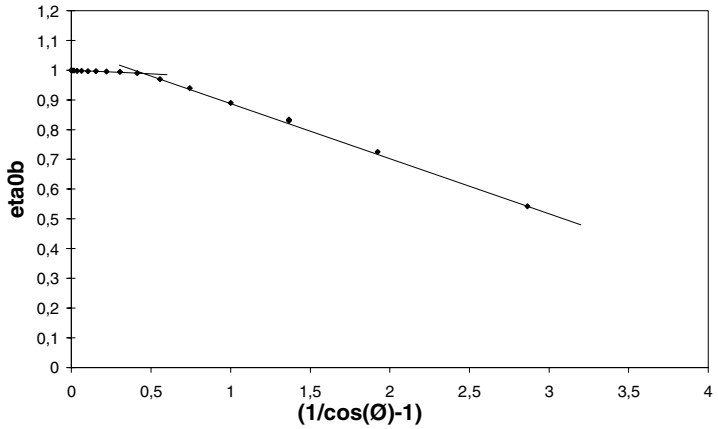

Figure 6.1 *$\eta_{0b}(\Theta)$, calculated from data measured on a flat-plate collector, plotted as a function of the factor (1/cos(Θ)-1). According to eq 6.3, the dots should form a single straight line if a single constant b_0 factor could be used for all incidence angles. (Paper III)*

6.2 Definition of different angles

Since the earth rotates, the position of the sun relative to the earth changes during the day. This means that the incidence angle of the radiation onto a collector surface will vary during the day. Since both the absorptance and the transmittance depend on the incidence angle, the optical properties of the collector also vary over the day. This is a matter that has to be considered when evaluating a solar collector.

The position of the sun relative to the collector can be described by using different angles (figure 6.2). The angle of incidence (Θ) of beam radiation onto the collector surface is the angle between the direction of the beam radiation and the normal vector to the surface. This angle can be calculated as (see appendix A):

$$\cos(\Theta) = \left(\sin(\alpha_s)\cos(\beta) + \cos(\alpha_s)\sin(\beta)\cos(\gamma_s - \gamma_c)\right) \qquad (6.4)^{21}$$

21. The symbols are explained in figure 6.2 and in the nomenclature list.

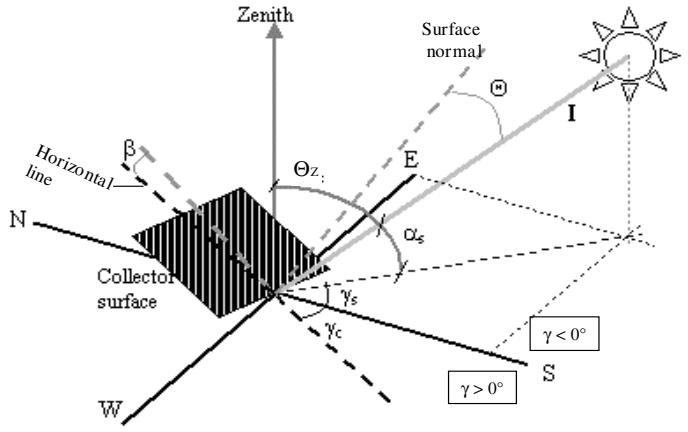

Figure 6.2 *Different angles describing the position of the sun relative to the collector surface: Θ_z = zenith angle, α_s = solar altitude angle, γ_s = solar azimuth angle, γ_c = surface azimuth angle, β = collector tilt, and Θ = incidence angle of beam radiation on collector surface.*

For an asymmetric collector (e.g. a MaReCo), the angle analysis has to be made in different directions. Figure 6.3 gives the definition of the transverse and the longitudinal analysis planes. The longitudinal plane is the plane including the surface normal and a line along the collector extension. The transverse plane includes the surface normal and is perpendicular to the longitudinal plane. For a south-facing collector trough with a horizontal axis, the transverse plane equals the vertical north-south plane.

The beam radiation onto the collector surface can be treated as a vector, which can be divided into two orthogonal components (figure 6.3). One component (I_T) is the projection of the radiation onto the transverse plane. The other component ($I_{//}$) is parallel to the collector glazing. Only the perpendicular component contributes to the energy output. The angle between I_T and the surface normal is the transverse incidence angle (Q_T). This angle is calculated as:

$$\Theta_T = 90 - \beta - \alpha_p \tag{6.5}$$

where α_p is the "profile angle" defined in figure 6.4. This angle determines whether the projected radiation is inside or outside the acceptance angle interval of the collector, i.e. whether the incident radiation is within the angle interval where it will be collected by the absorber. α_p is calculated as:

$$\tan(\alpha_p) = \frac{\tan(\alpha_s)}{\cos(\gamma_s - \gamma_c)} \tag{6.6}$$

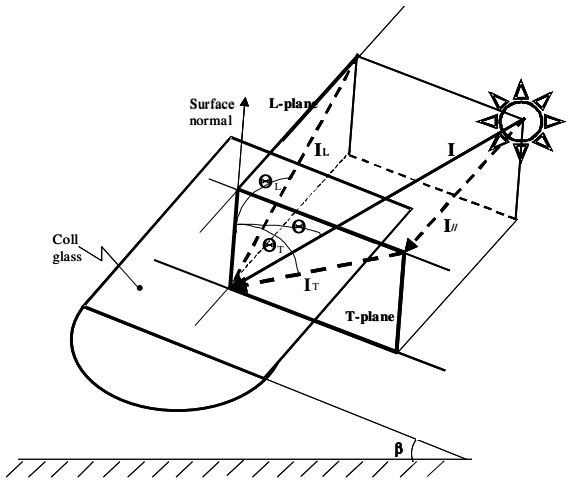

Figure 6.3 *Transverse (T) and longitudinal (L) planes and incidence angles (Θ_T and Θ_L respectively). Θ is the incidence angle between the solar radiation (I) and the surface normal. The radiation can be divided into two components: I_T (the projection on the transverse plane) and $I_{//}$ (a component along the glazing). I_L is the projection of I on the longitudinal plane.*

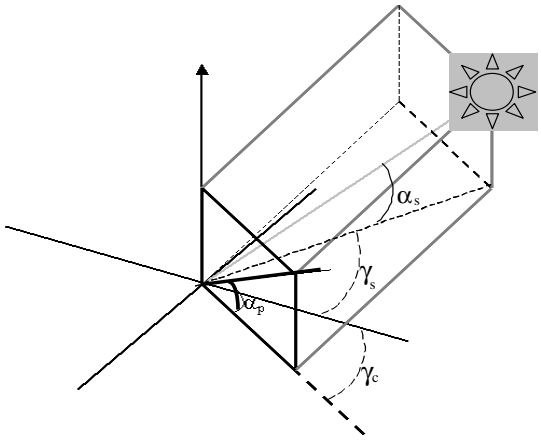

Figure 6.4 *α_p is the profile angle, i.e. the projection of α_s on a vertical plane, including the surface normal, perpendicular to the extension of the collector.*

For a south-facing collector, the profile angle is the same as the effective solar height (H_{eff}) for radiation projected in the vertical north-south plane. Figure 6.5 illustrates how this projected angle varies during the day for different dates during the year. For a south-facing collector, α_p coincides with the conventional solar height (α_s) at noon. During the equinoxes, the effective solar height is constant with a value of $(90 - \phi)°$. Note that the effective solar height has a minimum, and not a maximum, at noon during the summer months.

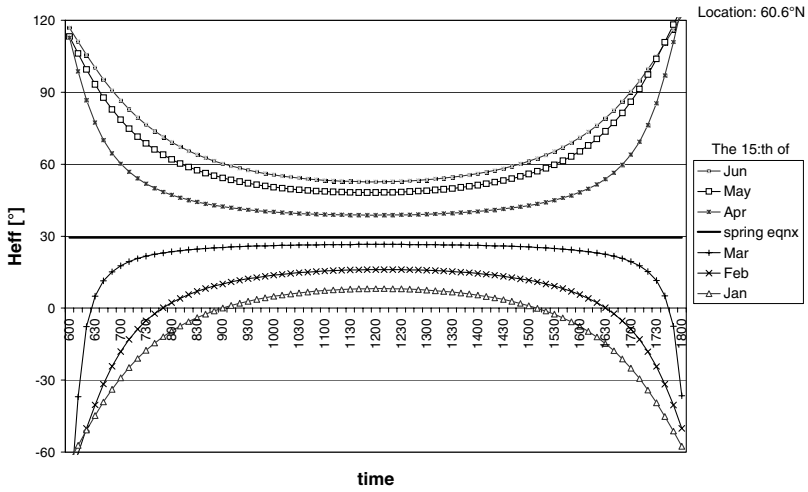

Figure 6.5 *The effective solar height (H_{eff}) in the north-south plane for different dates during the first six months of the year. The diagram is valid for Stockholm latitude.*

The angle between the projection of the solar radiation onto the longitudinal plane and the collector surface normal is the longitudinal incidence angle (Θ_L). This angle is calculated using the following relation:

$$\tan^2(\Theta) = \tan^2(\Theta_T) + \tan^2(\Theta_L) \tag{6.7}$$

Figure 6.6 shows the relation between the total incidence angle (Θ) and the two projected angles (Θ_T and Θ_L). Note that all shown combinations of the angles are not found for concentrating systems, since the combination of angles is determined by the movement of the sun and by the system geometry.

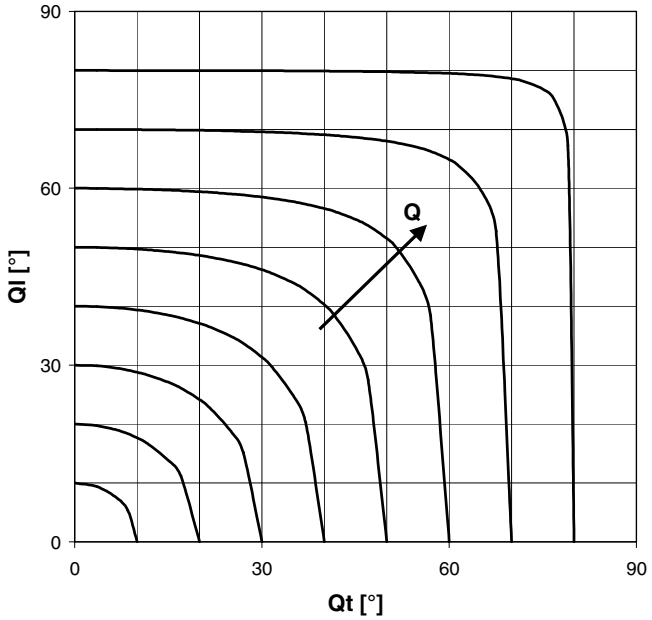

Figure 6.6 *Relation between Θ, Θ_L and Θ_T. The curves represent constant Θ (increasing in steps of 10° from 10° to 80°).*

Figure 6.7 shows the two projected incidence angles for a south-facing collector. During the equinoxes, Θ_T has a constant value of (ϕ - β), and for all days during the year, Θ_L has a minimum (0°) at noon. The minimum angle of incidence (and maximum direct irradiance) on a south-facing fixed surface is obtained if the surface is tilted with an angle (β) equal to the latitude (ϕ).

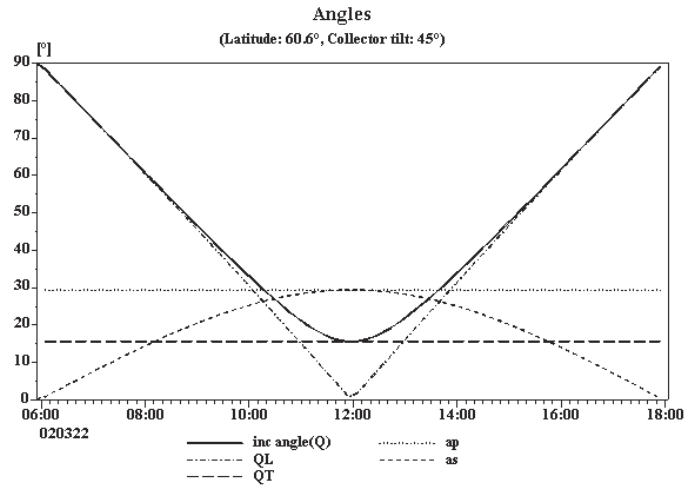

Figure 6.7 *The incidence angle (Q), the transverse (Q_T) and longitudinal (Q_L) incidence angles, the solar altitude (as), and the effective solar height (ap) for a south-facing collector on March 22 (when $\delta \approx 0°$). The figure shows that Θ_T and α_p are constant during that day. (The reason that Θ_L is not 0 exactly at noon is that the calculations were made for values from a database containing 10-minute mean values.)*

The angle calculations presented above are used in the work with the biaxial incidence angle modifier presented in chapter 8.

7 Measurements

7.1 Outdoor measurements

In order to evaluate the energy output from different collectors, prototypes were installed at VUAB´s laboratory in Älvkarleby (Sweden). Here a total of 15 collectors can be evaluated at the same time. The inlet temperature of the collectors can be controlled to get a variety of operating conditions, covering all main conditions which occur during a full year of operation. By running the pump in the collector loop continuously during the test period, all-day data, which increases the variation range for the input variables, can be used for the evaluation. This leads to a better accuracy for the individual parameters. The continuous operation also reflects the internal state of the collector during the preheating (and cooling) phase. Using data from the whole day therefore means that the model more accurately predicts the collector behaviour. The all-day measurements thereby lead to a better prediction of the long-term collector performance from a shorter test period. Six of the prototype collectors can be connected in series with a common flow. In this system, the water is cooled after each collector in order to get the same inlet temperature to all of them. This "common-flow system" facilitates comparisons between e.g. different glazings on similar collector boxes.

The evaluations in this work were done according to the principle of dynamic testing (chapter 6) where equation 7.1 is used for modelling the collector output.

$$\dot{q}_u = \eta_{0b}(\Theta) I_b + \eta_{0d} I_d - k_1 \Delta T - k_2 (\Delta T)^2 - (mC)_e \frac{dT_f}{d\tau} \qquad (7.1=6.1)$$

During the measurements the inlet (T_{in}) and the outlet (T_{out}) water temperatures were recorded together with the flow of water/glycol ($\dot{V}$) through the collector. It is important to note that the fluid temperature is determined correctly only if there is a mass flow in the collector loop. Also the total and the diffuse solar radiation (I_{tot} and I_d) and the ambient temperature (T_{amb}) were measured. Here it is important to shield the ambi-

ent temperature sensor from direct radiation from the sun. The radiation is measured with pyranometers on the horizontal plane and on collector planes of interest. Figure 7.1 shows the insolation on planes with different tilts (horizontal, 30°, and 45°) during a day with clear weather. The alignment of the pyranometers is crucial in order to get useful measured data. The diffuse radiation is measured by using a pyranometer equipped with a shadow ring. A correction factor is then applied to the measured data in order to determine the actual diffuse radiation. The radiation is also measured with a sun tracking pyranometer and a tracking pyrheliometer. The equipment used for most of the measurements in this work is specified in appendix B.

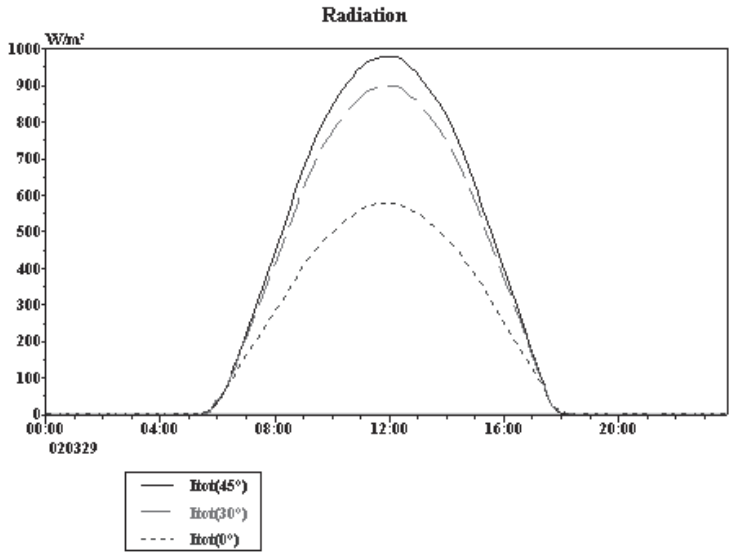

Figure 7.1 *Total insolation (Itot) onto the horizontal plane (0°) and onto planes with tilts of 30° and 45°.*

The measured data are sampled with a Campbell Scientific data logger each 20th second, and the sampled values are stored as 10-minute mean values for subsequent analyses. Since the one-node thermal capacitance term is based only on information of the fluid temperature variation within the time step, data gaps can be accepted. This means that erroneous data can be omitted from the database before the final parameter identification.

For the evaluation of the collected data, the statistics program SISS[22] was used. In the analyses, the beam radiation onto the collector plane was calculated together with different angles (e.g. the incidence angle and the effective solar height). Also the measured and the modelled output from the collector prototypes were calculated. The modelled (or "estimated") output is calculated with eq 7.1 and the measured (or actual) collector output ($\dot{q}_{um}$) is calculated as:

$$\dot{q}_{um} = \frac{\rho \dot{V} c_p (T_{out} - T_{in})}{A_c} \tag{7.2}$$

where ρ and c_p are the density and the specific heat of the collector fluid and A_c is the collector area.

7.2 Examples of evaluation

7.2.1 Description of the evaluation procedure

In order to exemplify the evaluation procedure, two evaluations are briefly described below. The studied collectors are one flat-plate collector and one MaReCo (figure 7.2). The flat-plate collector is used as a reference collector at Vattenfall's laboratory in Älvkarleby. This collector has a selective absorber, one cover glass and a Teflon foil between glass and absorber. The collector has an area of 13.1 m², is facing south, and has a tilt of 45°. The other example collector is an EPS-MaReCo further described in (Helgesson, 1999, and Helgesson et al, 2000a). The EPS-MaReCo has a glass tilt of 30° and an internal reflector made of laminated aluminum foil.

22. A statistics program distributed by the company ANASYS AB (www.anasys.se).

Figure 7.2 *Photos of a) the flat-plate collector used as a reference at VUAB's laboratory and b) the evaluated EPS-MaReCo.*

The first step in the analysis is to determine the collector parameters to be used in the collector model (eq 7.1). This is done by Multiple Linear Regression (MLR) on measured data from a number of days with varying operating conditions (section 7.1). The results from the two evaluations are given in table 7.1. More detailed printouts of the results are presented in appendix C. Figure 7.3 shows the energy output from the reference collector together with the total radiation onto the collector plane for a day with fairly clear weather.

Table 7.1 Collector parameters determined from evaluations of a flat-plate collector, and an EPS-MaReCo.

Collector	η_{0b} [–]	b_0 [–]	η_{0d} [–]	k_1 [W/m²,K]	k_2 [W/(m·K)²]	$(mC)_e$ [J/m²,K]
Flat-plate (ref)	0.792	0.20	0.705	2.02	0.03	7 004
EPS-MaReCo	0.51	0.26	0.38	1.22		863

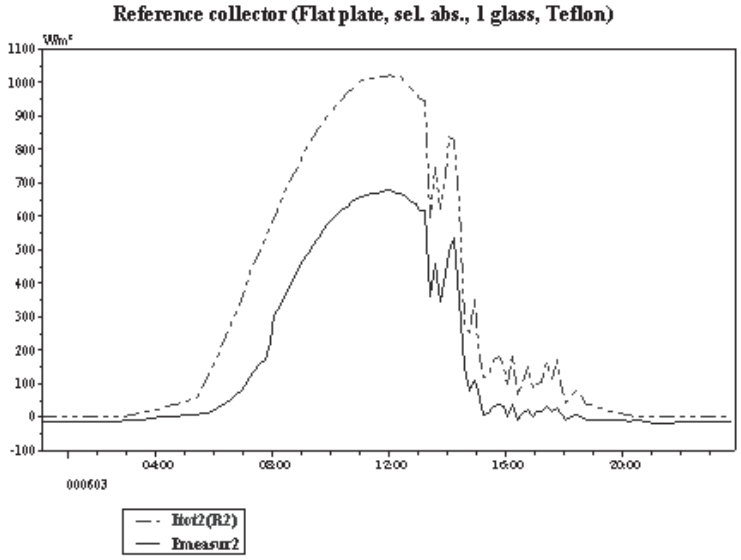

Figure 7.3 *Energy output (Pmeasur2) from the reference collector and total radiation onto the collector plane (Itot(R2)) for one evaluation day.*

In order to verify the model and the determined parameters, the modelled output (calculated with eq 7.1) is compared with the measured output in both a ”daily diagram” and a ”Pmodel/Pmeasure diagram”. Figure 7.4 shows the results for the flat-plate collector. In the Pmodel/Pmeasure diagram the modelled output is plotted as a function of the measured output. Ideally, the dots should be concentrated around a straight line with intercept 0 and slope 1. The two diagrams show that the model for the flat-plate collector agrees well with the true, measured, output.

Figure 7.5a is a daily diagram (also including the total insolation on the collector plane) for the EPS-MaReCo. This diagram shows that the modelled output follows the measured output well even if there are sudden changes in insolation, e.g. due to rapidly passing clouds. Figure 7.5b shows the Pmodel/Pmeasure diagram for the EPS-MaReCo. As can be seen from these two diagrams, the agreement between the modelled and the measured output is good, and therefore the determined parameters can be accepted also for the EPS-MaReCo.

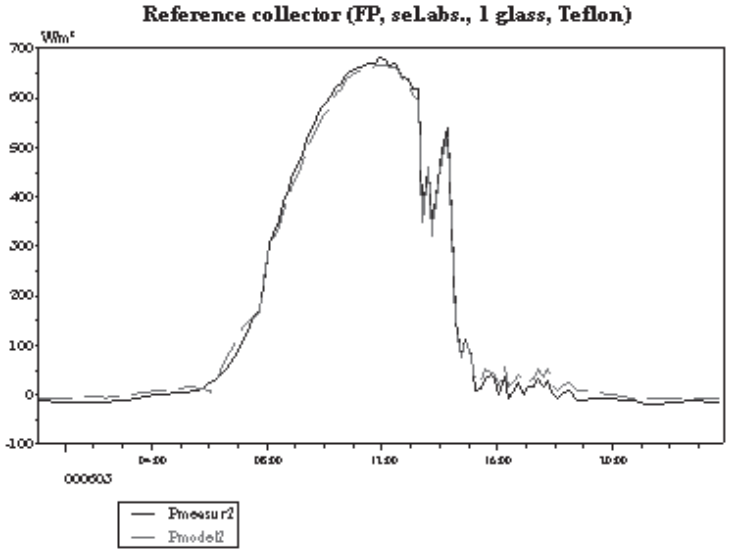

a)

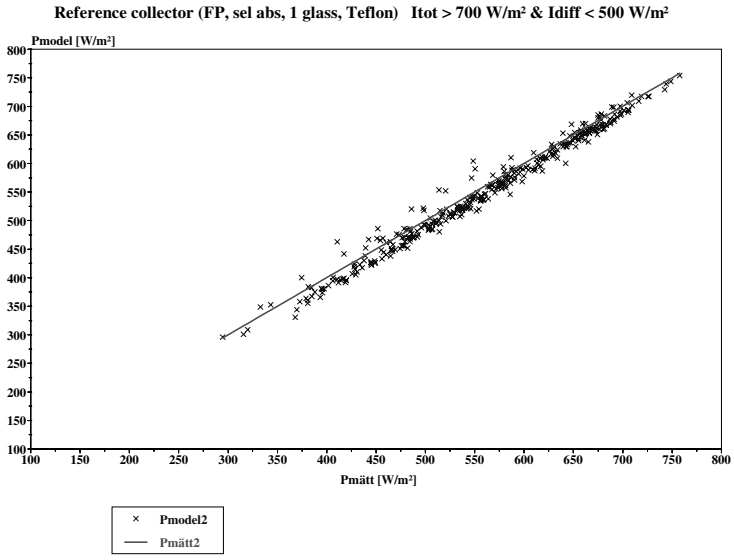

b)

Figure 7.4 *Examples of diagrams (a = a daily diagram, and b = a Pmodel/ Pmeasure diagram for June 2000) for verification of the collector model (Pmodel2) and the model parameters, according to table 7.1, for the evaluated flat-plate collector. Pmeasur2 is the measured energy output. The dots in diagram b should, ideally, concentrate around the straight line.*

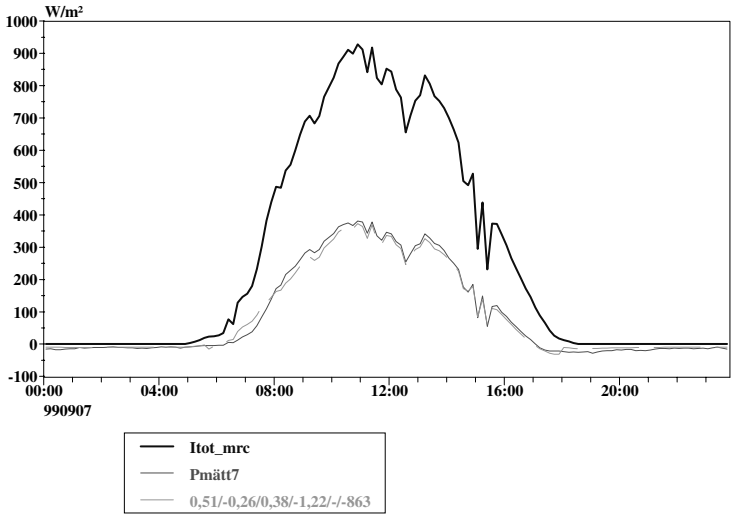

a)

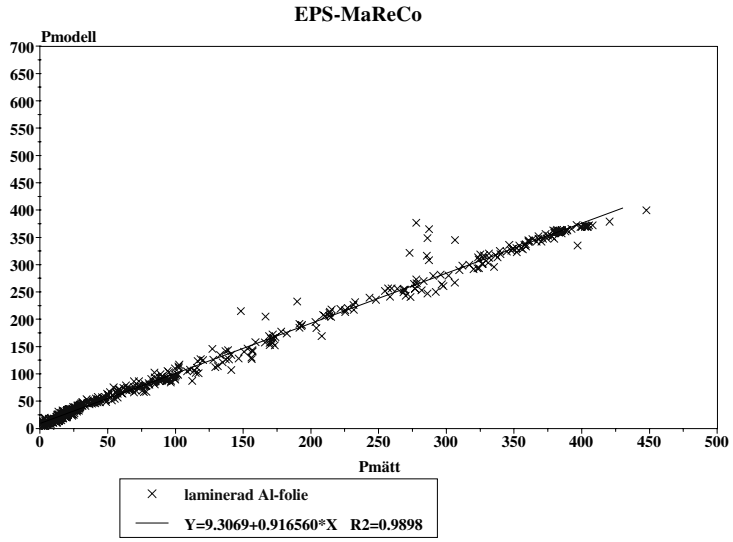

b)

Figure 7.5 *a) A "daily diagram" for verification of the collector model and the collector parameters determined from the evaluation of the EPS-MaReCo. Itot_mrc (blue solid thick line) is the total insolation onto the collector glazing, Pmätt7 (red line) is the measured output and the green dashed line is the modelled output.*
b) Pmodel/Pmeasure-diagram for the EPS-MaReCo. (Helgesson, 1999)

The last step in the analysis is to estimate the possible annual energy output from the collector. In order to do this the collector parameters are used in the simulation program MINSUN. Climatic data for Stockholm 1986 were used as a "reference year" for the simulations. Table 7.2 gives the estimated output from the flat-plate collector and the EPS-MaReCo evaluated above. The outputs are given for three different operating temperatures: 25°C (representative for pool heating), 50°C (domestic hot water heating systems), and 75°C (for combisystems). Due to higher heat losses, the output is lower at higher operating temperatures.

Table 7.2 Results from simulations with the MINSUN program for the two evaluated collectors. Energy output is given in kWh/m²,yr. Also the total insolation onto the collector planes is given.

T_{op}	25°C	50°C	75°C	I_{tot}
Flat-plate collector	683	491	308	1 129
EPS-MaReCo	351	288	242	1 113

The measured data can also be used to calculate the collector efficiency (η) as the ratio between the useful energy output and the total insolation onto the collector:

$$\eta = \frac{\dot{q}_{um}}{I_{tot}} = \eta_0 - U\frac{\Delta T}{I_{tot}} \qquad (7.3)$$

Figure 7.6a shows the "efficiency diagram" for the EPS-MaReCo evaluated above, and figure 7.9b shows a diagram where the efficiencies for some different collectors have been plotted versus the factor $\Delta T/I_{tot}$. According to eq 7.3 the dots should form a straight line with an intercept equal to η_0 and a slope representing the U-value. The diagram can be used for comparing the performance of different collectors in different temperature intervals.

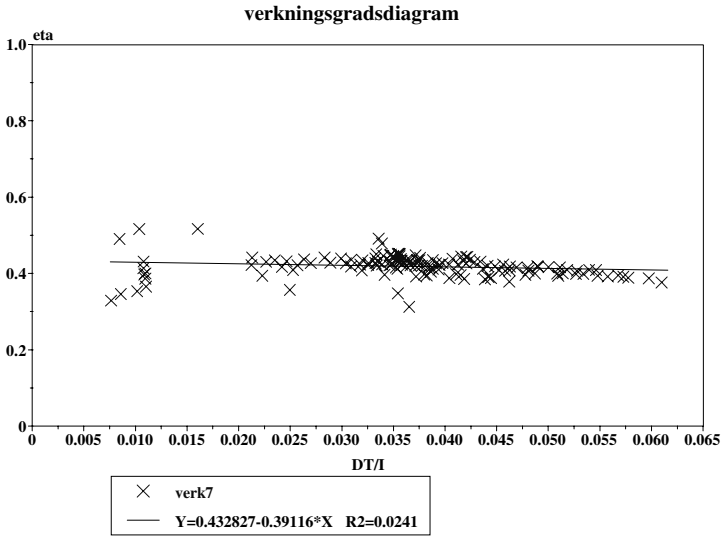

a)

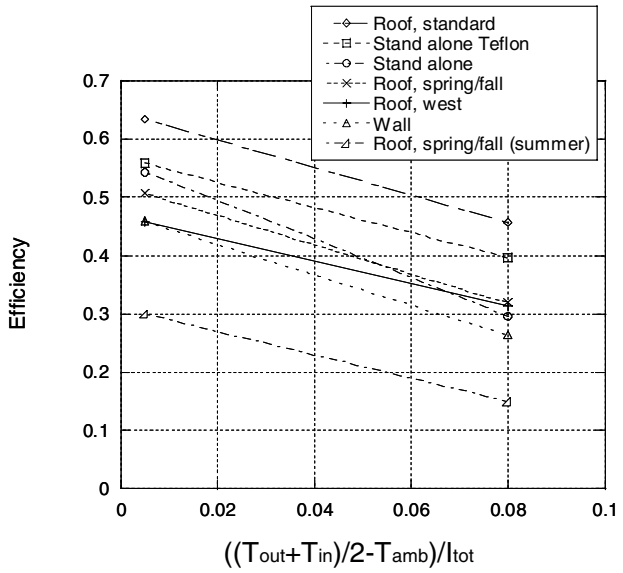

b)

Figure 7.6 *a) The efficiency diagram for the EPS-MaReCo (with I > 450 W/m²) (Helgesson, 1999).*
b) An efficiency diagram (with least square linear fit lines) comparing different investigated MaReCos (Paper IV).

Also the optical efficiency (η_0) for global irradiance can be calculated from the measurements:

$$\eta_0 = \left(\dot{q}_{um} + U\,\Delta T\right) \Big/ I_{tot} \tag{7.4}$$

The result for the flat-plate collector above is given in figure 7.7. The optical efficiency is greater than the total collector efficiency since the losses have then been removed.

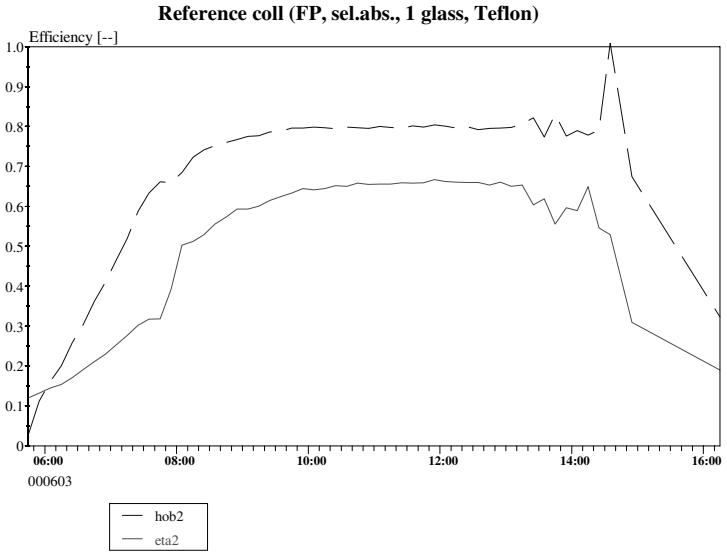

Figure 7.7: Measured total collector efficiency (eta2) and calculated optical efficiency (hob2) for the reference flat-plate collector.

The incidence angle dependence can be studied by plotting the optical efficiency versus the incidence angle. This is shown for the flat-plate collector in figure 7.8. The figure shows that the efficiency curve is relatively flat for lower incidence angles, but that it decreases rather steeply at higher angles.

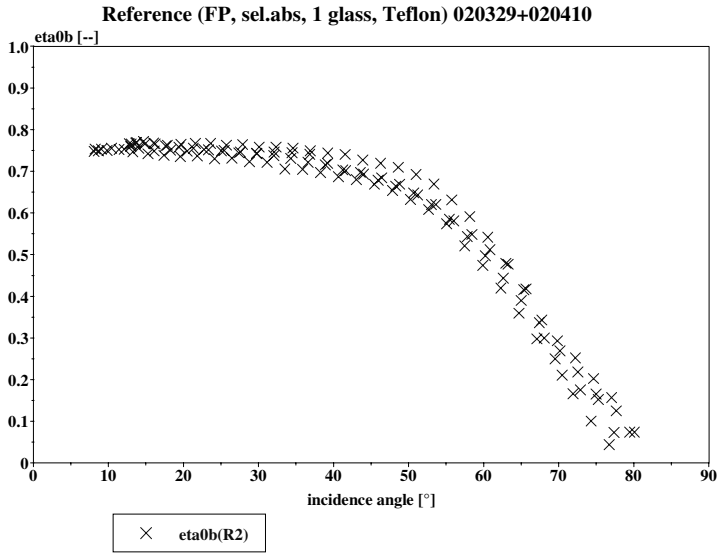

Figure 7.8 *Incidence angle dependence of the global optical efficiency for the reference collector. (Data from two days are used.)*

7.2.2 Evaluation of a combined solar collector + reflector

The optimal tilt for a collector placed in Sweden is between 30 and 60°. For flat horizontal roofs, there are few optimal solutions for solar energy applications. In a project (Paper I) a ”collector + reflector” combination was evaluated. The collector and the reflector are mounted on heavy concrete beams which distribute the load and keep the collector in place. The reflector has a parabolic shape and is made of laminated aluminum foil on plastic. Figure 7.9 shows a photo of the evaluated prototype.

Data from collector measurements made by SP were used in the evaluation together with a collector-reflector model and an assumed value of 0.80 for the total reflectance of the reflector. A MINSUN simulation estimates the yearly energy output to 499 kWh/m² (at T_{op} = 50°C) for the collector + reflector combination (figure 7.10). The evaluation shows that the reflector increases the energy output by about 23.5%. Even though the absolute increase is almost independent of the operating temperature, the relative increase is higher at higher temperatures.

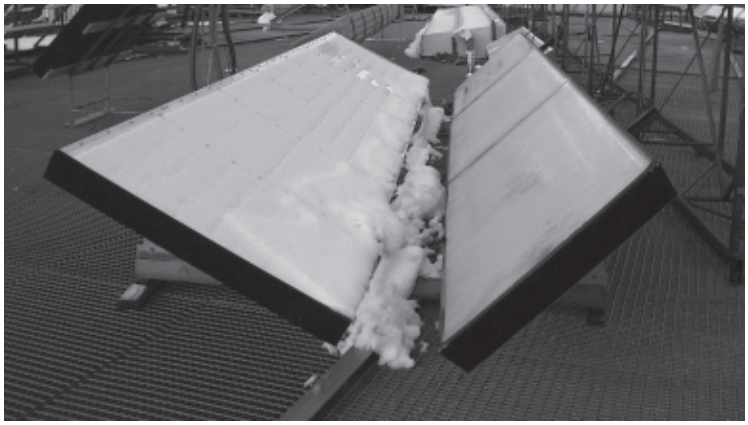

Figure 7.9 *The collector prototype that was evaluated at VUAB. The collector is tilted 45° and has an area of about 6.1 m². The collector box has a height of only about 90 cm.*

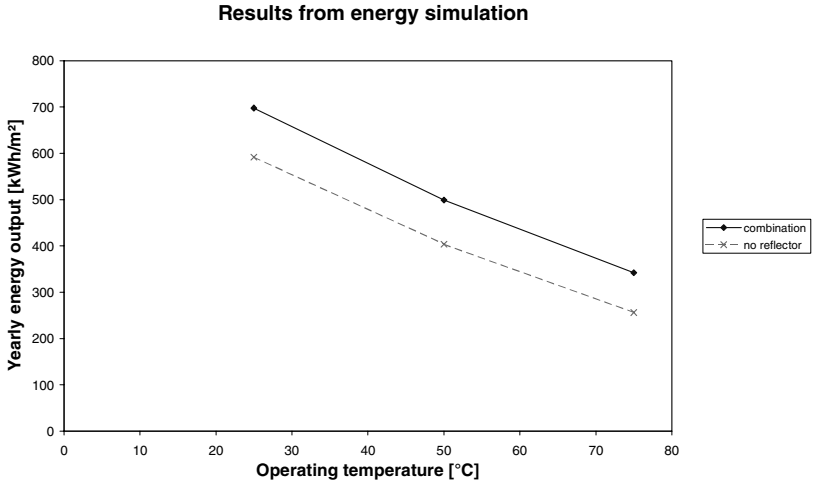

Figure 7.10 *Results from the simulation of yearly energy output. (Climatic data = Stockholm 1986.)*

The collector + reflector combination was also tested in a 210 m² large demonstration plant in Sweden. That investigation showed that the plant can give a yearly energy output of about 600 kWh/m² (at T_{op} = 40°C).

This is in agreement with the results in figure 7.10. A conclusion is that the evaluated construction is an interesting alternative for solar energy installations on horizontal roofs.

7.3 Measurements of incidence angle dependent optical properties

7.3.1 Solar absorbers

Although the solar absorptance of a collector absorber is a function of the incidence angle of the radiation onto the absorber, it is usually determined at near normal angle of incidence. The incidence angle dependence of the absorptance of two commercial selective solar absorbers was investigated in a project both by optical measurements at Uppsala University and by outdoor dynamic collector testing at VUAB's laboratory in Älvkarleby. The purpose of the study was to investigate how the incidence angle dependence of the absorptance affects the collector efficiency. Both absorbers had the same type of rolled aluminum substrate. One of the absorbers had a selective coating of electrochemically deposited nickel-pigmented anodized aluminum oxide (Ni-Al_2O_3) and the other had a coating of sputtered nickel/nickel oxide (Ni-NiO_x). Both types of coatings are absorbing in the solar spectral range due to small nickel metal particles, but the particle shapes, the oxide matrix, and the layer stratification differ. The angle dependent solar absorptance was, for different incidence angles, calculated from measurements of total spectral reflectance in the wavelength range 300 - 2 500 nm (Tesfamichael and Wäckelgård, 1999 and 2000). The result is given in figure 7.11, which shows the solar absorptance as a function of the incidence angle for the two tested absorbers. The reflectance of the coatings increases with increasing incidence angles. The difference between the two coatings is most pronounced at higher angles of incidence. The absorptance of the Ni-Al_2O_3 coating is almost constant over a wide range of incidence angles, with a steep drop at higher incidence angles. Due to thin film interference effects, the Ni-Al_2O_3-coated absorber (with a double-layer structure) has a better solar absorptance than the Ni-NiO_x coating at higher angles of incidence. The graded index structure of the sputtered Ni-NiO_x coating produces no interference patterns, and the solar absorptance decreases gradually already from near normal incidence, with a steep drop

at about 40°. A comparison of the two coatings shows that the solar absorptance of the NI-NiO_x coating starts to drop steeply at a lower angle of incidence.

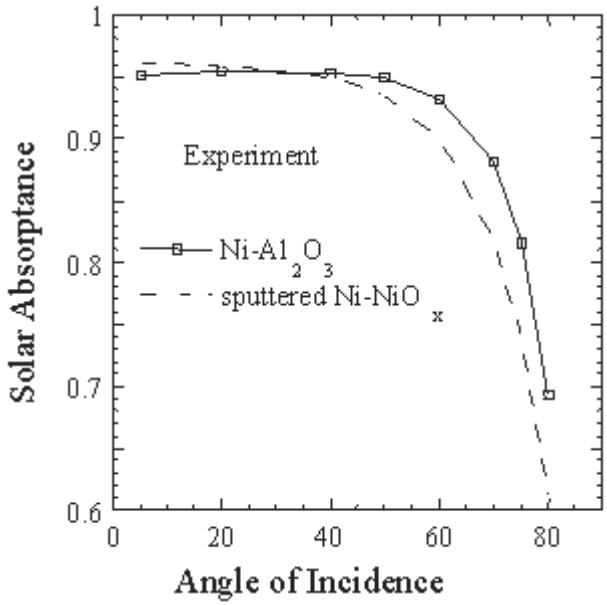

Figure 7.11 *Solar absorptance of two different coatings as a function of the incidence angle; nickel-pigmented aluminum oxide (Ni-Al_2O_3) and nickel/nickel oxide (sputtered Ni-NiO_x). (Paper II)*

The impact of the incidence angle dependent absorptance was also studied by outdoor testing (Paper II). In order to facilitate the comparison, the two absorbers were tested simultaneously in identical collector boxes. The evaluation was performed according to the principle of dynamic testing described in section 7.1. The results showed that there was no significant difference in the estimated yearly energy output between the two collectors (434 and 433 kWh/m² at T_{op} = 50°C for the Ni-Al_2O_3 and Ni-NiO_x surface respectively). The incidence angle dependence was studied by determining the optical efficiency for beam radiation in different incidence angle intervals. Figure 7.12 shows that the Ni-Al_2O_3 absorber has a slightly better performance at high incidence angles. This confirms the optical measurements according to figure 7.11. The difference is, however, smaller due to the impact of the cover glass,

Figure 7.12 *Comparison of the optical efficiency of the two tested solar collectors with different types of selective absorber.*

7.3.2 Solar glazings

In order to study the influence of different glazings on the collector output, comparative tests were made at VUAB in Älvkarleby. A method for careful outdoor characterization of the incidence angle dependent solar transmittance of solar glazings was developed (Paper III). The method was then used for investigating the performance of a structured glass (from AFG) and a flat glass (from Saint-Gobain). In the tests, the influence of antireflection treatment was also investigated. Four different cases were studied:

- Structured AFG glass with structure inwards
- AR-treated structured AFG, structure inwards
- AR-treated structured AFG, structure outwards
- AR-treated flat-plate glass.

In order to get comparative data between the different glazings, two identical collectors were connected in series, with a common flow, and one of the collectors was covered with a thin Teflon foil and was used as a reference case.

Figure 7.13 clearly shows the positive influence of AR treatment on the collector output. Collector #3 is the reference collector with Teflon glazing. On collector #2 the glazing was changed between infacing AFG glass with and without AR treatment three times during the day. An en-

ergy evaluation shows that commercial AR treatment can increase the solar transmittance by 4%, increasing the annual output by 9% (at T_{op} = 50°C).

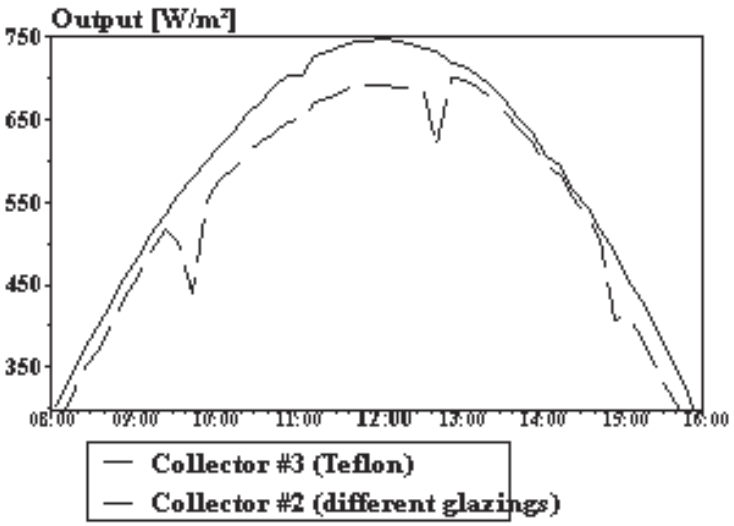

Figure 7.13 *Illustration of the influence of AR treatment. Collector #3 has a Teflon glazing. The glazing on collector #2 was changed, between AR-treated and non-AR-treated glass, three times during the day (starting with AR-treated AFG glass in the morning). (**Paper III**)*

The tests were carried out in a number of steps presented below:

1. Dynamic collector testing (section 7.1) was used in order to determine the heat loss factor, the diffuse optical efficiency, and the thermal capacitance. Equation 7.1 was used for modelling the output. In this case, the k_2 term was omitted since it did not improve the model.
2. The incidence angle dependent optical efficiencies of the collectors were determined by using equation 7.1 and eliminating the effect of heat losses and diffuse radiation using parameters from step 1:

$$\eta_{0b}(\Theta) = \left[\dot{q}_{um} - \left(\eta_{od} I_d - k_1 \Delta T - (mC)_e \frac{dT}{d\tau} \right) \right] \Big/ I_b \qquad (7.5)$$

3. Since the measurements of the different glazings were made on different days with different weather conditions, the data had to be ”normalized” in order to be comparable. The ratio between the optical

efficiency for each glazing and the reference Teflon film was calculated and plotted versus the incidence angle. One example is given in figure 7.14.

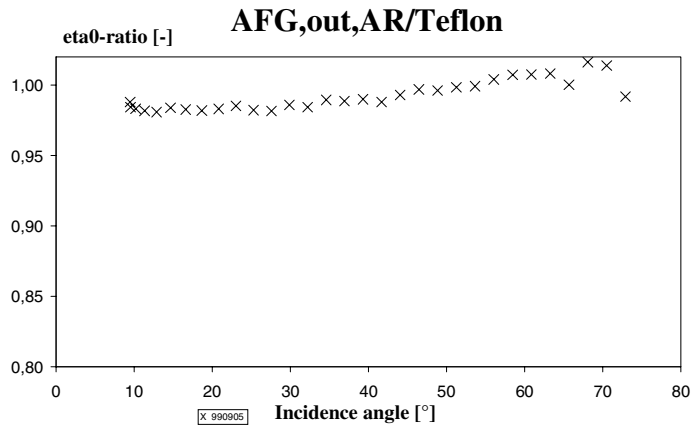

Figure 7.14 *Ratio between the optical efficiency for one of the tested glazings and the Teflon reference plotted as a function of the incidence angle.*

From one of the cases, a correction factor for the Teflon film was determined. This correction factor was then used to recalculate the optical efficiency for all glazings to comparable values, eliminating variations due to different measuring periods.

Both collectors were also tested covered with Teflon. Together with data of the angle dependent transmittance of Teflon, the results from this reference test were used to calculate the absolute values of the angle dependent optical efficiency of the four tested glazings. The use of a reference collector minimizes the influence of errors in the pyranometer measurements.

4. In order to estimate the dependence for large incidence angles, an extrapolation was made using the following expression:

$$\eta_0 = D\left(1 - b_0\left(\frac{1}{\cos(\Theta)} - 1\right)\right) \tag{7.6}$$

The b_0 factors were estimated from efficiency diagrams. The factor D was then determined by fitting calculated efficiency (eq 7.6) with the measured efficiency at an incidence angle of about 65 - 70°. The resulting diagrams are shown in figure 7.15.

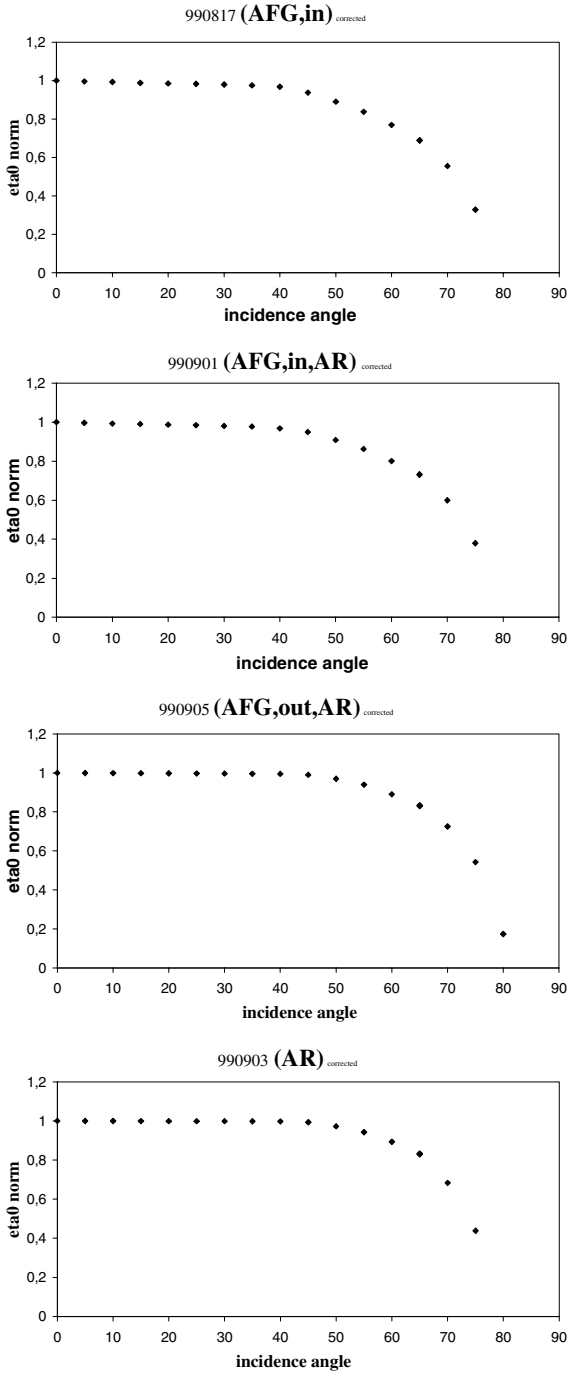

Figure 7.15 *Resulting incidence angle dependence of the optical efficiency for the four different glazings tested in the project.*

5. In order to estimate the influence of the different glazings on the annual energy output, the simulation program MINSUN was used. A detailed analysis of the incidence angle dependence indicates that the standard b_0 method does not model the angle dependence in a proper way (figure 6.1). In Paper III two simulations were made: one using the single-b_0 model (eq 6.3), and one using the incidence angle dependence according to figure 7.15 (with separate values of the optical efficiency in different incidence angle intervals). The results are given in table 7.3. A small difference in the estimation of the annual output can be noticed, where the constant b_0 method indicates a lower output. This is in agreement with the discussion in section 6.1.

Table 7.3 Estimated annual energy output in kWh/m² at T_{op} = 50°C for the studied glazings. Results from MINSUN simulation with climatic data for Stockholm 1986 and collector parameters from step 1.

	constant b_0 factor	η_{0b} according to figure 7.15
AFG,in	397	398
AFG,in,AR	432	436
AFG,out,AR	435	456
FP, AR	435	456

Samples of the glazings were also *optically characterized* by Uppsala University using a single-beam integrating sphere spectrophotometer (Nostell et al, 1999b). In the used, specially designed, integrating sphere, measurements on scattering samples can be made up to an incidence angle of 45°. Above 45° experimental problems occurs since the port of the sphere is too small, leading to too low recorded transmittance data.

Figure 7.16a shows that the increase in solar transmittance due to the *AR-treatment* is slightly higher than 3% at all incidence angles.

The most common way to install a structured glass is with the structure facing the absorber, although internal reflections in the structure may then decrease the transmittance at higher angles of incidence. Figure 7.16b shows the results from the characterization of the structured glass from AFG. This glass shows a similar incidence angle performance as a flat glass if the structure is turned outwards, but a lower transmittance for incidence angles exceeding 40° if the structure is turned inwards. The optical efficiency at high angles will therefore be better if

the structured side is turned outwards, and facing the *structure outwards* can increase the annual performance by 4% (at T_{op} = 50°C) (Paper III). This orientation of the structure might, however, increase the risk of dirt gathering on the glass, reducing the transmittance.

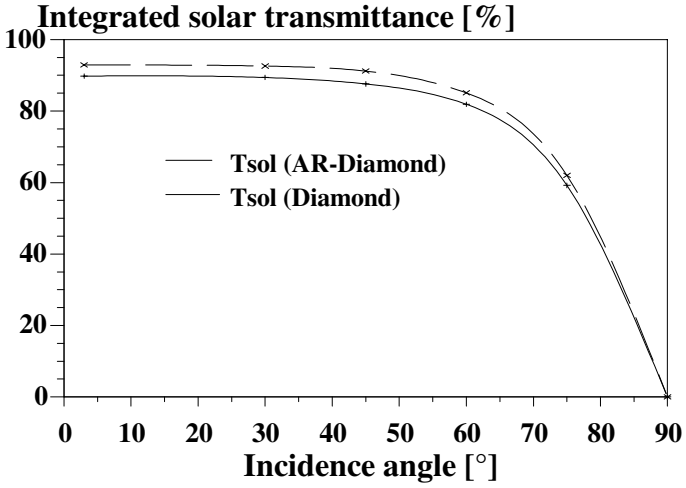

a)

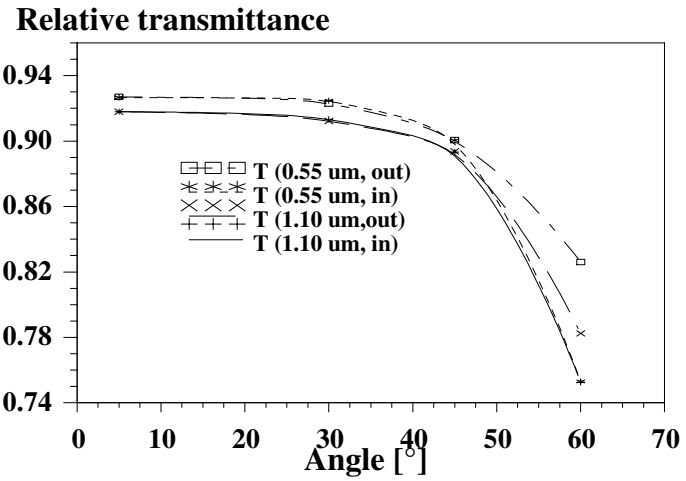

b)

Figure 7.16 *a) Integrated solar transmittance as a function of incidence angle for a Diamond flat glass with and without AR treatment. The markers correspond to values obtained from transmittance measurements.*
b) Relative transmittance at 0.55 and 1.10 mðm versus incidence angle for a structured glass with the structure facing either into or out of the sphere.

A comparison was also made between the results from the outdoor measurements and the transmittances from the spectrophotometric measurements (figure 7.17). For a flat AR-treated glass, the two methods agree. For the structured glass, the outdoor measurements give somewhat lower values. Since it is, in principle, difficult to characterize structured and partly scattering glazing in a conventional spectrophotometer, the outdoor method is supposed to be more reliable for testing structured glass.

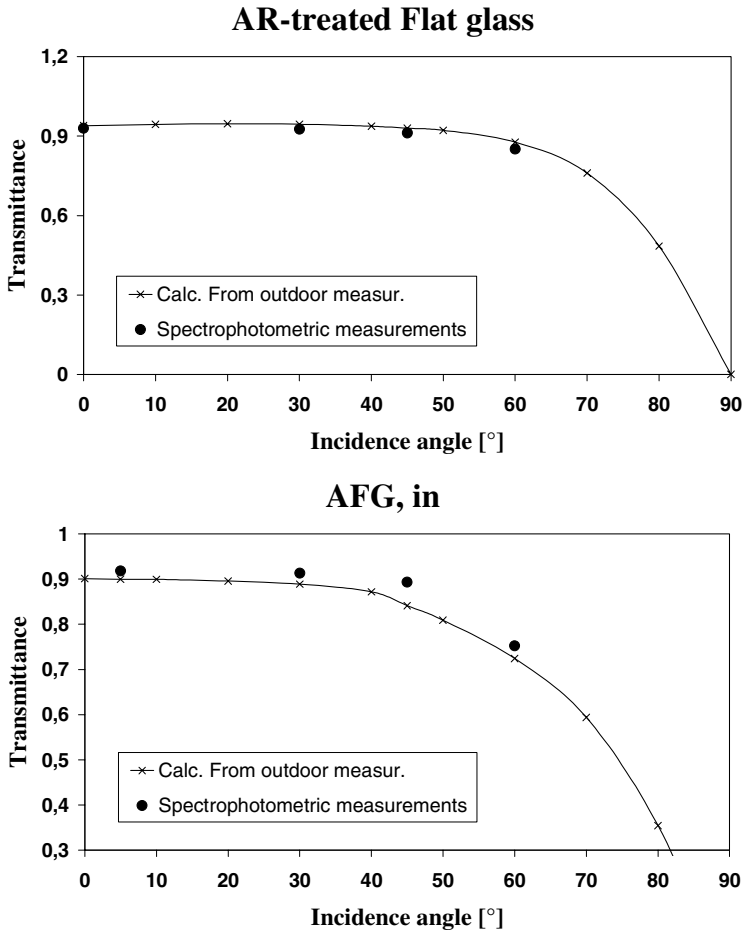

Figure 7.17 *Comparison between the outdoor measurements and the spectrophotometric measurements for determining the incidence angle dependence of the transmittance of different glazings.*

The results from the analyses above indicate that careful outdoor measurements can identify relatively small differences in optical efficiency between different collectors.

8 Asymmetric collectors

8.1 Introduction

An asymmetric collector, like the MaReCo described in chapter 3, has a complicated incidence angle dependence. The asymmetric shape gives rise to differences in incidence angle dependence of the optical properties in different directions. Figure 8.1 gives a definition of the longitudinal and the transverse directions of a concentrating system with cylindrical geometry. The incoming radiation is first transmitted through the glass and then reflected to the absorber. In the longitudinal plane, only the properties of the glass and the absorber affect the output when Θ_T is constant, and the incidence angle dependence is therefore similar to the dependence for a flat-plate collector (figure 8.2). This assumes that the reflectance of the reflector is independent of the incidence angle.

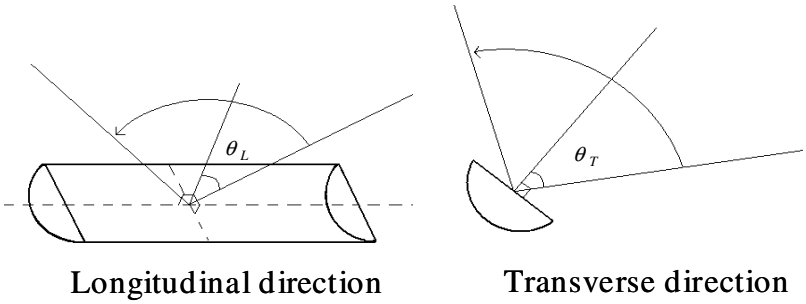

Figure 8.1 *Definition of the longitudinal and the transverse directions of a concentrating system with cylindrical geometry.*

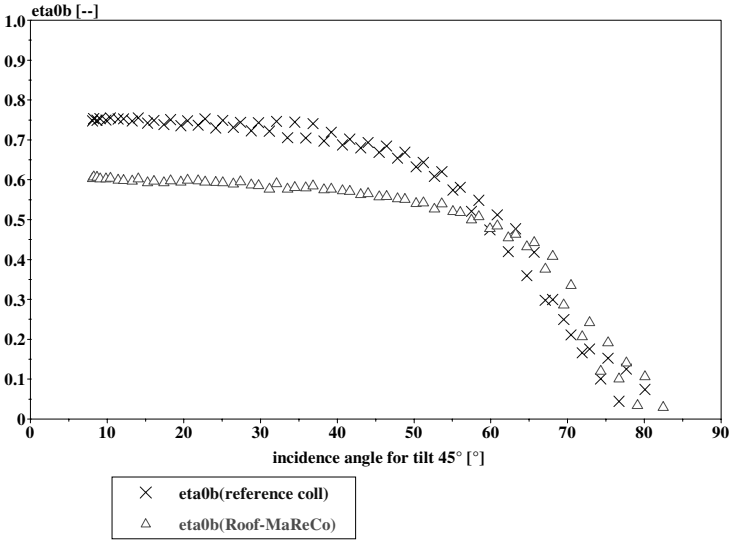

Figure 8.2 *Comparison of the optical efficiency for a conventional flat-plate collector (X) and for a Roof-MaReCo (Δ) in the longitudinal direction. (Paper VIII)*

In the transverse direction, the reflectivity and the geometry of the reflector also affect the performance. The concentration increases the radiation onto the absorber, but the reflector also introduces optical losses due to (multiple) reflections and absorption in the reflector material. The shape of the reflector affects the time of the day when the reflector is active. This is illustrated in figure 8.3b, showing the incident solar radiation onto and the energy output from a Roof-MaReCo placed with its longitudinal axis in the north-south direction (figure 8.3a). This diagram shows two distinctly different performance periods. Before about noon, the projected incidence angle is within the acceptance angle interval of the reflector, meaning that the reflector reflects the direct radiation onto the absorber. In the afternoon, the incidence angle is such that the reflector is no longer active and only radiation falling directly onto the absorber is contributing to the useful output.

a)

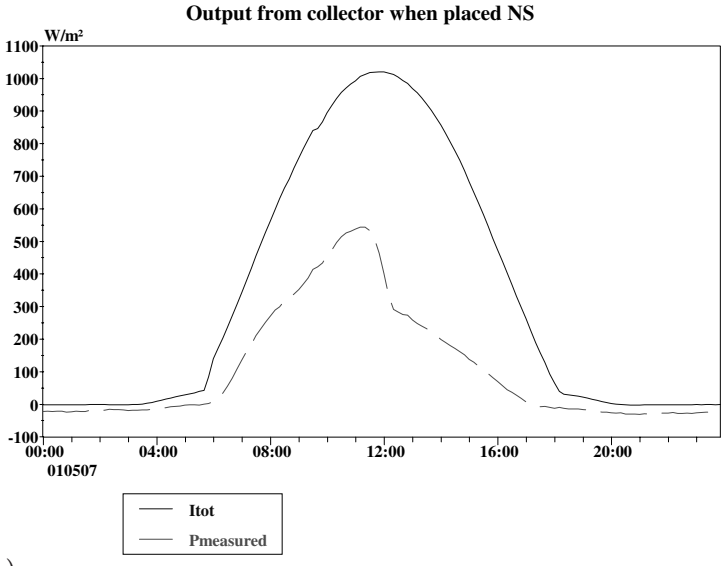

b)

Figure 8.3 *a) A MaReCo prototype placed with the reflector trough oriented north/south in order to study the transverse incidence angle behaviour.*
b) A daily diagram showing incident solar radiation onto and energy output from a Roof-MaReCo placed north/south.

The performance in the longitudinal and the transverse directions illustrated in figures 8.2 and 8.3 is typical of collectors with east-west symmetry.

8.2 A new suggested collector model

For a symmetric flat-plate collector, equation 6.3 can be used to model the incidence angle dependence. For an asymmetric collector, with different properties in different directions, this model is however not satisfactory. In this case, a biaxial overall incidence angle modifier can be used instead. This matter is discussed in (McIntire, 1982) where the incident angle modifier is approximated by factoring it into two components:

$$K(\Theta_L \Theta_T) \sim K(\Theta_L, 0) K(0, \Theta_T) \tag{8.1}$$

With this model, the incidence angle dependence of the collector is determined from measurements or calculations made in two orthogonal planes. In the equation above, index T denotes the transverse and L the longitudinal plane (figure 8.1). The factorisation of incidence angle modifiers for CPC collectors is also described in (Rönnelid et al, 1997b).

Using equation 8.1, the total incidence angle dependence, $K_{\tau\alpha}(\Theta)$, can be estimated as a "product model":

$$K_{\tau\alpha}(\Theta) = K_{\tau\alpha L}(\Theta_L) K_{\tau\alpha T}(\Theta_T) = f_L(\Theta_L) f_T(\Theta_T) \tag{8.2}$$

One shortcoming of this equation is that some optical effects (e.g. due to the glazing) are accounted for twice, i.e. in both $f_T(\Theta_T)$ and $f_L(\Theta_L)$. The model described by equation 8.2 is strictly correct only when radiation is incident in either the longitudinal or the transverse plane. For other angles, equation 8.2 will overestimate the optical losses due to the glazing. For an asymmetric collector, it is furthermore not always possible to determine the factor $K_L(\Theta_L,0)$ since $\Theta_T = 0$ may be outside the acceptance angle interval of the collector. This model is also not strictly correct for a symmetric collector.

In order to study the incidence angle dependence of the optical efficiency of MaReCo-type collectors, a project was carried out at Vattenfall Utveckling AB (Paper VII). In that project, a new expression for a biaxial incidence angle modifier was suggested (eq 8.3). In this model, the influence of the glazing and of the reflector on the optical efficiency is studied separately.

$$K_{\tau\alpha}(\Theta) = f_L(\Theta)\, g_{TL}(\Theta_T) \tag{8.3}$$

In this equation, the factor $f_L(\Theta)$ gives the influence of the glazing and $g_{TL}(\Theta_T)$ gives the influence of the reflector. Equation 8.3 is, in principle, different from equation 8.2 since Θ_L is not used. Below follows a discussion of the basic ideas behind this expression.

In order to avoid any contribution from the reflector, the influence of the glazing on the optical efficiency is studied by measurements made (close to the equinox) in the L plane. During the equinox (when Θ_T is constant), the incidence angle dependence should be determined by the angle Θ only. This is shown for the Roof-MaReCo in figure 8.4. This means that the influence of the glazing can be described by equation 6.2, using $b_0 = b_{0L}$ determined from measurements in the L direction. Since the optical path length and reflectance in the cover is determined by the incidence angle Θ, this angle, and not the longitudinal incidence angle Θ_L, should be used in the expression for modelling the influence of the glazing. Note that the b_0 value derived from the data in figure 8.4 will be different if it is determined as a function of Θ_L instead of Θ.

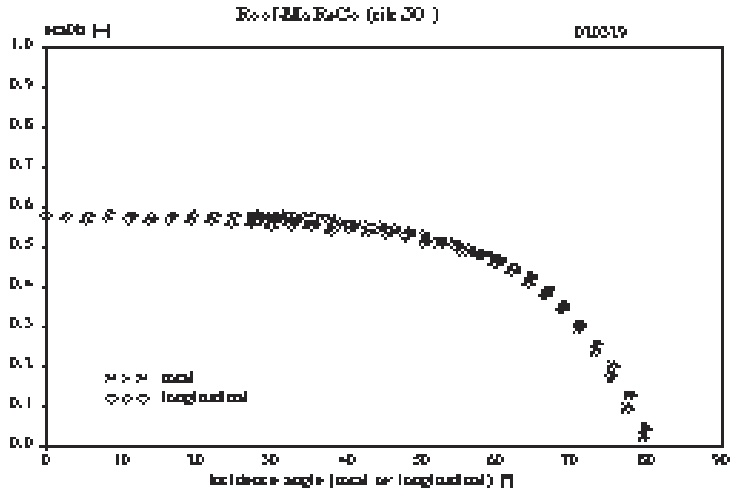

Figure 8.4 *Comparison of the incidence angle dependence of the optical efficiency in the total and in the L direction for the Roof-MaReCo during a day close to the spring equinox.*

The influence of the reflector on the optical efficiency depends on the absorption and on the multiple reflections in the reflector, and this is determined by the angle Θ_T. In order to find the influence of the reflec-

tor, measurements are made in the T direction when Θ_L is held constant. Due to geometrical effects and multiple reflections in the reflector, the total incidence angle dependence in the T plane should be stronger than in the L plane, where only the properties of the glass and the absorber are important. If the collector is covered with a glass, the measurements in the T direction will result in a factor that includes the influence of both reflector and glazing, i.e.:

$$F_T(\Theta_T) = f_L(\Theta_T) g_{TL}(\Theta_T) \tag{8.4}$$

where $f_L(\Theta_T)$ is the contribution from the glazing in the T direction, and $g_{TL}(\Theta_T)$ is the contribution from the reflector. If the glazing is considered to be isotropic, the incidence angle dependence of the transmittance of the glass is the same in both orthogonal planes, i.e. $f_T(\Theta_T) = f_L(\Theta_T)$. The ratio between the total dependence function in the T direction ($F_T(\Theta_T)$) and the f_L function (giving the influence of the glazing) should then only depend on the reflector geometry and can therefore be used as a "correction factor" accounting for the influence of the reflector:

$$g_{TL}(\Theta_T) = \frac{F_T(\Theta_T)}{f_L(\Theta_T)} \tag{8.5}$$

The product of the influence from the glazing ($f_L(\Theta)$) and from the reflector ($g_{TL}(\Theta_T)$) then gives the wanted biaxial incidence angle dependence as:

$$K_{\tau\alpha}(\Theta) = f_L(\Theta) \frac{F_T(\Theta_T)}{f_L(\Theta_T)} = f_L(\Theta) g_{TL}(\Theta_T) \tag{8.3}$$

Equation 8.3 is valid for asymmetric collectors like the MaReCo, and is fundamentally more correct than equation 8.2. It is also valid for flat-plate collectors, where $g_{TL}(\Theta_T) = 1$, resulting in $K_{\tau\alpha}(\Theta)$ being a function that is only dependent on Θ, just as desired. The equation is, however, not valid for values of Θ or Θ_T equal to 90°, but most useful energy will, anyhow, be collected at times when the incidence angle is less than that.

If the old and the suggested models are compared, the old model can be expressed as:

$$K_{\tau\alpha}(\Theta) = f_L(\Theta_L) f_L(\Theta_T) g_{TL}(\Theta_T) \tag{8.6}$$

This means that the transmittance of the glazing is modelled as a biaxial function.

8.2.1 Measurements performed to study the suggested model

The new suggested model was analysed by comparing the modelled output with data from outdoor measurements on a "Spring/Fall-MaReCo". This type of MaReCo is designed to give a high output during spring and fall (when heat is needed) without causing overheating during the summer (chapter 3).

In order to find the different factors in equation 8.3, the following measurements were made:

1. In a first step, the collector parameters were determined by an MLR analysis.
2. The factor $f_L(\Theta)$, which gives information about the influence of the glazing, is obtained from measurements in the L direction when Θ_T is constant, i.e. when the contribution from the reflector is constant. Since Θ_T has a constant value (of $(\phi - \beta)°$) during the equinoxes (see figure 6.5), the incidence angle dependence in the L direction is preferably studied at either spring or autumn equinox.
3. The factor $F_T(\Theta_T)$ is decided from measurements in the T direction when Θ_L is constant. This can be done either by performing an evaluation around noon (when $\Theta_L = 0°$) for a large number of days, or by rotating the collector to a north-south direction (like in figure 8.3a) and making measurements around the spring or autumn equinox. The latter method was used in the presented work.
4. The function $g_{TL}(\Theta_T)$ is modelled as the ratio $F_T(\Theta_T)/f_L(\Theta_T)$. This ratio gives the incidence angle dependence of the contribution from the reflector.

The measurements were made according to the method described in section 7.1. In order to determine the "no-loss efficiency", the effect of the heat losses etc was eliminated from the measured output ($\dot{q}_{um}$) as described in section 7.3.2.

$$\eta_{0b}(\Theta) = \left[\dot{q}_{um} - \left(\eta_{od} I_d - k_1 \Delta T - (mC)_e \frac{dT}{d\tau} \right) \right] \Big/ I_b \qquad (8.7=7.5)$$

The collector parameters used in equation 8.7 were determined with MLR on measured data (table 8.1). Since the Spring/Fall-MaReCo is designed to have a different performance during different parts of the year, the evaluation was divided into two periods (summer and autumn).

Table 8.1 Collector parameters for the studied Spring/Fall-MaReCo derived from MLR analyses.

	η_{0b}	b_0	η_{0d}	k_1	$(mC)_e$
summer	0.341	0.23	0.232	2.0	3 804
fall	0.56	0.09	0.31	2.0	2 227

Equation 8.3 requires more than one b_0 factor to be determined; one for the longitudinal plane (b_{0L}) and one during each evaluation period for the transverse plane (b_{0T}). The incidence angle dependences were determined by performing measurements around the equinox as discussed above.

The **b_{0L} factor** was found from an evaluation made during September 20 (when $\delta \approx 0$). From the analysis a value of 0.584 is found for $\eta_{0b(\Theta L=0)}$ and the b_{0L} factor is determined to 0.26. The diagrams in figure 8.5 show the optical efficiency as a function of the incidence angle (Θ) and as a function of the factor B_0 = (1/cos(Θ)-1) respectively. The data points in figure 8.5b form an almost straight line.

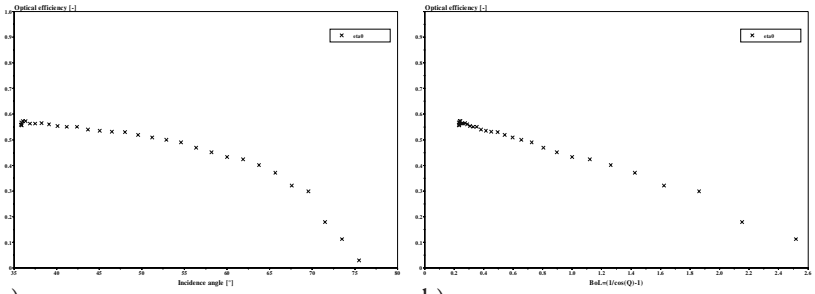

a) b)

Figure 8.5 *a) The optical efficiency plotted as a function of the incidence angle(Θ). (Data from September 20.)*
b) The optical efficiency plotted as a function of the factor (1/cos(Θ)-1)).

In order to find the **b_{0T} factor**, the collector was placed with the reflector trough extended in the north-south direction. With this orientation of the collector, two evaluations were made in order to separate periods when the reflector is active and when it is not active (compare figure 8.3). Figure 8.6 clearly shows that the no-loss efficiency follows different paths

depending on the incidence angle. In order to get a first estimate of the incidence angle dependence in the T direction, the same evaluation as in the L direction was done. The b_{0T} factor was estimated to be 0.20 when the reflector is active and 0.32 when it is not active (Helgesson and Karlsson, 2002a).

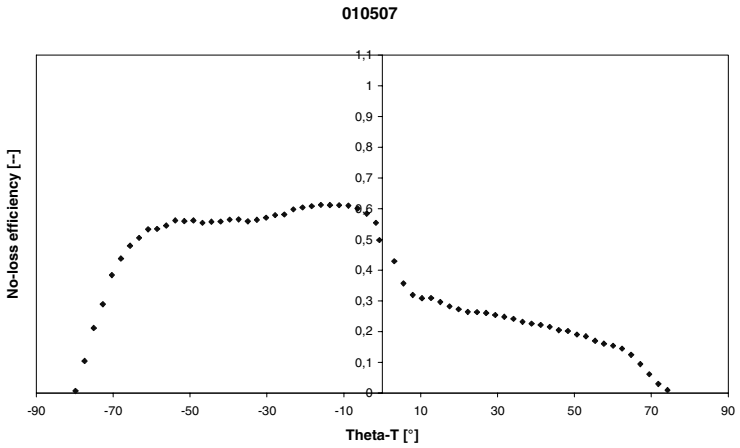

Figure 8.6 *"No-loss efficiency" as a function of the transverse incidence angle (Θ_T). The diagram shows that the reflector is only active before noon, giving two evaluation periods.*

The determined values of the b_0 factors were then used in equation 8.3 which was then used in equation 7.1 for calculation of the collector output using the suggested biaxial incidence angle dependence model. In order to verify the model it was compared with the measured output in a daily diagram (figure 8.7). The diagram shows that the model can be considered as acceptable to use, since it follows the actual output well. The deviation from the measured output is largest in the morning and in the afternoon, when the incidence angle is large.

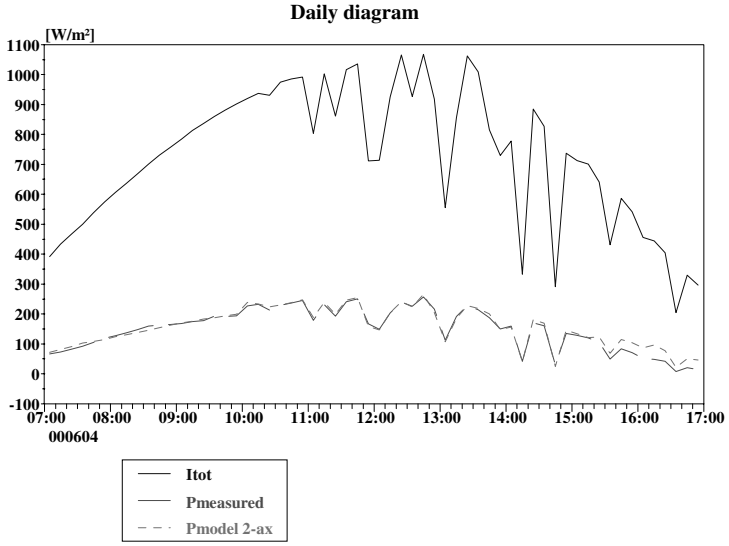

Figure 8.7 *A daily diagram for comparing the modelled output (Pmodel 2-ax) with the measured output ($P_{measured}$). The diagram also includes the incident solar radiation (I_{tot}).*

The results from this evaluation show that different b_0 factors can be used during different periods, but that a single b_0 factor cannot be used to model the dependence in the transverse direction for all angles of incidence. Problems still occur for incidence angles between the regions in figure 8.6.

8.2.2 Comparison between different models

The work presented above indicates that the new suggested expression for the biaxial incidence angle modifier (eq 8.7) can be used for modelling the collector output. Figures 8.8 and 8.9 show that the suggested biaxial model (P_{model} 2-ax) using equation 8.3 is better than the single-b_0 model (P_{model}) using equation 6.3 and also slightly better than the product model ($P_{model\ prod}$) using equation 8.2.

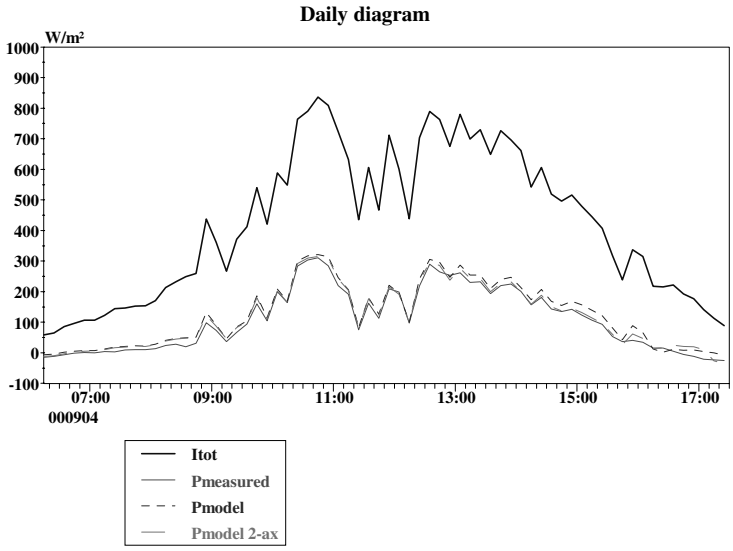

Figure 8.8 *Comparison between the new suggested biaxial model (P_{model} 2-ax) and the single-b_0 model (P_{model}). Pmeasured is the measured output and I_{tot} is the total radiation onto the collector.*

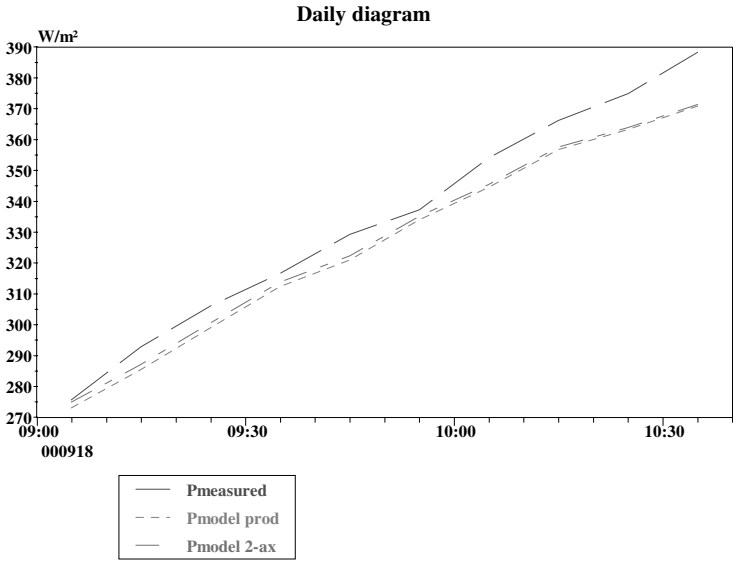

Figure 8.9 *A close-up diagram for comparison of the new suggested biaxial model (P_{model} 2-ax) and the model using eq 8.2 ($P_{model\ prod}$). $P_{measured}$ is the measured output.*

One drawback of the suggested method over the "single b_0 method" is that it requires measurements to be made at either spring or autumn equinox, or that the collector is mounted in such a way that it can be frequently redirected in order to keep Θ_T or Θ_L constant. It also gives problems for Θ_T close to the acceptance angles, where $F_T(\Theta_T)$ changes.

The same comparison between different incidence angle models as above was also made for a BoRö collector (Helgesson and Karlsson, 2003). The BoRö collector is a heavily truncated CPC collector with a bi-facial absorber. Each reflector trough has an acceptance angle interval of –90 to +40°. Figure 8.10 shows the collector and a daily diagram verifying the derived collector model and collector parameters. Outside the acceptance angle interval at 40° for each reflector trough, one part of the reflector is not active. This effect cannot, however, be identified in the diagram.

For this collector, the $F_T(\Theta_T)$ function was decided from a comparison of several different functions. Figure 8.11 presents the best function of the tested ones. The $f_L(\Theta_L)$ function was modelled as a conventional b_0 model.

A comparison between the single b_0 model, the product model, and the suggested biaxial model is given in figure 8.12. This comparison shows that there is no significant difference between the models. One conclusion from this is that the BoRö collector can be treated as a flat-plate collector. However, for collector types like the MaReCo, a biaxial model is required.

a)

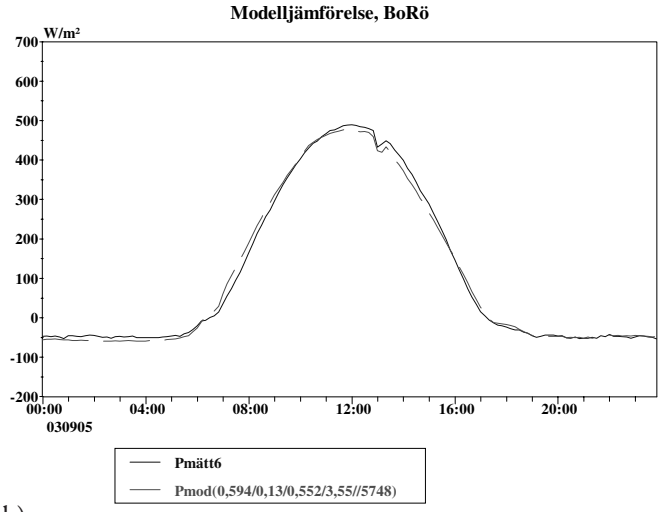

b)

Figure 8.10 *a) The studied BoRö collector, mounted for measurements in the T plane. b) A daily diagram used for comparing the modelled output (P_{mod}) with the measured ($P_{mätt}$).*

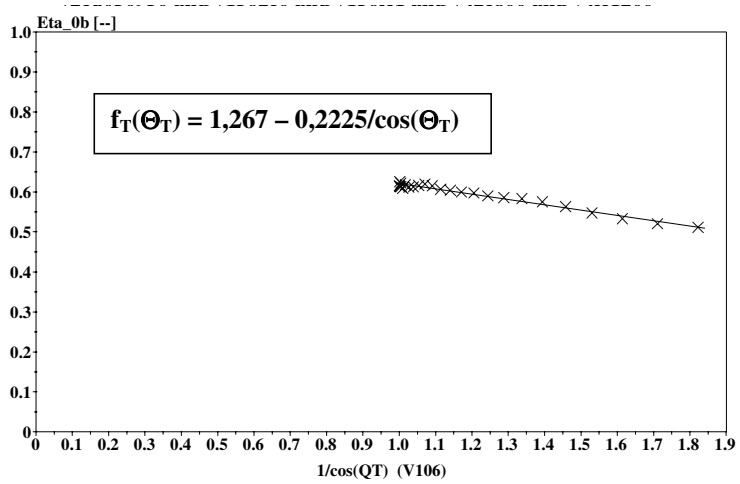

Figure 8.11 *Diagram for finding the function $F_T(\Theta_T)$ for the BoRö collector.*

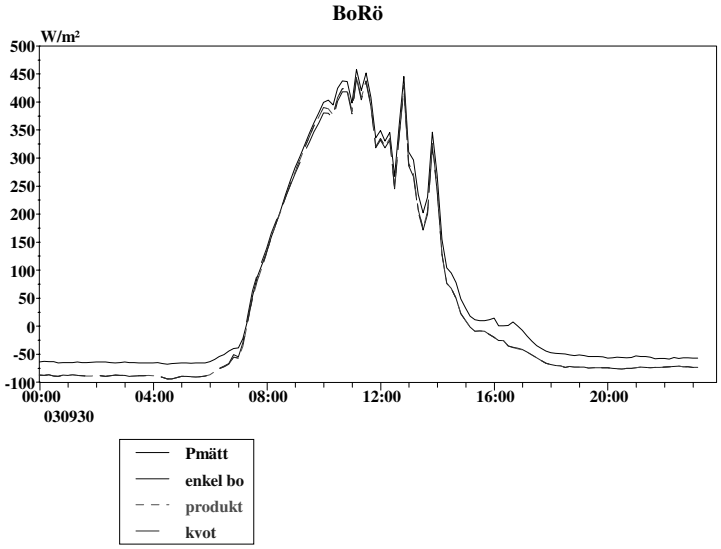

Figure 8.12 *Comparison of the three studied incidence angle dependence models with the measured output*

8.2.3 Energy output simulation

In order to study how the use of different incidence angle models influence the result when the energy output is simulated, the different models for the BoRö collector described above were used in MINSUN. In this case, the incidence angle dependence was given as a matrix with intervals of 10° for the angles Θ_T and Θ_L. The result (table 8.2) shows that there is no significant difference between the used models. The single-b_0 model indicates a somewhat lower energy output. This indicates that the single-b_0 model, which is also less time-consuming, might be good enough for predicting the energy output for a heavily truncated CPC collector.

Table 8.2 Predicted energy output (in kWh/m² at T_{op} = 50°C) when different incidence angle dependence functions for the BoRö collector in figure 8.10 were used in MINSUN.

model	**single b_0**	**product**	**new biaxial**
E_{50}	311	314	314

8.3 Further evaluation of the incidence angle dependence of asymmetric collectors

According to equation 8.3, the incidence angle dependence of the optical efficiency can be written as:

$$\eta_{0b}(\Theta) = \eta_{0b} F_{glas}(\Theta) G_{refl}(\Theta_T) \tag{8.8}$$

where the function $F_{glas}(\Theta)$ gives the dependence (in all directions) due to the cover, and $G_{refl}(\Theta_T)$ gives the dependence due to the reflector (only important in the T direction) (Paper VIII). Figure 8.13a shows the theoretical F_{glas} function (only considering the influence of the glazing) calculated with equation 6.2 using a b_0 value of 0.25. Figure 8.13b gives the measured function $G_{refl}(\Theta_T)$ for the MaReCo in figure 8.3a multiplied by the optical efficiency at normal incidence (η_{0b}). This figure has been obtained by correction for the glazing by dividing the optical efficiency in the T direction by data from figure 8.13a. The lower branch in the figure corresponds to values when the reflector is not active, i.e. when the incident radiation is outside the acceptance angle interval. (For a flat-plate collector, the dots in figure 8.13b should form a straight line with value = η_{0b}.)

Data from the two diagrams in figure 8.13 can be combined by using equation 8.8 in order to determine the incident angle dependent optical efficiency for different angles of incidence. The angle dependence in the transverse direction could be modelled as a function or given as a table in the simulation program. If e.g., for a certain occasion, $\Theta_T = \Theta_L = 45°$, then Θ = {eq 6.7} = 54.7°. From figure 8.13a, $F_{glas}(\Theta{=}54.7°) = 0.82$, and from figure 8.13b, $\eta_{0b} G_{refl}(\Theta_T{=}45°) = 0.65$. Equation 8.8 then gives $\eta_{0b}(\Theta{=}54.7°) = 0.82 \cdot 0.65 = 0.53$. If the standard biaxial model is used, the result would be (compare eq 8.6) $\eta_{0b}(\Theta{=}54.7°) = F_{glas}(\Theta_L{=}45°) \cdot F_{glas}(\Theta_T{=}45°) \cdot \eta_{0b} G_{refl}(\Theta_T{=}45°) = 0.89 \cdot 0.89 \cdot 0.65 = 0.52$. The difference between the results from the two models is then 2%.

In order to study the attainable solar fraction in a heating system, a simulation was made with the simulation program TRNSYS (Paper V). The incidence angle dependence of the MaReCo was modelled using the method described above. The results are given in figure 8.14. In order to attain the same solar fraction with the Spring/Fall-MaReCo as with the flat-plate collector, a larger collector area is needed. The overheating is, however, lower for the Spring/Fall-MaReCo. The TRNSYS simulation

indicates that the time spent at stagnation temperatures is smaller for the Spring/Fall-MaReCo than for the flat-plate collector. This means that it may be possible to use less expensive materials in the MaReCo.

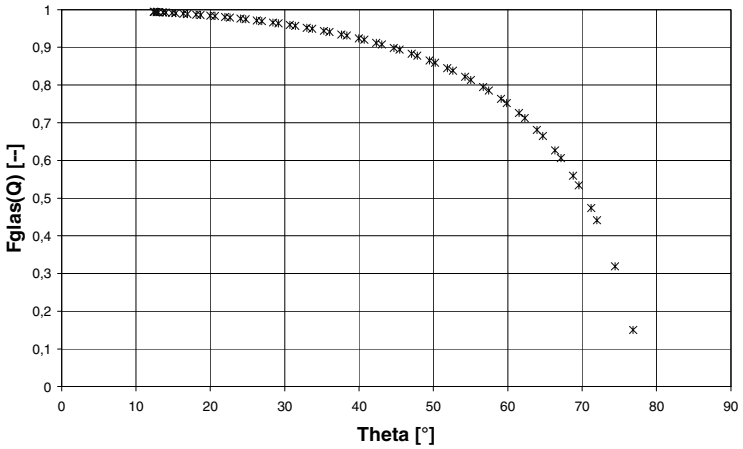

a)

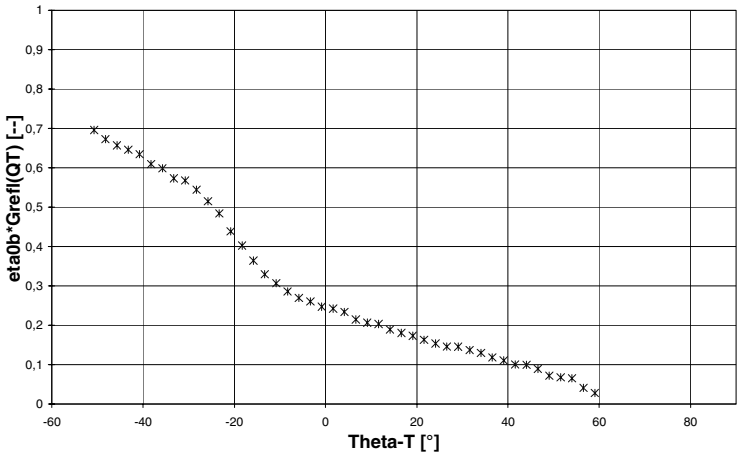

b)

Figure 8.13 *Evaluation of the MaReCo in figure 8.3a:*
a) Theoretical efficiency function, $F_{glas}(\Theta)$, according to eq 6.2 (with b_0 = 0.25) versus Θ.
b) Efficiency function $G_{refl}(\Theta_T)$ in the T direction. (Data from April 25 2002.)

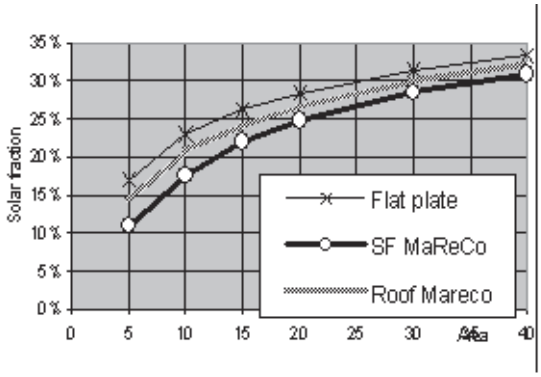

Figure 8.14 *Solar fractions for different collectors (flat-plate collector, Spring/Fall-MaReCo and Roof-MaReCo) with different areas. Collector tilt = 30°. Location: Stockholm, Sweden. Total load of space and water heating is 11 120 kWh.*

Due to the $G_{refl}(\Theta_T)$ function of the MaReCo, the MaReCo and the flat-plate collector have different performance for different tilt angles. This was investigated by combining Minsun simulations with a very simple system model. In these simulations, the optical efficiency was modelled according to equation 8.9, with the biaxial incidence angle dependence given as a table with intervals of 5°. The results of the simulations are presented in figure 8.15. This figure gives the estimated solar fractions of a domestic hot water system with either a flat-plate collector, a Roof-MaReCo or a Spring/Fall-MaReCo. The three systems are here individually dimensioned to exactly cover the heat load during July. The maximum collector area for avoiding overproduction in July is estimated as:

$$A_{c,July} = \frac{L_{July}}{E_{July}} \quad [m^2] \tag{8.9}$$

where L is the total heat load for the system and E is the simulated energy production per m² from the collector at an operating temperature of 50°C. The solar fraction of the system is then calculated as:

$$SF = \frac{total\ \ production}{total\ load} = \frac{A_{c,July} * E_{yr}}{L_{yr}} = \left[\frac{L_{July}}{L_{yr}}\right]\left[\frac{E_{yr}}{E_{July}}\right] \tag{8.10}$$

where the first bracket includes a parameter only depending on the load, and the second a parameter only depending on the solar collector. This means that the solar fraction, in a simplified way, can be estimated as a product of a load factor and a collector factor. Furthermore, for a given system, the load factor is a constant. In the domestic hot water system studied here this factor is 1/12. The collector factor varies, however, with the tilt angle.

Figure 8.15 shows that the Spring/Fall-MaReCo gives the highest solar fraction for low tilt angles, that the Roof-MaReCo is the best system for tilt angles between 40° and 70°, and that the flat plate collector gives the highest solar fraction for near vertical collectors. The collector area for maximum solar fraction for both the Roof-MaReCo and for the Spring/Fall-MaReCo systems is 14.8 m². The vertical flat-plate collector has an area of 15.4 m². The flat-plate system has a maximum solar fraction of 0.80, whereas the Roof-MaReCo system has a maximum solar fraction of 0.71, and the Spring/Fall-MaReCo system a solar fraction of 0.62.

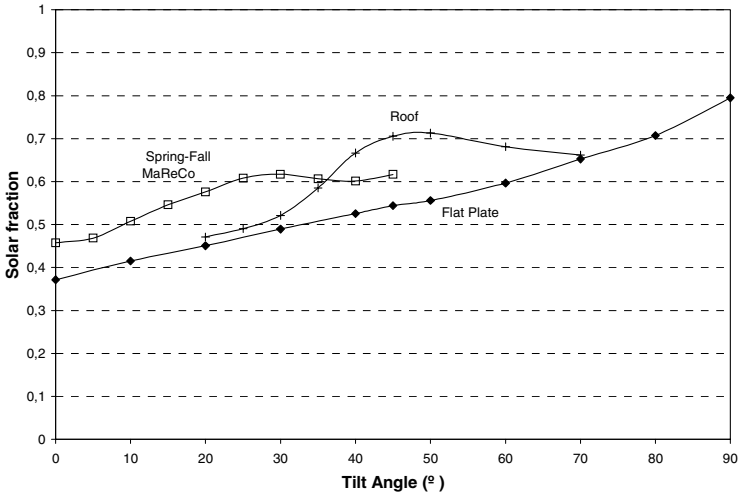

Figure 8.15 *Solar fraction (for a heat load of 400 kWh/month) as a function of tilt angle for three different collectors.*

8.4 Study of the incidence angle dependence angle by angle

According to figure 6.1, a single b_0 factor is not enough to describe the optical performance of a solar collector for all incidence angles. An alternative method can be to divide the incidence angle interval into several smaller parts and to use the following expression to model the incidence angle dependence (Helgesson and Karlsson, 2002a):

$$\eta_{0b}(\Theta) \cdot I_b = \sum_i \eta_{0b,i} I_{b,i} \tag{8.11}$$

In this method, the beam radiation is sorted into different classes depending on the incidence angle. Several MLR analyses are then performed in order to determine the optical efficiency in each class. One optical efficiency is obtained in each interval from these analyses. This "incidence angle divided" method is compared with the "single-b_0 model" (eq 6.2) in figure 8.16. The figure shows that these two methods give very similar results. The single-b_0 method requires, however, less evaluation work, and can therefore be a good choice for evaluation, at least for symmetric collectors. The angle dependence of a structured glass, with the structure facing inwards, cannot, however, be modelled correctly with a b_0 function (Paper III).

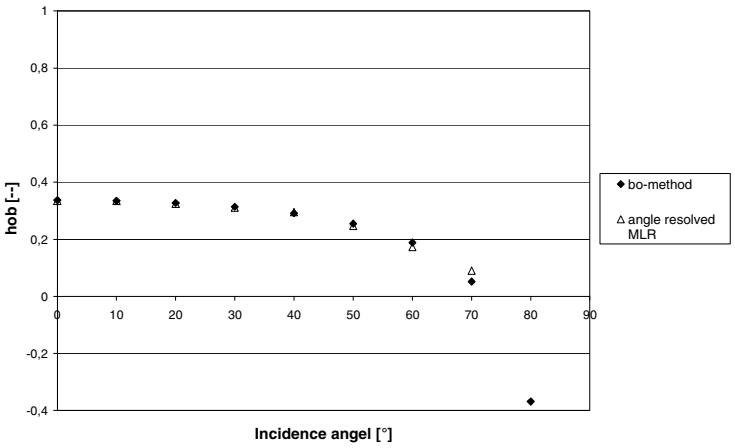

Figure 8.16 *The optical efficiency (hob), for the collector in figure 8.3, versus the incidence angle. A comparison is made between the "single-b_0 method" (eq 6.2, and the incidence angle divided method (according to eq 8.11).*

The method of dividing the incidence angle interval can be extended further by looking at the performance in two directions. In this way, a matrix with different incidence angle modifier values can be formed. This matrix can then be used in an adapted MINSUN version in order to study the yearly energy output.

8.5 Incidence angle dependence of some PV modules

In Paper IX, the proposed biaxial model for the incidence angle dependence of the optical efficiency is used for a PV module equipped with an asymmetric east/west aligned reflector.

$$\eta_0 = R_T(\Theta_T) f_L(\Theta) \tag{8.12}$$

The studied system consists of a thin film CIGS module and a parabolic overedge reflector of anodized aluminum (figure 8.17). By placing the module with the cells perpendicular to the extension of the concentrator, all series-connected cells get equal irradiance. The optical axis of the reflector is inclined at an angle of v = 25° over the horizon, meaning that it reflects all radiation at Θ_T > 25° onto the absorber. Below 25°, only direct irradiance on the module gives a contribution to the electricity production. The module plane has an inclination of β = 20°. The geometrical concentration ratio (C) of the construction is 3.

As a reference, a vertical module of the same size, but without a reflector, was used.

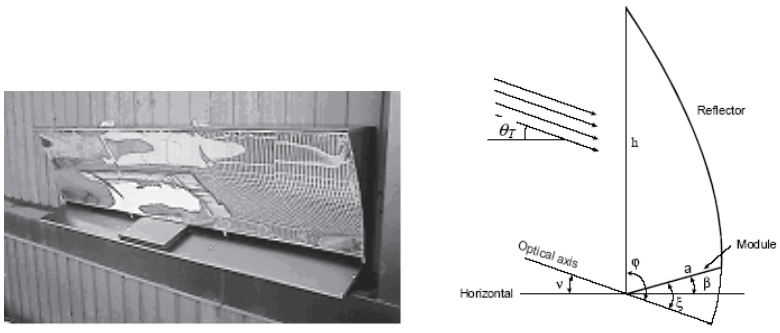

a) b)

Figure 8.17 The 3X concentrating PV system with overedge reflector, a) photo, b) schematic sketch of the cross section.

The optical efficiency of the PV module is calculated from measurements of the short-circuit current from the module ($I_{SC,conc}$) and from the reference module ($I_{SC,plan}$):

$$\eta_0 = \frac{1}{C}\frac{I_{SC,conc}}{I_{SC,plan}} \tag{8.13}$$

In the paper, it is shown that the optical efficiency of the reflector is independent of the longitudinal angle of incidence (Θ_L). This can be seen in figure 8.18, which shows the results from measurements made when Θ_T was almost constant (and about 30°). The angle Θ_L, however, varies from –90° to +90° over the day (from 6.00 AM to 6.00 PM).

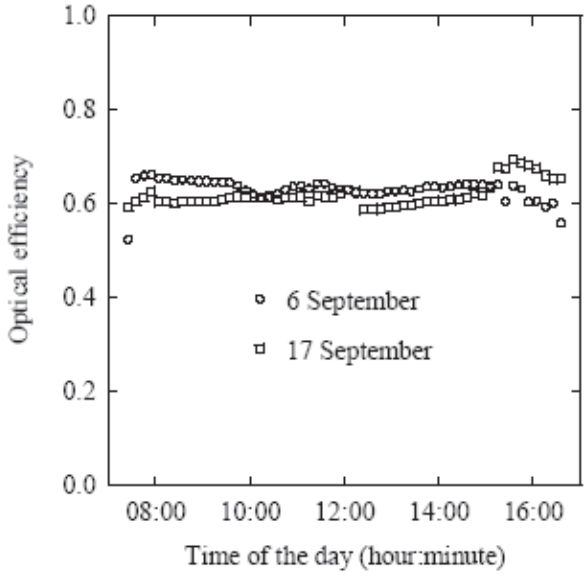

Figure 8.18 *Optical efficiency of the parabolic overedge reflector as a function of the time of the day for two days near the autumn equinox. (Θ_T~30°)*

Figure 8.19 shows how the short-circuit current from the module with the overedge reflector and from the reference module varies during a test day close to the equinox when $\Theta_T \approx$ constant. During these measurements, the reflector was directed north/south and tilted so that the sun moved in the T plane of the system. The figure also shows the optical efficiency of the reflector (R_T).

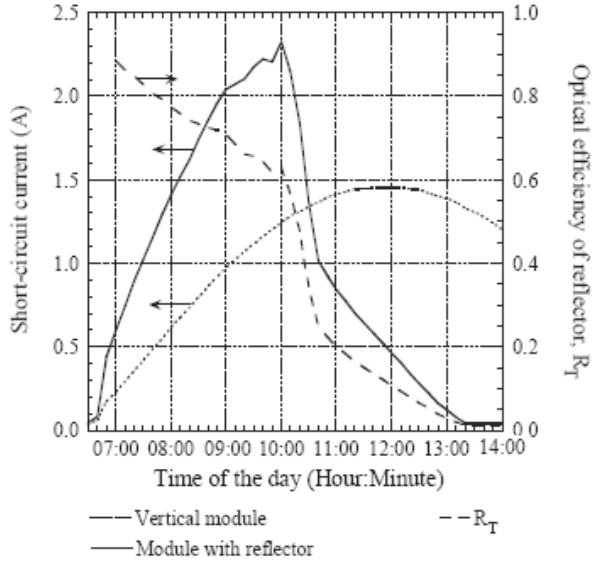

Figure 8.19 *Short-circuit currents from the concentrating and from the reference systems during 24 September 2003. R_T is the optical efficiency of the reflector. The systems are rotated north/south.*

Due to the geometry of the construction, irradiation at $\Theta_T < 25°$ is not reflected to the module. Direct radiation will, however, reach the module at an angle of incidence that is $(70 - \Theta_T)°$. For $\Theta_T > 25°$, part of the beam radiation reaches the module directly and part is reflected before reaching the module. Assuming only one reflection, the Θ_T dependence of the optical efficiency can be formulated as:

$$R_T(\Theta_T) = \begin{cases} \dfrac{a\cos(70-\Theta_T)}{h\cos(\Theta_T)} & \text{for } \Theta_T < 25° \\ \rho + (1-\rho)\dfrac{a\cos(70-\Theta_T)}{h\cos(\Theta_T)} & \text{for } \Theta_T \geq 25° \end{cases} \tag{8.14}$$

where ρ is the reflectance of the reflector and a and h are lengths defined in figure 8.17.

In order to study how well the model describes the real system efficiency, measured short-circuit currents from the vertical reference module were used with the parametric model (eq 8.14) to predict the gener-

ated short-circuit current from the reflector module. The comparison of the predicted and the measured I_{SC} shows that the model describes the optical efficiency well (figure 8.20).

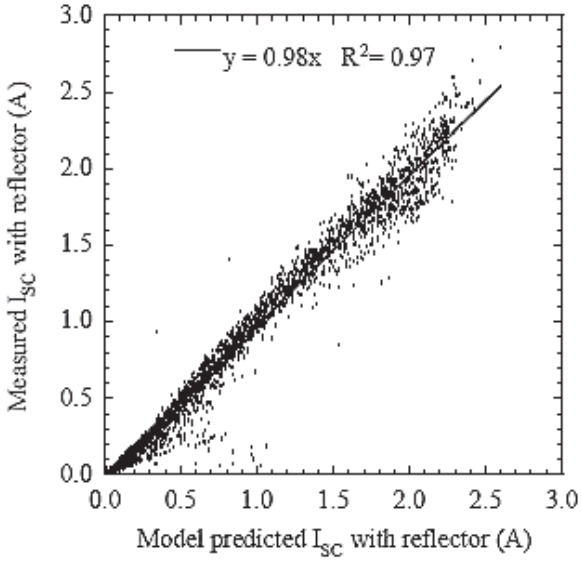

Figure 8.20 *Comparison between modelled and measured I_{SC} from the module with the overedge reflector. Data from the period 10th July to 12th September 2003. One data point for every 10th minute, 7:00 – 17:00, is included in the graph.*

The function f_L can e.g. be modelled (with a b_0 expression) or measured. Figure 8.21 shows the f_L and the R_T functions that determine the optical efficiency of the studied PV system with a parabolic overedge reflector and a vertical glazing. The f_L function is here obtained from a Fresnel calculation assuming a 3 mm glass. The optical efficiency at any given moment in time is obtained by taking the product of $f_L(\Theta)$ and $R_T(\Theta_T)$, using the real angle of incidence (Θ) and the transverse projection angle (Θ_T) at that time.

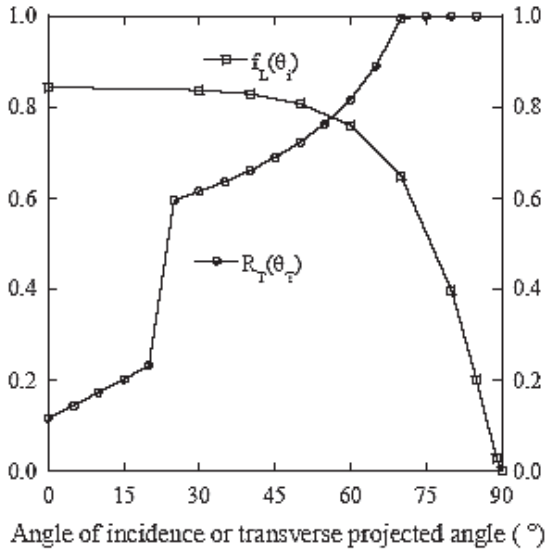

Figure 8.21 *The factors $f_L(\Theta)$ and $R_T(\Theta_T)$ for the studied concentrating PV-system.*

A comparison of the suggested model with a commonly used biaxial model shows that the difference between the models can be a couple of percentage points. The suggested model is valid for most types of concentrating systems (as well as for flat-plate solar collectors).

9 Summary and Discussion

9.1 Summary of the papers

This work concentrates on outdoor measurements of different solar collectors. For the evaluations, a dynamic test method has been used. Examples of outdoor measurements made for evaluation of different collectors are given in the presented papers. The aim has been to study the incidence angle dependence of flat plate and asymmetric collectors. Detailed measurements of structured and antireflection treated glazings have been performed. A new biaxial model has been suggested and a method for outdoor characterization of asymmetric collectors has been tried experimentally. The suggested method has also been tested on a PV module with a concentrator.

In paper I, a collector with an external reflector is evaluated. The reflector parameters were determined by predicting a value of the reflectance of the reflector and then comparing modelled and measured data of the collector + reflector combination. In order to estimate the possible yearly energy output, the results were used together with a simulation tool.

In order to study how different solar collector materials affect the output, measurements have been made on flat-plate collectors for both different absorbers and different glazings (Papers II and III). The outdoor measurements were compared, and in good agreement, with optical measurements made by Uppsala University. In Paper II, the incidence angle dependence of different absorbers was studied. The angle dependence was determined by dynamic testing using a single b_0 model and an evaluation of the optical efficiency in different incidence angle intervals.

In Paper III, a method for detailed outdoor characterization of the incidence angle dependence of solar collectors is developed. In this method, two identical collector boxes are used and series connected in order to get an identical flow of water. One of the collectors is covered with a thin Teflon foil and used as a reference collector. This collector is, in principle, used as an irradiance monitor since it is easier to align two large collectors than to align a solar collector and a pyranometer. Teflon

is used as a reference since it has a well documented transmittance, very low absorptance and a minimal angular dependence. The other collector box was used for analyzing different glazing. The method is carried out in a number of steps: 1) The collectors are long term tested in order to get the collector parameters, especially the U-values and the optical efficiency for diffuse irradiance. 2) The effect of heat losses and diffuse irradiance is eliminated, giving the optical efficiencies for beam irradiance of the collectors. 3) In order to make the measurements for the different tested cases comparable, the ratio between the optical efficiencies of the test and the reference collectors is calculated. 4) By testing both collectors with a Teflon film as a cover, the relative optical efficiency of the collector is derived. This is then used, together with the known angular transmittance of Teflon, to calculate the absolute value of the angular dependent transmittance of the tested glazings. The method was used to study the impact of antireflection treatment. The results show that antireflection treatment can increase the annual energy output by 9%. The results also show that a structured glass should be mounted with the structure facing outwards.

At VUAB, a special reflector collector, the MaReCo, has been developed. In the work, the performance of different MaReCo prototypes have been studied and reported in different papers. Since the MaReCo is asymmetric, the modelling of the incidence angle dependence of the optical properties is rather difficult, and a new biaxial model has been suggested and tried experimentally. In Paper IV, evaluations of asymmetric collectors for stand-alone, roof or wall integrated installation are presented. For these evaluations, the incidence angle dependence was modelled with the standard b_0 function. The evaluation gave the highest annual energy output for a roof mounted MaReCo (336 kWh/m² at an operating temperature of 50°C) and for a stand-alone MaReCo with Teflon (282 kWh/m²).

In Papers V and VI, a "Spring/Fall MaReCo" was evaluated. This collector is designed to suppress the energy output during the summer. In this way a larger collector area can be installed in order to increase the solar fraction of the system without causing overheating during the summer. A Spring/Fall MaReCo was outdoor tested during a whole year. The study shows that the efficiency decreases, as wanted, during the summer. According to an energy simulation with Minsun, the annual energy output is estimated to approximately 222 kWh/m². The Spring/Fall MaReCo was also installed and tested in a system with a determined hot water load. The yearly collector output was, from this test, estimated to 165 kWh/m². The lower solar fraction than expected is explained by poor stratification in the tank.

In Papers VII and VIII, a new method for evaluation of the incidence angle dependence of the optical efficiency based on outdoor measurements is developed and tested. For flat-plate collectors, the incidence angle dependence is often modelled with the standard b_0 model:

$$\eta_{ob}(\Theta) = \eta_{ob} \cdot \left[1 - b_0 \left(\frac{1}{\cos(\Theta)} - 1 \right) \right]$$

For asymmetric collectors, like e.g. the MaReCo, this model may however not work satisfactorily since the incidence angle dependence is then different in different directions. Biaxial models, based on projected incidence angles, may be used to estimate the annual performance of asymmetric collectors. However, the use of projected angles tends to underestimate optical losses in the cover glass. In the work, a biaxial model, which uses the transverse projected incidence angle for determining the influence of the reflector and the real incidence angle to determine the influence of the glazing, is proposed: $K_{\tau\alpha}(\Theta) = f_L(\Theta)\, g_{TL}(\Theta_T)$. In this equation, the factor $f_L(\Theta)$ gives the influence of the glazing and $g_{TL}(\Theta_T)$ gives the influence of the reflector. This model gives an absolute value of the optical efficiency and is valid for all types of concentrating systems, as well as for flat-plate collectors. In order to find the $f_L(\Theta)$ and the $g_{TL}(\Theta_T)$ factors, the following measurements were made:

- The factor $f_L(\Theta)$ is obtained from measurements in the L direction when Θ_T is constant, i.e. when the contribution from the reflector is constant. This measurement is preferably done at either spring or autumn equinox when Θ_T has a constant value.
- The factor $F_T(\Theta_T)$ is decided from measurements in the T direction when Θ_L is constant. This is done by rotating the collector to a north-south direction and making measurements around the equinox. The function $g_{TL}(\Theta_T)$ is then modelled as the ratio $F_T(\Theta_T)/f_L(\Theta_T)$. In this way the influence of the glazing is eliminated and the ratio gives the incidence angle dependence of the contribution from the reflector.

When determining the optical efficiency in the different directions, the method developed in Paper III was used. The collector parameters were determined by dynamic testing.

In Paper VII, the new suggested method was tested on a Spring/Fall MaReCo. The results show that the new method can be used for modelling the collector output and that it is better than the single b_0 model. The results show that different b_0 functions can be used during different periods, but that the incidence angle dependent performance can not be

modelled with a single b_0 function during the period when the optical efficiency of the reflector changes. One drawback of the suggested method over the single b_0 method is, however, that it requires measurements to be made at either spring or autumn equinox. In Paper VIII, the method is further studied on different asymmetric collectors. The incidence angle dependence in the T and the L direction is here studied in more detail and the method for combining these dependencies to an overall optical efficiency is described.

In Paper IX, the new suggested biaxial model for the incidence angle dependence of the optical efficiency is used for a PV module with an east-west aligned asymmetric parabolic reflector. It is shown that the dependence of the optical efficiency of the reflector on the longitudinal incidence angle is negligible. The model is also compared with a commonly used biaxial model and it is found that the difference is a couple of percentage points when the difference between the longitudinal projected incidence angle and the real incidence angle is large and the angle of incidence on the glass is high.

9.2 Summary of the studies of collector performance and of the incidence angle dependence

Solar energy has the advantage of being a clean and sustainable energy source. One problem, though, is the high installation costs. By R&D activities, it is, however, possible to improve the output/cost ratio. This can be done either by increasing the collector performance or by reducing the costs, e.g. by using cheaper materials or more rational manufacturing methods. One example of an attempt to improve the output/cost ratio is the development of the MaReCo collector. This is an asymmetric reflector collector that is specially designed for the insolation conditions in Sweden. The major advantage of the MaReCo is the low material content, and thereby the low material costs.

The output from a collector depends on both optical (α, ε, and τ) and thermal (U) properties. Examples of improvements to increase the output are the use of:

- selective absorbers (having a high absorptance but a low emittance)
- AR-treated cover glass (having a high transmittance)
- transparent insulating material (e.g. Teflon that reduces the heat losses)

- different reflector arrangements (placed between collector rows in a large collector field or inside the collector as in the MaReCo).

In order to evaluate how different designs affect the performance of the collector, measurements are needed. In order to save time, a dynamic evaluation procedure can be used to estimate the annual energy output instead of performing year long measurements. The energy output can be modelled as:

$$\dot{q}_u = \eta_{0b}(\Theta) I_b + \eta_{0d} I_d - k_1 \Delta T - k_2 (\Delta T)^2 - (mC)_e \frac{dT_f}{d\tau} \qquad (7.1)$$

where Θ is the incidence angle, i.e. the angle between the beam radiation and the normal to the glass, and where

$$\eta_{0b}(\Theta) = \eta_{0b}\left[1 - b_o\left(\frac{1}{\cos(\Theta)} - 1\right)\right] \qquad (6.3)$$

This expression is, however, not valid for all incidence angles, since the collector properties depend on the incidence angle. The evaluation will be even more difficult if the collector is asymmetric, since the angle dependence must then be studied in two perpendicular planes of the collector (longitudinal, and transverse). In this work, a novel expression for modelling a biaxial incidence angle dependence has been suggested:

$$K_{tot}(\Theta) = f_L(\Theta) g_{TL}(\Theta_T) \qquad (8.3)$$

where the factor $f_L(\Theta)$ gives information about the influence of the glazing and $g_{TL}(\Theta_T)$ accounts for the influence of the reflector. Measurements have been made on different collectors in order to study the suggested model experimentally. The results indicate that the suggested expression can be used for accurate modelling of the collector output. It does not, however, differ significantly from the more simple single b_0 model, and that model may therefore be considered good enough for collector evaluations. One drawback of the suggested method is also that the measurements must be made in a way so that Θ_T or Θ_L are held constant in order to decide the factors f_L and g_{TL}. If a more thorough evaluation of an asymmetric collector is needed, the biaxial model should be used instead of the single b_0 method.

9.3 Suggestions for future work

For future work, continued measurements on both flat-plate and asymmetric collectors (e.g. MaReCos, and vacuum tubes) are suggested in order to further study the collector performance and to find those collector designs that are likely to achieve the best output at the specific location. In order to better consider the incidence angle dependence, alternative methods for modelling the angle dependence must be suggested and evaluated. Different biaxial methods should be compared by performing measurements and ray tracing studies.

References

Adsten, M., & Perers, B. (1999). *Simulation of the influence of tilt and azimuth angles on the collector output of solar collectors at northern latitudes*. Paper presented at North Sun Conference, Edmonton, Canada.

Adsten, M., Joerger, R., Järrendahl, K., & Wäckelgård, E. (2000). *Optical Characterization of Industrially Sputtered Nickel-Nickel Oxide Solar Selective Surface*. J. Solar Energy, vol 68, no 4, pp 325 - 328.

Adsten, M., Hellström, B., & Karlsson, B. (2001). *Measurement of radiation distribution on the absorber in an asymmetric CPC collector*. Submitted to J. Solar Energy.

Adsten, M., Perers, B., & Wäckelgård, E. (2002a). *The influence of climate and location on collector performance*. Renewable energy 25, pp 499 – 509.

Adsten, M., Wäckelgård, E., & Karlsson, B. (2002b). *Calorimetric measurements of heat losses form a truncated asymmetric solar thermal concentrator*. Ångström Laboratory, Uppsala University. Submitted to Journal of Solar Energy.

Adsten, M. (2002c). *Solar Thermal Collectors at High Latitudes - Design and Performance of Non-Tracking Concentrators.* Uppsala: Uppsala University.

Carvalho, M.J., Collares-Pereira, M., Gordon, J.M., & Rabl, A. (1985). *Truncation of CPC solar collectors and its effect on energy collection*. J. Solar Energy, vol 35, no 5, pp 393 – 399.

Cathro, K., Constable, D., & Solaga, T. (1984). *Silica low-reflection coatings for collector covers, by a dip-coating process*. J. Solar Energy, vol 32 (5).

Chant, V.G., & Håkansson, R. (1985). *The MINSUN simulation and optimisation program. Application and users guide*. IEA SH & C Task VII, Ottawa.

Collaires-Pereira, M., & Rabl, A. (1979). *Simple procedure for predicting long-term average performance of nonconcentrating and of concentrating solar collectors*. J. Solar Energy 23, 235.

Duffie, J.A., & Beckman, W.A. (1991). *Solar engineering of thermal processes; second edition*. New York: John Wiley & Sons, Inc.

Fischer, S., Müller-Steinhagen, H., Perers, B., & Bergquist, P. (2001). *Collector test method under quasi-dynamic conditions according to the European Standard EN 12975-2*. Contribution to the ISES conference.

Helgesson, A. (1999). *Utvärdering av EPS-MaReCo med konvektionskylning*. VUAB Report: UR 99:21. Älvkarleby: Vattenfall Utveckling AB. {Project report concerning the evaluation of an EPS-MaReCo.}

Helgesson, A., Karlsson, B., & Perers, B. (2000a). *Evaluation of a MaReCo-prototype*. Contribution to EuroSun in Copenhagen.

Helgesson, A. (ed), et al (2000b). *Solvärme - Slutrapport för FUD-program Solvärme 1996 – 99*. Report: UD 00:12, Älvkarleby: Vattenfall Utveckling AB. {Final report for the Swedish RD&D-programme concerning solar heating.}

Helgesson, A. (2001). *Utvärdering av solvärmeanläggning i Torsåker*. UD 01-02. Älvkarleby: Vattenfall Utveckling AB. {Project report concerning the evaluation of a solar energy plant in Torsåker, Sweden.}

Helgesson, A., & Karlsson, B. (2002a). *Infallsvinkelberoende från utomhusmätningar på MaReCo-solfångare*. Report: U 02:110. Älvkarleby: Vattenfall Utveckling AB. {Project report on incidence angle dependence from outdoor measurements on a MaReCo.}

Helgesson, A., Karlsson, B., & Fahlström, A. (2002b). *MaReCo-Hybrid i Hammarby Sjöstad – inledande prototypmätningar*. Report: 03:9, Elforsk AB. {Project report describing a MaReCo-hybrid.}

Helgesson, A., & Karlsson, B. (2003). *Utvärdering av ny metod för vinkelberoende*. Report: U 03:74. Älvkarleby: Vattenfall Utveckling AB. {Project report regarding evaluation of a biaxial incidence angle dependence model.}

Helgesson, A. (ed), Larsson, S., Karlsson, B., & Krohn, P. (2004). *FUD-program "Solvärme 2001 – 2003", Slutrapport*. ER 26:2004, Eskilstuna: Statens Energimyndighet. {Final report for the Swedish RD&D-programme concerning solar heating.}

Hellström, B., Adsten, M., Nostell, P., Wäckelgård, E., & Karlsson, B. (2000). *The impact of optical and thermal properties of the performance of flat plate solar collectors*. Contribution to EuroSun 2000 in Copenhagen.

Hellström, B. (2004). *Derivation of efficiency factors for uneven irradiation on a fin absorber.* J. Solar Energy, 77, pp 261 – 267.

Hollands, K.G.T., Brunger, A.P., & Morrison, I.D. (1991). *Evaluating improvements to a low-concentration-ratio, non-evacuated, non-imaging solar collector*. Submitted to ISES Conference.

Karlsson, B., & Wilson, G. (2000a). *MaReCo design for horizontal, vertical or tilted installation*. Contribution to EuroSun 2000 in Copenhagen.

Karlsson, B., Larsson, S., Wilson, G., & Andersson, A. (2000b). *MaReCo for large systems*.

Karlsson, B., Helgesson, A., & Svensson, L. (2003). *Development of a MaReCo-hybrid*. Contribution to the ISES Congress in Gothenburg.

Kerskes, H., Asenbeck, S., Heidemann, W., & Müller-Steinhagen, H. (2003). *Angepasste Kollektoren für Kombianlagen – Der IAM macht's möglich*. Institut für Thermodynamik und Wärmetechnik.

Larsson, S. (2003). *The Swedish national solar heating R&D-programme*. Contribution to the ISES conference in Gothenburg.

Mills, D.R., & Giutronich, J.E. (1978). *Asymmetrical non-imaging cylindrical solar concentrators*. J. Solar Energy, 20, pp 45 - 55.

Mills, D.R., Monger, A., & Morrison, G.L. (1994). *Comparison of fixed asymmetrical and symmetrical reflectors for evacuated tube solar receivers*. J. Solar Energy, vol 53, no 1, pp 91 – 104.

McIntire, W.R. (1982). *Factored approximations for biaxial incident angle modifiers*. J. Solar Energy, vol 29, no 4, pp 315 – 322.

Nayak, J.K., & Amer, E.H. (2000). *Experimental and theoretical evaluation of dynamic test procedures for solar flat-plate collectors*. J. Solar Energy 69 (5), pp 377 – 401.

Norton, B., Eames, P.C., & Yadav, Y.P. (1991). *Symmetric and asymmetric linear compound parabolic concentrating solar energy collectors: The state-of-the-art in optical and thermophysical analysis*. International Journal of Ambient Energy, vol 12, no 4, pp 171 - 190.

Nostell, P., Roos, A., & Karlsson, B. (1997). *Optical characterisation of solar reflecting surfaces*. In proceedings of SPIE, paper 3138-20, pp 163 - 172, San Diego, USA.

Nostell, P., Roos, A., & Karlsson, B. (1998a). *Ageing of solar booster reflector material*. J. Solar Energy Materials and Solar Cells 54, pp 235 - 246.

Nostell, P., Roos, A., & Karlsson, B. (1998b). *Antireflection of glazings for solar energy applications*. Sol. Energy Mat. Solar Cells (54).

Nostell, P., Roos, A., & Karlsson, B. (1999a). *Optical and mechanical properties of sol-gel antireflective films for solar energy applications*. J. Thin solid films 351, pp 170 - 175.

Nostell, P., Roos, A., & Rönnow, D. (1999b). *Single-beam integrating sphere spectrophotometer for reflectance and transmittance measurements versus angle of incidence in the solar wavelength range on diffuse and specular samples*. Rev. Sci. Instrum., vol 70 (5), pp 2 481 – 2 494.

Nostell, P. (2001). *Antireflexbehandling av solfångartäckglas genom doppning, samt förbättringar av mekaniska filmegenskaper genom värmebehandling*. Stockholm: Optronic Consulting. {Report concerning AR-treatment of collector glazing by a dip-coating method, and improvements of the mechanical properties by heat treatment.}

Perers, B., & Karlsson, B. (1990). *An annual utilisability method for solar collectors in the Swedish climate*. Contribution to the NorthSun Conference.

Perers, B., Bergkvist, M., & Karlsson, B. (1992). *Booster reflectors in large collector fields. Promising reflector materials.*, Contribution to the NorthSun Conference in Trondheim.

Perers, B. (1993a). *Dynamic method for solar collector array testing and evaluation with standard database and simulation programs*. J. Solar Energy, vol 50, no 6, pp 517 - 526.

Perers, B., & Karlsson, B. (1993b). *External reflectors for large solar collector arrays, simulation model and experimental results*. J. Solar Energy, 51 (5), pp 327 - 337.

Perers, B., Karlsson, B., & Bergkvist, M. (1994). *Intensity distribution in the collector plane from structured booster reflectors with rolling grooves and corrugation*. J. Solar Energy 53, pp 215 - 226.

Perers, B. (1995). *Optical Modelling of Solar Collectors and Booster reflectors under Non Stationary Conditions*. Uppsala: Uppsala University.

Perers, B. (1997). *An improved dynamic solar collector test method for determination of non-linear optical and thermal characteristics with multiple regression*. J. Solar Energy, vol 59, no 4 - 6, pp 163 - 178.

Perers, B., Nilsson, L., Helgesson, A., & Larsson, S. (2003). *Comparison of different solar heating plants in Sweden*. Contribution to the ISES congress in Gothenburg.

Rabl, A. (1976). *Comparison of solar concentrators*. J. Solar Energy 18, pp 93 - 111.

Rabl, A., Goodman, N.B., & Winston, R. (1979). *Practical design considerations for CPC solar collectors*. J. Solar Energy 22, pp 373 - 381.

Rabl, A., O'Gallagher, J., & Winston, R. (1980). *Design and test of non-evacuated solar collectors with compound parabolic concentrators*. J. Solar Energy, vol 25, pp 335 – 351.

Rönnelid, M., & Karlsson, B. (1996a). *Experimental investigation of heat losses from low-concentrating non-imaging concentrators*. J. Solar Energy vol 57, no 2, pp 93 - 109.

Rönnelid, M., Karlsson, B., & Gordon, J.M. (1996b). *The impact of high latitudes on the optical design of solar systems*. Proc. EuroSun 96, Freiburg, Germany, pp 341 - 345.

Rönnelid, M., & Karlsson, B. (1997a). *Irradiation distribution diagrams and their use for estimating collectable energy*. J. Solar Energy 61, pp 191 - 201.

Rönnelid, M., Perers, B., & Karlsson, B. (1997b). *On the factorisation of incident angle modifiers for CPC collectors*. J. Solar Energy, vol 59, no 4 – 6, pp 281 – 286.

Rönnelid, M., & Karlsson, B. (1998). *Optical acceptance function of modified compound parabolic concentrators with linear corrugated reflectors.* Solar Energy Research Center, Högskolan Dalarna, Sweden. Applied Optics 37, 5222-5226.

Rönnelid, M., & Karlsson, B. (1999). *The use of corrugated booster reflectors for large solar collector fields*. J. Solar Energy, 65, 343 - 351.

Rönnelid, M., & Karlsson, B. (2003). *Optimised truncation of a wide acceptance angle CPC*. Contribution to ISES.

Tripanagnostopoulos, Y., Yianoulis, P., Papaefthimiou, S., & Zafeiratos, S. (2000). *CPC solar collectors with flat bifacial absorbers*. J. Solar Energy 69, pp 191 – 203.

Tesfamichael, T., & Wäckelgård, E. (1999). *Angular solar absorptance of absorbers used in solar thermal collectors*. J. Applied optics, vol 38, no 19, pp 4 189 – 4 197.

Tesfamichael, T., & Wäckelgård, E. (2000). *Angular solar absorptance and incident angle modifier of selective absorbers for thermal collectors*. J. Solar Energy, vol 68, no 4, pp 335 – 341.

Veenstra, A. (1999). *European product standards for solar domestic hot water systems reaching maturity*. Contribution to Industry Workshop for Solar Combisystems (IEA-Task 26), in Stuttgart.

Appendix A

Derivation of some "angle equations"

A.I The incidence angle

The incidence angle (Θ) is the angle between the vector describing the beam radiation (**I**) onto a surface and the normal vector (**n**) to that surface (figure A.1). An expression for calculating this angle can be derived from the following relation:

$$\mathbf{I}\cdot\mathbf{n} = |I||n|\cos(\Theta) \Rightarrow \cos(\Theta) = \frac{I \cdot n}{|I||n|} \qquad \text{(A.1)}$$

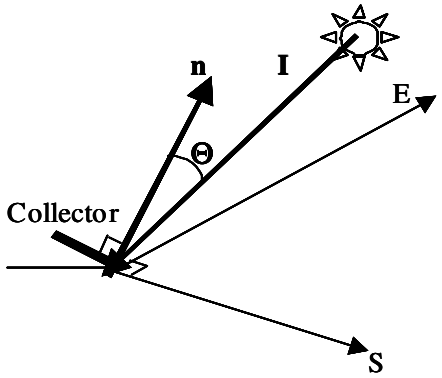

Figure A.1 *Definition of the incidence angle (Θ). S shows the south direction and E the east direction. **I** is the beam radiation from the sun to the collector and **n** is the vector normal to the collector glazing.*

From figure A.2 it can be realized that the two vectors above can be expressed as:

$$\left.\begin{aligned}\mathbf{I} &= (I_S, I_E, I_z) = I\left(\cos(\alpha_s)\cos(\gamma_s), \cos(\alpha_s)\sin(\gamma_s), \sin(\alpha_s)\right)\\ \mathbf{n} &= (n_S, n_E, n_z) = n\left(\sin(\beta)\cos(\gamma_c), \sin(\beta)\sin(\gamma_c), \cos(\beta)\right)\end{aligned}\right\} \quad \text{(A.2)}$$

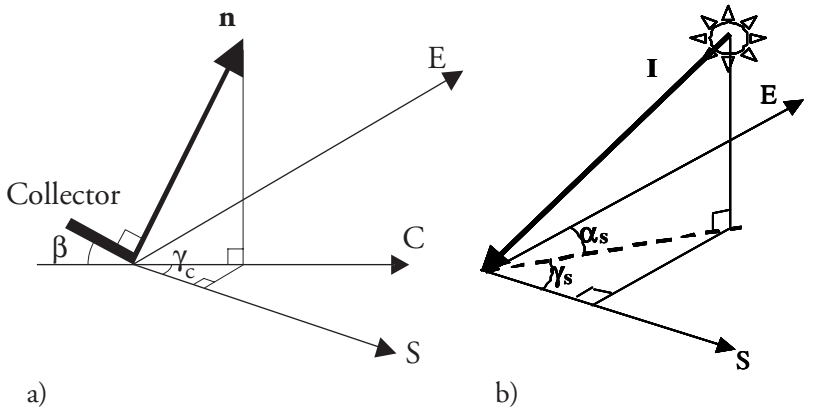

Figure A.2 *Characterization of the vectors used for deriving an expression for calculation of Θ. S = south, E = east, C = collector direction. a) The normal vector of the collector surface (**n**), b) The vector of beam irradiation (**I**).*

Using equations A.2 in eq A.1 gives the following relation:

$$\cos(\Theta) = \frac{In\left(\cos(\alpha_s)\sin(\beta)\cos(\gamma_s)\cos(\gamma_c) + \cos(\alpha_s)\sin(\beta)\sin(\gamma_s)\sin(\gamma_c) + \sin(\alpha_s)\cos(\beta)\right)}{\sqrt{I^2\left(\cos^2(\alpha_s)\left(\cos^2(\gamma_s) + \sin^2(\gamma_s)\right) + \sin^2(\alpha_s)\right)}\sqrt{n^2\left(\sin^2(\beta)\left(\cos^2(\gamma_c) + \sin^2(\gamma_c)\right) + \cos^2(\beta)\right)}} =$$

$$= \left\{\sin^2(A) + \cos^2(A) = 1\right\} = \frac{In\left(\cos(\alpha_s)\sin(\beta)\left(\cos(\gamma_s)\cos(\gamma_c) + \sin(\gamma_s)\sin(\gamma_c)\right) + \sin(\alpha_s)\cos(\beta)\right)}{In} =$$

$$= \sin(\alpha_s)\cos(\beta) + \cos(\alpha_s)\sin(\beta)\cos(\gamma_s - \gamma_c) \quad \text{(A.3)}$$

A.II The profile angle (α_p)

Using figure A.3, the following relations can be found:

$$\tan(\alpha_p) = a/b \quad \text{(A.4)}$$

$$\tan(\alpha_s) = {}^{a}\!/_{d} \tag{A.5}$$

$$b = d\,\cos(\gamma_s - \gamma_c) \tag{A.6}$$

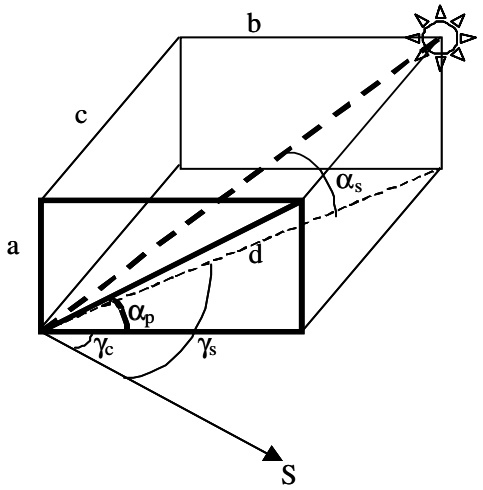

Figure A.3 *Definitions of symbols used in the calculation of the profile angle (α_p). α_s is the solar altitude angle and γ is the azimuth angle for the sun ($_s$) and the collector ($_c$) counted from the south direction (S). a, b, c and d are lengths of interest for the calculations.*

Using eq A.5 and A.6 in eq A.4 gives:

$$\tan(\alpha_p) = \frac{d\,\tan(\alpha_s)}{d\,\cos(\gamma_s - \gamma_c)} = \frac{\tan(\alpha_s)}{\cos(\gamma_s - \gamma_c)} \tag{A.7}$$

A.III Determination of Θ_T

The transverse incidence angle is identified in figure A.4. From this figure Θ_T is calculated as:

$$\Theta_T = 90 - \beta - \alpha_\pi \tag{A.8}$$

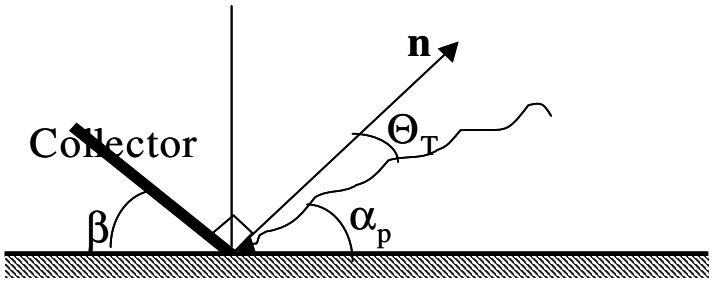

Figure A.4 *Sketch for finding an expression for the transverse incidence angle (Θ_T). (The cut is made perpendicular to the collector extension, i.e. in the transverse plane.) α_p is the profile angle, β is the tilt of the collector, and n is the collector normal vector.*

A.IV Determination of Θ_L

From figure A.5 it is easy to find the following expressions, using the Pythagorean theorem and common trigonometric relations:

$$d^2 = b^2 + c^2 \tag{A.9}$$

$$\tan(\Theta_T) = b/a \Rightarrow b = a\tan(\Theta_T) \tag{A.10}$$

$$\tan(\Theta_L) = c/a \Rightarrow c = a\tan(\Theta_L) \tag{A.11}$$

$$\tan(\Theta) = d/a \Rightarrow d = a\tan(\Theta) \tag{A.12}$$

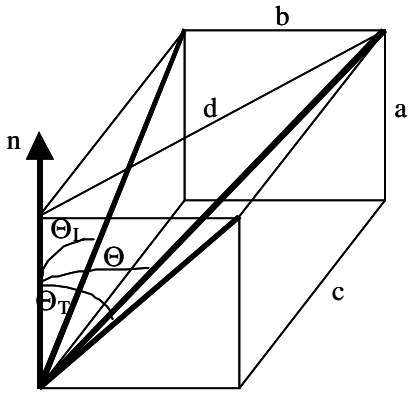

Figure A.5 *Definition of the angles Θ, Θ_T, and Θ_L. (The figure is drawn in such a way that the normal vector of the collector is pointing upwards.)*

Equations A.9 – A.12 then gives:

$$\tan^2(\Theta) = \tan^2(\Theta_T) + \tan^2(\Theta_L) \quad \text{(A.13)}$$

For a south facing collector, the projected incidence angles can also be calculated as:

$$\tan(\Theta_L) = \tan(\Theta)\sin(\gamma_s) \quad \text{(A.14a)}$$

$$\tan(\Theta_T) = \tan(\Theta)\cos(\gamma_s) \quad \text{(A.14b)}$$

where γ_s is the solar azimuth angle.

Appendix B

Measurement equipment

B.I Equipment used at the Älvkarleby laboratory

At Vattenfall's laboratory in Älvkarleby, 15 different collectors can be evaluated at the same time. The collectors are placed on the roof of the laboratory (figure B.1). The heated water is led into the laboratory and cooled in a heat exchanger (figure B.2) before it is circulated back to the collector. The collectors are connected to either of two systems, one in which the inlet temperature at each collector can be controlled, and one where the collectors are connected in series with a common flow. By controlling the inlet temperature, it is possible to cover a large variety of operating conditions. The common flow system facilitates comparisons between different collectors, since uncertainties in flow measurements then do not affect the comparison. In this system, the water is cooled after each collector in order to get the same inlet temperature for all collectors.

Figure B.1 *A photo from the "solar roof" at the Älvkarleby laboratory. Different prototype collectors can be seen.*

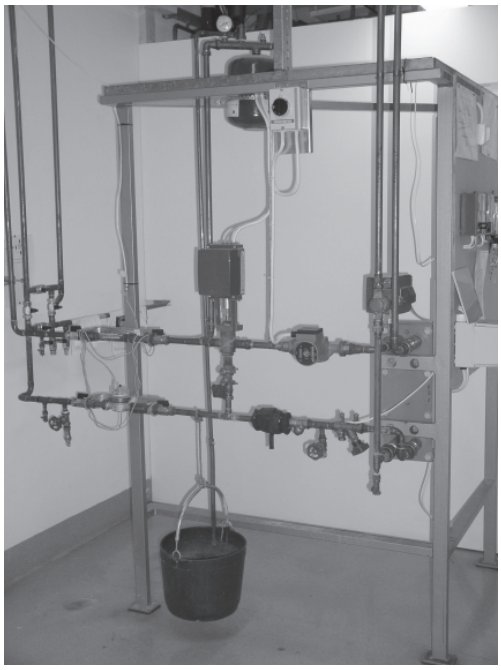

Figure B.2 *A photo showing flow meter (to the left), expansion tank, pump, different valves, and heat exchanger for one of the collector "stations".*

Some comments about the measuring equipment are given in table B.1. Figure B.3 shows some of the used sensors. More information about solar energy measurements can be found in (Perers et al, 2003).

Table B.1 Comments about different equipment used for solar energy measurements.

Measured variable	Type of sensor	Comments
Temperature	PT 100	• Sensors for measuring inlet and outlet water/glycol temperatures shall be installed pointing against the flow direction in a rising part of the pipes. It is also a good advice to place the sensor after a pipe bend, where the fluid is well mixed. The outer parts of the pipe, where the sensor is placed, should be thoroughly insulated. • The sensor used for measuring the temperature of the ambient air must be protected from direct radiation from the sun, and it must also be well ventilated.
Flow (of water/glycol)	Turbine flowmeter	In order to minimize disturbances, the flow meter should be installed in a straight pipe run.
Radiation	• Kipp & Zohnen solarimeter • Eppley pyrheliometer	• The solarimeters are used for measuring radiation on horizontal and tilted planes. By using a shading ring, the diffuse radiation can be determined. • The radiation is also measured with a sun tracking pyrheliometer.
Data logger	Campbell Scientific data logger (CR10)	Used for collecting the measured data and storing (10 minutes) mean values. It is important to check the clock.
At the laboratory, it is also possible to measure/register wind speed, with an anemometer, wind direction, and heat radiation, with a pyrgeometer.		

Figure B.3 *Instruments for climatic measurements. Pyranometers (to the right in the figure) for measuring total and diffuse radiation on a horizontal surface and on a surface tilted 45°, sun tracking pyrheliometer and pyranometer (to the left), and radiation shielded sensor for measuring T_{amb} (under the desk).*

B.II Some equations used during evaluation

Declination:

$$\delta = 23.45 \sin(360\ (284+n)/365) \qquad \text{(B.1)}$$

n = day number

Älvkarleby location: N 60.6°, E 17.4°

Hour angle:

$$\upsilon = (A + 4\,(L_{st} - L_{loc}) + B)\ 15° \tag{B.2}$$

A = time of day
$B = 9.87 \sin(2C) - 7.53 \cos(C) - 1.5 \sin(C)$
$C = 360\ (n - 81)/364$

Solar altitude:

$$\sin(\alpha_s) = \sin(\phi)\sin(\delta) - \cos(\phi)\cos(\delta)\cos(\upsilon) \tag{B.3}$$

Solar azimuth:

$$\cos(\gamma_s) = (\sin(\delta)\cos(\phi) + \cos(\delta)\sin(\phi)\cos(\upsilon))/(-\cos(\alpha_s)) \tag{B.4}$$

Calculation of the product "density · specific heat" for water:

$$\rho \cdot c_p = 4\,208 - 1{,}649\ T_{in} \tag{B.5}$$

Appendix C

Evaluation results

C.I MLR analysis

Example of results from MLR analyses performed on measured data for a flat-plate collector and an EPS-MaReCo. The bold values give the wanted collector parameters. (I_b => η_{0b}, I_bB_o/I_b => b_0, I_d => η_{0d}, DT => k_1, dyn => $(mC)_e$). The values of R^2, std, and the T-ratios can be used to decide if the determined parameters are useful. R^2, the coefficient of determination (or the square of the correlation coefficient), should be as high as possible (i.e. close to 1). The standard deviation, std, should be as low as possible, and the absolute value of the T-ratio should be higher than 1 if the parameter is to improve the model.

MLR-analysis on reference *Flat-Plate* collector

Select: Itot0° > 500 W/m², Idiff45° < 500 W/m², Q < 89°, Pmeasured >5 W/m²

```
(V92GT5) AND (V70GT500) AND (V62LE89) AND (V159LE500)
    M u l t i p e l   L i n j ä r   R e g r e s s i o n s a n a l y s
Oberoende  Medel      Standard     Korrelation    Regression     Medelfel     Beräknad
variabler  värde      avvikelse     X mot Y       Koefficient    hos reg.koe  T-värde
Ib(R2)     579.69135   614.33954    0.98068       0.79151714     0.00222     356.19128
IbBoR2     110.53317   152.35364    0.58505      -0.15708686     0.00433     -36.31343
Id(R2)     181.20540   207.87213    0.80649       0.70474660     0.00534     131.94968
DT2         32.08218    34.02106    0.88470      -2.02372074     0.15366     -13.17047
dyn2         0.00061     0.00417    0.06737   -7004.11328125    84.07988     -83.30309
DT22      1157.43274  1387.44678    0.76956      -0.02567692     0.00228     -11.24514
  Beroende
 Pmätt2      470.45407    491.14645

 Konstant term                      0.00000
 Multipel korrelation               0.99956
 Förklarad proportion (R2)          0.99913
 Residualernas std.                14.54810

 Variansanalys
Variationsorsak        Frihets          Kvadrat     Medel    F-värde
                       grader           summa          kvadrat
 Regressionen            6 435994144.00000  72665688.00000343333.9688
 Residualer           1803    381600.00000       211.64725
 Total                1808 436375744.00000
```

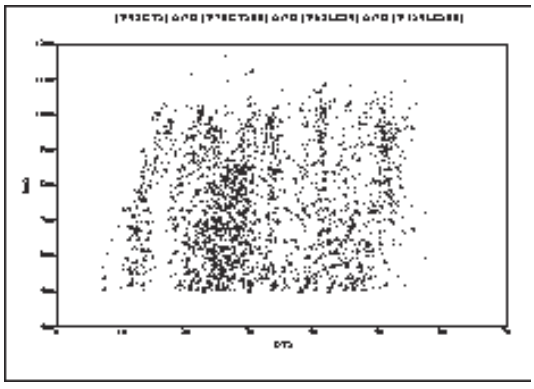

(The $I_{tot}/\Delta T$-diagram shows the data used for the MLR analysis. The larger the diagram area that is covered with dots, the greater the number of different operating conditions that are covered in the analysis.)

MLR-analysis on *EPS-MaReCo* with laminated Al foil.

Select: Itot0° > 50 W/m², Idiff45° < 500 W/m², Q < 85°, Pmeasured >0 W/m²

```
(V2LE990905 OR (V2GE990914 AND V2LE990921) OR V2GE990923)AND V8GE50 AND V77LE5
 M u l t i p e l   L i n j ä r   R e g r e s s i o n s a n a l y s
Oberoende Medel  Standard  Korrelation Regression Medelfel    Beräknad
variabler värde  avvikelse  X mot Y    Koefficient  hos reg.koe T-värde
Ib_mrc   193.65940  345.56790  .96507    .50513780   .00597   84.61800
IbBo     34.66054   62.21832  .89930    -.13287180  .02698   -4.92544
Idmrc3   157.07080  174.86610  .68054    .37707520   .00772   48.86269
DT7      17.47366    20.13632  .89917   -1.22011700  .10168  -11.99995
dyn7       .00035    .00201   .21679  -863.63760000337.07310  -2.56217
Beroende
Pmätt7     129.23550    184.52020

 Konstant term                  .00000
 Multipel korrelation             .99705
 Förklarad proportion (R2)        .99411
 Residualernas std.             14.22979

                     Variansanalys
Variationsorsak        Frihets     Kvadrat         Medel      F-värde
                        grader       summa       kvadrat
Regressionen              5  16855920.00000   3371185.00000 16648.9100
Residualer              493     99826.00000       202.48680
Total                   497  16955750.00000
```

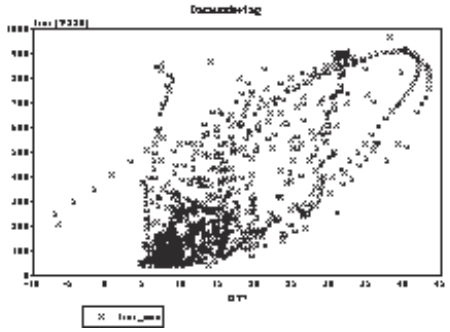

The determined collector parameters from the analysis above are presented in table C.1.

Table C.1 Collector parameters determined from MLR analysis of the flat-plate collector, and the EPS-MaReCo.

Collector	η_{0b} [–]	b_0 [–]	η_{0d} [–]	k_1 [W/m²,K]	k_2 [W/(m·K)²]	$(mC)_e$ [J/m²,K]
Flat-plate (ref)	0.792	0.20	0.705	2.02	0.03	7 004
EPS-MaReCo	0.51	0.26	0.38	1.22		863

These parameters are then used in MINSUN in order to estimate the yearly energy output. The MINSUN-simulations for the flat-plate collector and the EPS-MaReCo are presented in the next session.

C.II MINSUN simulation

When running the simulation, the collector parameters ($F'(ta)b = \eta_{0b}$, $F'UL0 = k_1$, $F'UL1 = k_2$, bo, tilt = β, dir = γ_c, rho = ρ_g, $(mC)_e$, $F'(ta)d = \eta_{0d}$) are given together with the acceptance angle interval (Hsouth max/min). Relevant climatic data (here Stockholm 1986) and a model for calculating tilted radiation are chosen. The result part gives the insolation H (beam, horizontal, and onto collector plane) and the collector output, Q_u, at 5 different operating temperatures (including 25, 50, and 75°C). Optime is the annual operating time if the collector has the given operating temperature the whole year.

MINSUN-run for the *Flat-plate collector*.

```
MINSUN (UMSORT) VERSION [REFTES15] 96-08-22 BP VATTENFALL  UTVECKLING AB
DYNAMIC COLL.MODEL INCL. UNGLAZED+EXTERNAL REFLECTOR+ANGULAR RESOLVED IAM.
+ HSOUTH (MIN / MAX) + BACKSIDE IRRADIATION VACUUM COLLECTOR 2-AXIS TRACKING PTC
     MONTH END DAYS  31  28  31  30  31  30  31  31  30  31  30  31
*COLLECTOR SWITCHES 1=ON,0=OFF
*FLAT PLATE=1 SALT POND=0 EVAC TUBE=0 CENTRAL RECV=0 PARB TROUGH=0 SHAL POND=0
*TILTED RADIATION MODEL=2 (0=Isotropic, 2=Hay & Davies)
*Hsouth max=180.0  Hsouth min=   .0    FnO backside for vacuumcollector=  .00

*F`(ta)b F`UL0  F`UL1    b0  TILT  DIR  RHO (mC)e F`(ta)d F`ULw F`ULsky F`(ta)w
   .792  2.020   .030   .198 45.0   .0   .3  7.004   .705   .000   .000   .000

*NOTE ! REFLECTOR MODEL NOT ACTIVE IN THIS RUN AS Lr/H NEGATIVE=-2.00****
*NOTE ! Value given for F`(ta)d is used for sky diffuse radiation.
*F`(ta)diffuse from reflector is calculated in this run
*from Kta beam data and F`(ta)beam assuming isotropic diffuse distribution

*LATITUDE Acoll/Agrnd    OPEATING TEMPERATURES    LONGDIFF TMAMB   TROOM
   59.33     .01        25.0 40.0 50.0 60.0 75.0     3.1    10.0    18.0
*INCIDENCE ANGLE Kta = BO FUNCTION Kta=1-BO*(1/COS(0)-1)
*Ktad for diffuse radiation from sky + ground=  .89
*Ktad for diffuse radiation from reflector=  .00
*Effective incidence angle for diffuse radiation from reflector= 90.0 deg
*IEA UMSORT OUTPUT SUMMARY * FOR COLLECTOR NUMBER:  1  FOR LOCATION: st86
- TEMPERATURES IN DEGREES CELCIUS  - ALL ENERGIES IN KWH/(M2*MONTH) OR YEAR
*********************************************************************************
*   MONTH    *  J *  F *  M *  A *  M *  J *  J *  A *  S *  O *  N *  D * YEAR *
*********************************************************************************
*Ta     st86 -3.7 -7.4  1.0  2.5 12.6 16.0 17.0 13.6  8.8  7.2  5.1 -1.1*  6.0 *
*Taload st86 -3.7 -7.4  1.0  2.9 14.9 17.2 17.6 16.3 11.0  8.3  5.4 -1.0*  6.9 *
*********************************************************************************
*Hbeam  st86  10.  48.  53.  85. 208. 187. 150.  67. 123.  50.  23.   8.* 1011.*
*Hhoris st86   7.  33.  53.  97. 173. 175. 158.  97.  88.  34.  12.   5.*  934.*
*********************************************************************************
*Hcoll  st86  15.  64.  77. 118. 190. 173. 161. 102. 131.  61.  28.  11.* 1129.*
*********************************************************************************
*Top/Qu 25.C   4.  29.  40.  67. 125. 114. 107.  62.  82.  34.  14.   4.*  683.*
*Top/Qu 40.C   3.  22.  31.  53. 109.  99.  90.  48.  69.  28.  11.   3.*  567.*
*Top/Qu 50.C   2.  18.  26.  45.  98.  88.  80.  40.  60.  24.   9.   2.*  491.*
*Top/Qu 60.C   1.  14.  21.  38.  87.  77.  69.  31.  51.  20.   7.   1.*  417.*
*Top/Qu 75.C   0.   8.  14.  27.  68.  60.  53.  21.  38.  15.   4.   0.*  308.*
*********************************************************************************
*Optime 25.C  23. 115. 164. 257. 377. 412. 430. 350. 274. 149.  59.  21.* 2630.*
*Optime 40.C  17.  88. 124. 198. 290. 301. 305. 246. 225.  93.  42.  15.* 1945.*
*Optime 50.C  15.  71. 100. 161. 269. 265. 256. 194. 198.  81.  40.  14.* 1665.*
*Optime 60.C  13.  62.  85. 131. 249. 234. 233. 154. 170.  66.  33.  12.* 1443.*
*Optime 75.C   4.  47.  64. 104. 207. 209. 198. 104. 139.  54.  24.   7.* 1162.*
*********************************************************************************
```

MINSUN-run for the *EPS-MaReCo*.

```
TILTED RADIATION MODEL=2 (0=Isotropic, 2=Hay & Davies)
*Hsouth max= 65.0  Hsouth min= 20.0    FnO backside for vacuumcollector=  .00
*F`(ta)b F`UL0  F`UL1    b0  TILT  DIR  RHO (mC)e F`(ta)d F`ULw F`ULsky F`(ta)w
   .505  1.220   .000   .260 30.0   .0   .3   .863   .377   .000   .000   .000
*NOTE ! REFLECTOR MODEL NOT ACTIVE IN THIS RUN AS Lr/H NEGATIVE=-2.00****
*NOTE ! Value given for F`(ta)d is used for sky diffuse radiation.
*F`(ta)diffuse from reflector is calculated in this run
*from Kta beam data and F`(ta)beam assuming isotropic diffuse distribution
*LATITUDE Acoll/Agrnd    OPEATING TEMPERATURES    LONGDIFF TMAMB   TROOM
   59.33     .01        25.0 40.0 50.0 75.0 90.0     3.1    10.0    18.0
*INCIDENCE ANGLE Kta = BO FUNCTION Kta=1-BO*(1/COS(0)-1)
*Ktad for diffuse radiation from sky + ground=  .75
*Ktad for diffuse radiation from reflector=  .00
*Effective incidence angle for diffuse radiation from reflector= 90.0 deg
*IEA UMSORT OUTPUT SUMMARY * FOR COLLECTOR NUMBER:  1  FOR LOCATION: st86
- TEMPERATURES IN DEGREES CELCIUS   - ALL ENERGIES IN KWH/(M2*MONTH) OR YEAR
*****************************************************************************
*  MONTH   *  J *  F *  M *  A *  M *  J *  J *  A *  S *  O *  N *  D * YEAR *
*****************************************************************************
*Ta    st86 -3.7 -7.4  1.0  2.5 12.6 16.0 17.0 13.6  8.8  7.2  5.1 -1.1 * 6.0 *
*Taloadst86 -3.7 -7.4  1.0  2.9 14.9 17.2 17.6 16.3 11.0  8.3  5.4 -1.0 * 6.9 *
*****************************************************************************
*Hbeam st86  10.  48.  53.  85. 208. 187. 150.  67. 123.  50.  23.   8.* 1011.*
*Hhoris st86  7.  33.  53.  97. 173. 175. 158.  97.  88.  34.  12.   5.*  934.*
*****************************************************************************
*Hcoll st86  13.  56.  72. 116. 193. 181. 167. 104. 122.  55.  24.  10.* 1113.*
*****************************************************************************
*Top/Qu 25.C   0.   2.  22.  40.  71.  61.  59.  36.  46.  13.   0.  0.*  351.*
*Top/Qu 40.C   0.   2.  19.  35.  65.  55.  52.  30.  41.  11.   0.  0.*  310.*
*Top/Qu 50.C   0.   2.  17.  32.  62.  52.  49.  27.  38.  10.   0.  0.*  288.*
*Top/Qu 75.C   0.   1.  14.  26.  55.  45.  42.  20.  31.   9.   0.  0.*  242.*
*Top/Qu 90.C   0.   1.  12.  23.  50.  41.  38.  17.  28.   8.   0.  0.*  219.*
*****************************************************************************
```

Table C.2 summarizes the energy output at three interesting temperatures. Also the total insolation onto the collector planes is given.

Table C.2 Results from MINSUN simulations for the two evaluated collectors. Energy output is given in kWh/m²,yr. I_{tot} = the total insolation onto the collector planes.

T_{op}	25°C	50°C	75°C	I_{tot}
Flat-plate collector	683	491	308	1 129
EPS-MaReCo	351	288	242	1 113

Appendix D

Summaries of the Papers

D.I Summary of the work

The work concentrates on outdoor measurements of different solar collectors. For the evaluations, a dynamic test method has been used. Examples of outdoor measurements made for evaluation of different collectors are given in the Papers I and VII

In order to study how different solar collector materials affect the output, measurements have been made on flat-plate collectors for both different absorbers and different glazings (Papers II and III). These outdoor measurements were also compared, and in good agreement, with measurements made by Uppsala University. The method to study the optical efficiency developed in Paper III was then used in the work with the biaxial incidence angle modifier.

At VUAB, a special reflector collector, the MaReCo, has been developed. The performance of different MaReCo prototypes has been studied and reported in Papers IV - VI. Since the MaReCo is asymmetric, the modelling of the incidence angle dependence of the optical properties is rather difficult. A new biaxial model has been suggested and tried experimentally (Papers III, V, VII - X). The development of this method is described in Papers VII and VIII. Papers V and IX present two examples where this method has been used.

D.II List of papers

[I] Helgesson A., Karlsson B. & Perers B. (Vattenfall Utveckling AB), "*Development and evaluation of a combined solar collector + reflector*". Contribution to NorthSun 99 in Edmonton.
My contribution is evaluation of the prototype and editing of the paper.

[II] Tesfamichael T. & Wäckelgård E. (Department of Materials Science, Uppsala University) & Helgesson A. (Vattenfall Utveckling AB), "*Impact of angular solar absorptance on collector performance investigated by dynamic collector testing and optical angular characterization of solar absorbers*".
Contribution to NorthSun 99 in Edmonton, Canada, 1999.
My contribution is outdoor evaluation in Älvkarleby.

[III] Helgesson A. & Karlsson B. (Vattenfall Utveckling AB) & Nostell P. (Dep. of Material Science, The Ångström Laboratory, Uppsala University), "*Angular dependent optical properties from outdoor measurements of solar glazings*".
Contribution to EuroSun 00 in Copenhagen, Denmark, 2000. (Also published in Solar Energy, vol 69, nos 1 – 6, pp 93 - 102, 2000.)
My contribution is development of the method for and outdoor evaluations in Älvkarleby and editing of the paper.

[IV] Adsten M. (The Ångström Laboratory, Uppsala University), Helgesson A. & Karlsson B. (Vattenfall Utveckling AB), "*Evaluation of CPC-collector designs for stand-alone, roof- or wall installation*".
Submitted to Solar Energy 2004.
My contribution is parts of the collector evaluations.

[V] Helgesson A. & Karlsson B. (Vattenfall Utveckling AB) & Nordlander S. (SERC, Högskolan Dalarna) "*Evaluation of a Spring/Fall-MaReCo*".
Contribution to EuroSun in Bologna, 2002.
My contribution is outdoor evaluations, Minsun simulation and editing of the paper.

[VI] Karlsson B. & Helgesson A. (Vattenfall Utveckling AB), "*System testing of a MaReCo with suppressed summer performance*".
Contribution to the ISES Congress in Gothenburg, 2003.
My contribution is system evaluations and editing of the paper.

[VII] Helgesson A. & Karlsson B. (Vattenfall Utveckling AB), "*Study of incidence angle dependence on optical efficiency based on outdoor measurements, modelling of incidence angle dependence of non-symmetrical collectors*".
Contribution to NorthSun in Leiden, 2001.
My contribution is evaluations, development and use of the new biaxial method, and editing of the paper.

[VIII] Helgesson A. & Karlsson B. (Vattenfall Utveckling AB), "*Incidence angle dependence of an asymmetric collector*".
Contribution to EuroSun in Bologna, 2002.
My contribution is parts of the evaluations and editing of the paper.

[IX] Brogren M., Roos A. (Solid State Physics, Engineering Science, Uppsala University), Karlsson B. & Helgesson A. (Vattenfall Utveckling AB), & Nilsson J. (Energy and Building Design, Lund University), "*Biaxial model for the incidence angle dependence of the optical efficiency of photovoltaic and solar thermal systems with asymmetric reflectors*".
Contribution to the ISES Congress in Gothenburg, 2003 and also submitted to Solar Energy.
My contribution is development of the biaxial method for PV-modules and part of the evaluations.

[X] Helgesson A. (Vattenfall Utveckling AB), Nilsson J. & Karlsson B. (Energy and Building Design, Lund University), "*A new model and method for determination of the incidence angle dependence of the optical efficiency of solar collectors*".
Submitted to Solar Energy.
My contribution is development of the biaxial method and editing of the paper.

D.III The abstracts of the papers

D.III.I Development and evaluation of a combined solar collector + reflector

This project is a part of a large Swedish National Solar Thermal R&D-program for solar energy heating. In the project a solar collector + reflector combination was constructed for easy application on flat ground or non-tilted roofs. A prototype with a 6 m^2 collector and an adherent parabolic reflector was built. An interesting detail of the construction is the mounting on heavy beams made of concrete. This makes it possible to avoid making holes in the roofs and thereby makes the mounting easier and cheaper. In order to get an estimation of the possible yearly output, measurements of flow and temperatures were used together with a simulation tool. The results show that a yearly gain of about 500 kWh/m^2 is possi-

ble at an operating temperature of 50°C and that the reflector gives a contribution of about 23%. The collector + reflector combination has also been tested in a 210 m^2 large collector field in Örebro.

D.III.II Impact of angular solar absorptance on collector performance investigated by dynamic collector testing and optical angular characterization of solar absorbers

The purpose of this study was to investigate how the angular solar absorptance of the solar absorber influences the efficiency of the whole solar thermal collector. Two types of absorbers (aluminum strip with either nickel-pigmented anodic aluminum oxide coating or nickel/nickel oxide coating) were tested in the same type of collector box. The collectors were evaluated according to the principle of dynamic testing. This evaluation showed no significant difference in yearly energy output between the two absorbers. The optical evaluation of the angular solar absorptance was made from angular spectral reflectance using an optical measuring system equipped with an integrating sphere. The measurements showed a better optical performance of the nickel-pigmented aluminum oxide absorber at higher angles of incidence, but this effect is reduced by the glazing. This result is confirmed by the dynamic testing.

D.III.III Angular dependent optical properties from outdoor measurements of solar glazings

A method for careful outdoor characterization of the angular dependent solar transmittance of solar glazing is developed and used for investigating the performance of structured and antireflection treated glass. Two identical collectors are series connected in order to get an identical flow. The reference collector is always covered with a thin Teflon foil and the test collector is furnished with the investigated covers. The method is carried out in six steps: 1) The collectors are long term tested in order to get the collector parameters, especially the U-values. 2) The performances of the collector at a temperature close to ambient are monitored during a clear day. 3) The effect of heat losses is eliminated from the knowledge of the U-values, and the optical efficiencies of the collectors are derived. 4) The ratio between optical efficiency of the test- and the reference collector is calculated. 5) Both collectors are tested with a Teflon film, with well-known optical properties, as a cover and the relative optical efficiency is derived. 6) From the relative transmittance between the

investigated glazings and Teflon, the absolute value of the angular dependent transmittance is derived. The results show good agreement with conventional optical characterization. The commercial antireflection treatment increases the solar transmittance with 4 % and the annual output with 9 %. The structured glass, shows similar angular performance as a flat glass if the structure is faced outwards, but shows a lower transmittance for incidence angles exceeding 40° if the structure is faced inwards. This means that the annual performance is decreased by 4 % by facing the structure inwards instead of outwards.

D.III.IV Evaluation of CPC-collector designs for stand-alone, roof- or wall installation

An asymmetrically truncated non-tracking compound parabolic concentrator type collector design concept has been developed. The collector type has a bi-facial absorber and is optimised for northern latitudes. The concept is based on a general reflector form that is truncated to fit different installation conditions. In this paper collectors for stand-alone, roof and wall mounting are studied. Prototypes of six different collectors have been built and outdoor tested. The evaluation gave high annual energy outputs for a roof mounted collector, 925 MJ/m², and a stand-alone collector with Teflon, 781 MJ/m², at an operating temperature of T_{op} = 75°C. A special design for roofs facing east or west was also investigated and gave an annual energy output of 349 (east) and 436 (west) MJ/m² at T_{op} =75°C. If a high solar fraction over the year is the objective, a load adapted collector with a high output during spring/fall and a low output during summer can be used. Such a collector had an output of 490 MJ/m² at T_{op} = 75°C. Finally a concentrating collector for wall mounting was evaluated with an estimated annual output of 194 MJ/m² at T_{op} = 75°C. The concentrator design concept can also be used for concentrators for PV-modules.

D.III.V Evaluation of a Spring/Fall-MaReCo

One problem associated with solar energy is that the heating demand is largest during the winter, while the solar supply is largest during the summer. In order to contribute to the space heating during spring and fall, a relatively large collector area is needed. This will, however, increase the risk of overheating during the summer. To avoid this problem, a special collector, the “Spring/Fall-MaReCo”, has been constructed. The purpose of a MaReCo is to reduce the costs for solar energy by using internal

reflectors. The collector consists of a parabolic reflector trough with a bifacial absorber fin. The shape of the reflector affects the collector performance and the Spring/Fall-MaReCo is designed to suppress the energy output during the summer. In this way a larger collector area can be installed in order to increase the solar fraction of the system without causing overheating. The paper presents results from the collector evaluation.

D.III.VI System testing of a MaReCo with suppressed summer performance

One problem with solar energy is that the heating demand is largest during the winter, while the solar supply is largest during the summer. In order to avoid overheating during the summer, but still contribute to the heat load during spring and fall, a special collector with reduced summer efficiency has been constructed. In this way, a larger collector area can be installed in order to increase the solar fraction of the system without the risk of overheating during the summer. This "Spring/Fall-MaReCo" is a reflector collector designed for roof-installation. The collector principally consists of an asymmetric reflector trough with a bifacial absorber. The low material content keeps the collector cost low. Vattenfall Utveckling AB has evaluated the performance of a prototype of the Spring/Fall-MaReCo. This study shows that the efficiency decreases, as wanted, during the summer. According to an energy simulation, the annual energy output is estimated to approximately 222 kWh/m².

D.III.VII Study of incidence angle dependence on optical efficiency based on outdoor measurements, modelling of incidence angle dependence of non-symmetrical collectors

The annual energy output from a solar collector can be estimated by using collector performance parameters in a simulation program. For flat plate collectors, the incidence angle dependence is often modelled with the following expression

$$\eta_{ob}(\Theta) = \eta_{ob} \cdot \left[1 - b_0 \left(\frac{1}{\cos(\Theta)} - 1 \right) \right]$$

where Θ is the incidence angle and b_0 is an incidence angle modifier. For a non-symmetrical collector, like e.g. an asymmetric CPC or a MaReCo (i.e. a reflector collector specially designed for high latitudes and extended in the east-west direction), this model may however not work satisfactorily since the incidence angle dependence then will be different in different directions. In this paper is a method for investigating the performance of non-symmetrical collectors developed. This method builds on a biaxial incidence angle modifier with two b_0-factors, one in the transverse (T) and one in the longitudinal (L) direction:

$$K_{tot}(\Theta) = (1 - bo_L \cdot (1/\cos(\Theta) - 1)) \cdot \frac{(1 - bo_T \cdot (1/\cos(\Theta_T) - 1))}{(1 - bo_L \cdot (1/\cos(\Theta_T) - 1))}$$

In order to study how well the new suggested expression describes the actual collector performance, outdoor measurements were made on a MaReCo-prototype during summer-autumn 2000. The evaluation of the measurements shows that the suggested model is a good way to describe the collector output. The paper also gives suggestions to continued work in this area.

D.III.VIII Incidence angle dependence of an asymmetric collector

The MaReCo is a special reflector collector adapted for northern latitudes. The collector consists of an asymmetric reflector trough with a single bifacial absorber running along the trough. Since the collector is asymmetric, the incidence angle dependence of the optical efficiency is different in different directions. Outdoors measurements have been performed on different MaReCo prototypes in order to study the incidence angle dependence of the optical efficiency. In the paper, energy output from and efficiency of three different MaReCos are presented.

D.III.IX Biaxial model for the incidence angle dependence of the optical efficiency of photovoltaic and solar thermal systems with asymmetric reflectors

The optical efficiency of concentrating solar thermal and photovoltaic systems with cylindrical geometries is asymmetrical about the optical axis. Biaxial models, based on projected incidence angles, are often used to

estimate the annual performance of asymmetric concentrators. However, the use of projected angles tends to underestimate optical losses in the cover glass. In this work, a biaxial model for the incidence angle dependence of the optical efficiency, which uses the transverse projected incidence angle for determining the influence of the reflector and the real incidence angle to determine the influence of the glazing is proposed: $\eta_{0pt} = R_T(\Theta_T)f_L(\Theta_i)$. The model gives an absolute value of the optical efficiency and it is valid for all types of concentrating systems, as well as for flat plate collectors and planar PV modules. The model is validated for a system with an east-west aligned asymmetric parabolic reflector without a cover glass and it is shown that the dependence on the optical efficiency of the reflector on the longitudinal angle of incidence is negligible. The model is compared with the commonly used biaxial model and it is found that the difference is a couple of percentage points when the difference between the longitudinal projected incidence angle and the real incidence angle is large and the angle of incidence on the glass is high.

D.III.X Development and testing of a new model and method for the incidence angle dependence of the optical efficiency of different solar collectors

A new biaxial method for modelling the incidence angle dependence of the optical efficiency of asymmetric collectors is developed. This method is based on measurements in both the longitudinal and the transverse planes of the collector. The model includes a function, $f_L(\Theta)$, that considers the influence of the glazing, and a function, $g_{TL}(\Theta_T)$, that considers the influence of the reflector. The analysis procedure is carried out in a number of steps. First the dependence of the glazing is derived from measurements in the longitudinal direction at times when Θ_T is constant. Then the influence of the reflector is determined from measurements in the transverse direction for constant Θ_L. The suggested method is evaluated by performing outdoor measurements on some different MaReCos. The results show that the suggested model is accurate and better than a common single b_0 model for evaluation of asymmetric collectors. The paper also includes a discussion of the solar fraction of collector systems. A special expression for estimating the solar fraction is derived.

LUND UNIVERSITY
Lund Institute of Technology

ISSN 1671-8136
ISBN 91-85147-07-9